Theses and Dissertations

Spring 2016

Effects of mechanical stimulation on fibroblast-guided microstructural and compositional remodeling

Aribet M. De Jesús

University of Iowa

Recommended Citation

Follow this and additional works at: http://ir.uiowa.edu/etd

Part of the Biomedical Engineering and Bioengineering Commons

www.manaraa.com

EFFECTS OF MECHANICAL STIMULATION ON FIBROBLAST-GUIDED

MICROSTRUCTURAL AND COMPOSITIONAL REMODELING

by

Aribet M. De Jesús

A thesis submitted in partial fulfillment
of the requirements for the Doctor of Philosophy
degree in Biomedical Engineering
in the Graduate College of
The University of Iowa

May 2016

Thesis Supervisor: Assistant Professor Edward A. Sander

Graduate College
The University of Iowa
Iowa City, Iowa

CERTIFICATE OF APPROVAL

_____

PH.D. THESIS

_____

This is to certify that the Ph.D. thesis of

Aribet M. De Jesús

has been approved by the Examining Committee
for the thesis requirement for the Doctor of Philosophy
degree in Biomedical Engineering at the May 2016 graduation.

Thesis Committee: _____
                              Edward A. Sander, Thesis Supervisor

                              _____
                              Michael Mackey

                              _____
                              James Ankrum

                              _____
                              Madhavan Raghavan

                              _____
                              Sarah Vigmostad

To mami, papi, and my beloved papá Juan.

The increase of scientific knowledge lies not only in the occasional milestones of science, but in the efforts of the very large body of men (and women) who with love and devotion observe and study nature.

Polykarp Kusch

ACKNOWLEDGMENTS

I would like to thank my thesis advisor, Dr. Edward Sander, for taking a chance, and giving me the opportunity to become a PhD student. It has been a challenging, and exciting five-year journey, and I truly appreciate the academic guidance, and the support that he has given me along the way. I would also like to thank my committee members, Dr. Michael Mackey, Dr. Sarah Vigmostad, Dr. James Ankrum, and Dr. Madhavan Raghavan for sharing their valuable insight, knowledge and suggestions.

I would also like to acknowledge Sathivel Chinnathambi for having the patience to teach me many lab techniques that became essential to the completion of this dissertation and for providing useful and insightful ideas and suggestions. I want to thank Mariam El-Hattab, and Zack Seikel for their help as undergraduate researchers. Many thanks to all of my other labmates, Hoda Zarkoob, Maziar Aghvami, Andrew Wagner, and Keerthi Atluri for their help, support and stimulating conversations. I would like to acknowledge support from the Department of Education Graduate Assistantships in Areas of National Need (GAANN) program and the University of Iowa College of Engineering for financial support.

To my friends Camila Ramírez, Richard González, Nelson Colón, my beautiful, loving siblings, Amarilis De Jesús and Anthony De Jesús, and Aaron Wells, many thanks for being my safety net, for helping me maintain my sanity, and for always supporting me and motivating me to keep going. Lastly, I could not be more appreciative of the amazing human beings that I have had the privilege to call my family. Mami, y papi, thank you for always inspiring me to dream big, to work hard, and to always try despite the fear of failure.

ABSTRACT

Many physiological and pathological processes, such as wound healing and tissue remodeling, are heavily influenced by continuous mechanical cell-cell and cell-ECM communication. Abnormalities that may compromise the biomechanical communication between the cells and the ECM can have significant repercussions on these physiological and pathological processes. The state of the mechanical environment and the reciprocal communication of mechanical signals between the ECM and the cell during wound healing and aged dermal tissue regeneration may be key in controlling the quality of the structure and physical properties of regenerated tissue.

This dissertation encompasses a series of studies developed for characterizing the effects of mechanical cues on altering and controlling tissue remodeling, and regeneration in the context of controlling scar formation during wound healing, and the maintenance and regeneration of the dermal extracellular matrix (ECM) during aging. In order to achieve this goal, *in vitro* models that contained some features of the provisional ECM, and the ECM of the dermis were developed and subjected to an array of quantifiable mechanical cues. Wound models were studied with different mechanical boundary conditions, and found to exhibit differences in initial short-term structural remodeling that lead to significant differences in the long-term synthesis of collagen after four weeks in culture. Dermal models seeded with fibroblasts from individuals of different ages were treated with a hyaluronic acid (HA)-based dermal filler. Changes in the mechanical environment of the dermal models caused by swelling of the hydrophilc HA, resulted in changes in the expression of mechanosensitive, and ECM remodeling genes, essential for

the maintenance and regeneration of dermal tissue. Taken together, these data provide

new insights on the role of mechanical signals in directing tissue remodeling.

PUBLIC ABSTRACT

The integrity, composition and function of cutaneous tissue is highly dependent on the physical interactions that occur between fibroblasts and the composite of proteins that make up the structural frame-work of said tissue. Many physiological and pathological processes depend on the ability of the fibroblast to sense mechanical cues from its environment and respond by altering its tissue remodeling capabilities in order to maintain equilibrium and the structural integrity of tissue.

This dissertation describes a series of studies that were developed for characterizing the effects of different mechanical cues on altering tissue remodeling, regeneration and repair in the context of controlling scar formation during wound healing and the maintenance and regeneration of the aged dermis. To achieve this goal, in vitro models of the wound and the extracellular matric (ECM) of the dermis were developed and were subjected to an array of quantifiably mechanical cues. Wound models were subjected to different physical constraints and were found to exhibit differences in initial short-term structural remodeling that lead to significant differences in the long-term synthesis of collagen after four weeks in culture. Dermal models seeded with fibroblasts from individuals of different ages were treated with a hyaluronic acid (HA)-based dermal filler. Changes in the mechanical environment of the dermal models caused by swelling of the hydrophilc HA, resulted in changes in the expression of mechanosensitive, and ECM remodeling genes, essential for the maintenance and regeneration of dermal tissue. Taken together, these data provide new insights on the role of mechanical signals in directing tissue remodeling.

TABLE OF CONTENTS

LIST OF TABLES

LIST OF FIGURES

xiv

CHAPTER 1: MOTIVATION

1.1. Introduction

Connective tissues encompass a diverse range of tissues that provide resistance to a variety of external and internal loads. Much like a composite material, connective tissues are comprised of a variety of proteins and cells that together provide properties required for its maintenance and function. The nature of the morphological and compositional organization of the extracellular matrix (ECM) of different types of tissues is highly dependent on the function and location of the tissue and is therefore a product of the loads that it must bear. From the intrinsic forces generated from underlying skeletal growth to gravitational forces, soft connective tissue must constantly respond and adapt to a variety of mechanical forces.

The maintenance of physiological function of connective tissue in response to changes in loading, rupture, or damage is possible due to the presence of fibroblasts [2-4]. Fibroblasts are connective tissue cells that are derived from mesenchymal stem cells [5-7]. Mechanical forces that are applied to tissues at a macroscopic level are transmitted through the fibrous network of the ECM, down to the microscopic level where they cause changes to the local environment. These changes are sensed by resident fibroblasts that respond by altering their contractile behavior and increasing the expression of growth factors and ECM proteins [8, 9]. In turn, microscopic responses of individual elements of the ECM can alter the macroscopic mechanical behavior of the tissue. So, through dynamic reciprocal multi-scale communication of mechanical loads between the cell and the ECM, fibroblasts can respond to physical and biochemical signals, remodel, and

1

restore homeostasis to the ECM [8]. Interactions that occur between fibroblasts and their mechanical environment are key in the progression of a large number of physiological processes such as wound healing, tissue growth, development, and regeneration. Inefficient communication between the cells and the ECM are hypothesized to be the cause of pathological behavior that may result in inefficient tissue regeneration during wound healing, fibrosis, and aging [10-15].

<div align="center">

1.2. Multiscale Mechanical Interactions In the Wound

Healing Process

</div>

Cutaneous wound healing is a complex physiological process that occurs in response to injury or insult to connective tissue. This response involves the coordinated activation of multiple cell types and growth factors, and the dynamic crosstalk between the mechanical environment of the wound bed and the contractile fibroblast [16, 17]. This dynamic and complex process involves four overlapping phases: hemostasis, inflammation, proliferation and remodeling, which, under normal physiological conditions, result in the restoration of structure, composition and function of the injured tissue [18, 19].

Normal wound healing commences upon injury. The process of hemostasis begins when activated platelets first aggregate within the wound and secrete various biochemical factors and growth factors, such as platelet-derived growth factor (PDGF) and transforming growth factor (TGF-β), which results in the formation of the provisional fibrin matrix of a clot. The inflammatory phase follows as leukocytes, such as neutrophils and macrophages, migrate to the wound site to clean up the damaged tissue and remove

2

foreign bodies. During the proliferative phase, the release of cytokines and growth factors attracts budding endothelial cells to vascularize the granulation tissue and the migration of fibroblasts from surrounding tissues. Fibroblasts play a key role during the remodeling phase of the wound healing process and are essential to dermal wound healing, as they are responsible for the secretion of ECM matrix proteins and wound contraction[20-23]. As the remodeling phase progresses, the fibroblast, in response to growth factors and tension, differentiate into highly contractile myofibroblasts. In addition to generating large traction forces, myofibroblasts synthesize ECM proteins, such as hyaluronic acid, fibronectin, and collagen [24-26]. Through the expression of α-smooth muscle actin (α-SMA) myofibroblasts exert contractile forces that allow them to reorganize newly synthesized proteins, and close the wound margins. But this regenerated tissue is far from perfect. The collagen matrix of connective tissue scars is poorly reconstituted, organized in dense parallel bundles that differ from the mechanically efficient basket-weave meshwork of collagen in unwounded dermis (Fig. 1) [27].

3
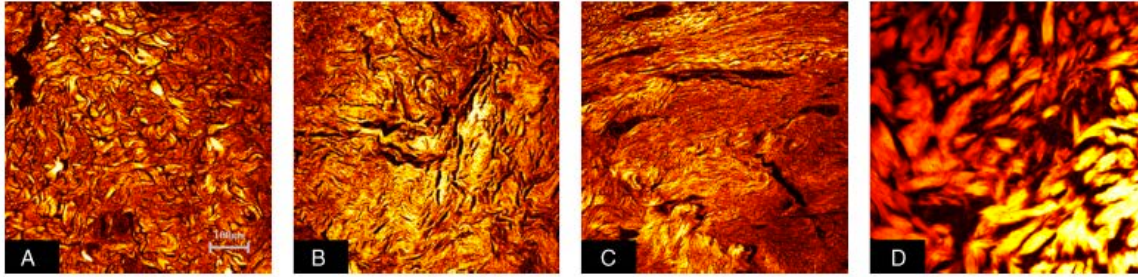
Figure 1. Differences in collagen architecture between A) normal skin, B) normotrophic scars, C) hypertrophic scars, and D) keloids [27] observed via confocal microscopy. The images highlight differences in collagen organization in normal skin and scar tissue in the order of increasing hypertrophy. Collagen fibers in normal, unwounded skin exhibit an isotropic organization. Collagen fibers in normotrophic, hypertrophic and keloid scars assume a more aligned orientation. Keloid scars also contain significantly thicker bundles of collagen as compared with normal, normotrophic and hypertrophic scars.

Furthermore, under pathological conditions, an increased state of tension can perpetuate the presence of the myofibroblast, causing increased collagen production that can result in the formation of hypertrophic scars [28]. In fact, some wound healing strategies are based on reducing the state of tension in the wound in order to reduce scarring, such as negative pressure therapy and compression [29].

1.3. Modeling the Wound Healing Process

1.3.1. *In Vitro* Models

Scratch wound assays are a common and simple method used to study cell migration and repopulation upon injury. This assay consists in disrupting a monolayer of a confluent population of cells by creating a "scratch" or incision along the surface of the substrate [30-32]. This assay has been used extensively to study re-epithelialization, but keratinocyte monolayer cultures have demonstrated hyperproliferative growth and limited stratification under these simplified, *in vitro* conditions. Though helpful in providing

4

information on the migratory behavior of keratinocytes upon injury, the lack of complexity of this model limits the study of keratinocyte and epithelial-mesenchymal cross-talk during wound healing and provides no information on the behavior and role of the fibroblast.

Deformable substrates with tunable mechanical properties are a common model used to investigate the effects of physical forces on cell behavior *in vitro*. The culture of fibroblasts on substrates such as polyacrylamide gels has aided in elucidating the role of mechanical tension on regulating the expression of ECM proteins, α-SMA, and pro-fibrotic chemokines [14]. Therefore, also supporting the hypothesis that mechanical tension and fibroblast mechanosensing are factors in wound fibrosis. The study of keratinocyte mechano-response using similar systems has linked mechanical forces to keratinocyte proliferation, migration, and colony formation, features that are important in re-epithelialization during normal and diseased wound healing [33, 34]. Despite the many advances that two-dimensional wound models have provided, these systems do not provide a realistic representation of the complex, three-dimensional environment of physiological cutaneous tissue.

The need for models that better represent the physiological environment of the ECM has lead to the development of *in vitro* systems based on the use of protein-rich hydrogels. The cell-populated collagen gel models described in the previous section have been extensively used as dermal equivalents and as representative models of different phases of the wound healing process, particularly of the transition from granulation tissue to scar tissue [35-37].

5

As previously described, the attached cell-seeded collagen gel model, defined by the development of isometric tension by the highly contractile myofibroblast due to the presence of lateral fixed boundary conditions, is representative of granulation tissue. Granulation tissue is the temporary matrix that develops in a wound 4-5 days after injury, densely populated by different cell types and rich vasculature [38]. The stress relaxation or released cell-populated collagen gel is used as a model for the acellular, and relatively avascular scar tissue that replaces granulation tissue after wound contracture. Fibroblasts in granulation tissue possess a bipolar morphology and extend along vectors of tension, perpendicular to the direction of wound contraction. A similar morphology is observed in fibroblasts seeded within attached collagen matrices where they exhibit actin-rich bundles aligned in the direction perpendicular to the fixed boundary of the gel [39] Fibroblasts in scar tissue, like fibroblasts in stress-released collagen gels, begin to lose their extended, bipolar morphology and the appearance of stress fibers. During the transition from granulation tissue to scar in the wound, and from attached to a released state in the collagen gel, the cell population dwindles and the volume of the tissue decreases. Many researchers have built upon these models to examine the role of a variety of physical and biochemical factors on different aspects of the wound healing process as well as other regenerative processes. Rouillard *et al.* explored the effects of anisotropic mechanical boundaries on fibroblast invasion from a collagen gel into a fibrin gel polymerized in the cell-seeded collagen-based dermal equivalent as a model of a wound [40].

These *in vitro* systems have offered more physiologically relevant models that incorporate the dynamics of three-dimensional cell-matrix interactions. Mechanical manipulation of these constructs through the use of different boundary conditions and

6

applied forces by means of stretching devices has provided a large body of evidence that supports the role that physical forces play in controlling the regenerative and remodeling capabilities of fibroblasts in a plethora of physiological and pathological processes. But, despite the many advantages that these models offer, their use in experimental studies and as a representation of the physiological milieu are limited. While granulation tissue is composed of a variety of proteins such as fibronectin, tenascin, and hyaluronan, that is slowly replaced by collagen type III, and collagen type I, the ECM of cell-populated collagen models only consists of collagen type I. These models also lack the multi-cellularity that identifies the wound milieu. While physiological wounds are invaded by macrophages, platelets, and fibroblasts, cell-seeded collagen gels are commonly inhabited solely by fibroblasts. Finally, the absence of multiple layers is another limitation that leads to the overlook of the cross-talk between different skin compartments.

Human skin and scar explants have been used to study the effects of the healing process on the compositional and mechanical properties of skin ECM. Histological analyses of scar tissue show structural and compositional differences in collagen type I deposition as compared to healthy, unwounded skin [27]. The collagen matrix of connective tissue scars is poorly reconstituted, and is organized in dense, parallel bundles that differ from the mechanically efficient basket-weave meshwork of collagen in the unwounded dermis. These findings are consistent with studies that have revealed that human scar tissue is stiffer than unwounded skin [41].

It is clear that mechanical tension impacts tissue remodeling, regeneration and healing by controlling cell behavior. This is seen clinically in scar formation in wounds formed on areas of the skin that are under greater stress such as the shoulders and knees.

7

As an attempt to uncover the effects of the state of stress in the wound on structural arrangement and their role in guiding *de novo* ECM synthesis and organization. The first portion of this thesis describes efforts to develop a simple fibrin-based model of the remodeling phase of the wound healing process. This model can be used to easily quantify patterns of deformation and fiber alignment that are dependent on cell traction force generation, applied boundary conditions, and the geometry of the gel.

1.4. Multiscale Mechanical Interactions in Aging of the
Dermal ECM

Another example of how the mechanical environment can impact cell behavior and the maintenance and regeneration of connective tissue can be observed in aged skin. The dermal ECM is composed of an extensive variety of proteins that provide structural support to the skin and maintain its function. Proteoglycans, and glycosaminoglycans make up only a portion of the ECM, while collagen type I comprises up to 66-69% of its mean fractional volume [42]. Mechanically responsive fibroblasts secrete and organize fibrillar collagen type I, creating a three-dimensional network that provides mechanical integrity to the skin.

Dynamic mechanical interactions between fibroblasts and the collagenous network regulate cell morphology and function and help maintain a strong, healthy dermis. As we age, the health, structure and appearance of skin deteriorates. Chronologically aged skin is characterized by the presence of wrinkles, increased fragility, and a loss of elasticity. These drastic changes in the mechanical properties of skin are hypothesized to occur due to a loss of structural integrity and a loss of

8

mechanical tension in the dermal ECM that occurs as a result of inefficient collagen degradation [43].

Inefficient collagen degradation occurs due to two inherent properties of collagen: (1) a long half-life [44], and (2) cross-links resistant to biosynthesis/degradation [45]. Histological studies have revealed drastic changes in fibroblast morphology in aged skin. Cells in the aged dermis assume a rounded, collapsed shape that is characteristic of mechanically inactive, and quiescent cells [11]. The loss of a homeostatic level of tension in the skin due to the breakdown of collagen fibers, could result in a loss of mechanical communication to the cell, causing cells to cease collagen production and to increase their catabolic activity. As a result, collagen synthesis is decreased and matrix metalloproteinase (MMP) synthesis is increased, causing further degradation and collapse of the network [11, 43, 46]. This kind of catabolic response accompanied by fibroblast inactivity has been observed experimentally in tension-free collagen gels [47, 48]. Nakagawa *et al.* used attached and free-floating cell-seeded collagen gel models to prove that fibroblasts that were allowed to achieve high levels of tension in tethered gels remained synthetic and produced collagen. Those cultured under tension-free conditions in free-floating gels, synthesized little to no collagen [48]. It has also been reported by Langholz *et al.* that fibroblasts that are grown in these stress-relieved collagen gels down-regulate the expression of genes encoding for collagen while up-regulating MMP1 mRNA through integrin-collagen interactions [49]. The details of these kinds of models are discussed in more detail in the next section.

9

1.5. The Mechanosensitive Fibroblast

As members of the family of connective-tissue cells, fibroblasts are responsible for the production and maintenance of the ECM of most connective tissues. Fibroblasts secrete and structurally organize an assortment of proteins including collagens type I and III, glycosaminoglycans, and elastin. The mechanical environment of the ECM plays a pivotal role in controlling the differentiation and function of the fibroblast. The mechanical feedback loop that exists between fibroblasts and the ECM is central to its function of maintaining structural and compositional integrity of the connective tissue it inhabits. Early *in vitro* studies revealed the presence of different fibroblast phenotypes within 3D collagen gels cultured under different states of tension [22, 48, 50]. Fibroblasts, as well as several other cell types, such as smooth muscle cells and endothelial cells, contract collagen matrices through the contractile activity of actin stress fibers. Forces generated by the actin cytoskeletal machinery are translated to collagen fibers via integrin complexes that connect the cytoskeleton to ECM proteins. This behavior results in the reorganization and densification of the fibrous collagen network. The mechanism and extent of contraction is dependent on the fibroblast phenotype, which in turn, is dependent on the state of tension in the collagen matrix. Physical loading caused by cell-generated tension or by externally applied tension regulates the release of transforming growth factor beta (TGF-β), as well as the activation of matrix-stored form of latent TGF-β. This multifunctional cytokine belongs to the TGF-β superfamily that includes three different isoforms, known to induce alpha smooth muscle actin (α-SMA) formation and myofibroblast differentiation and has been implicated in collagen synthesis [51, 52].

10
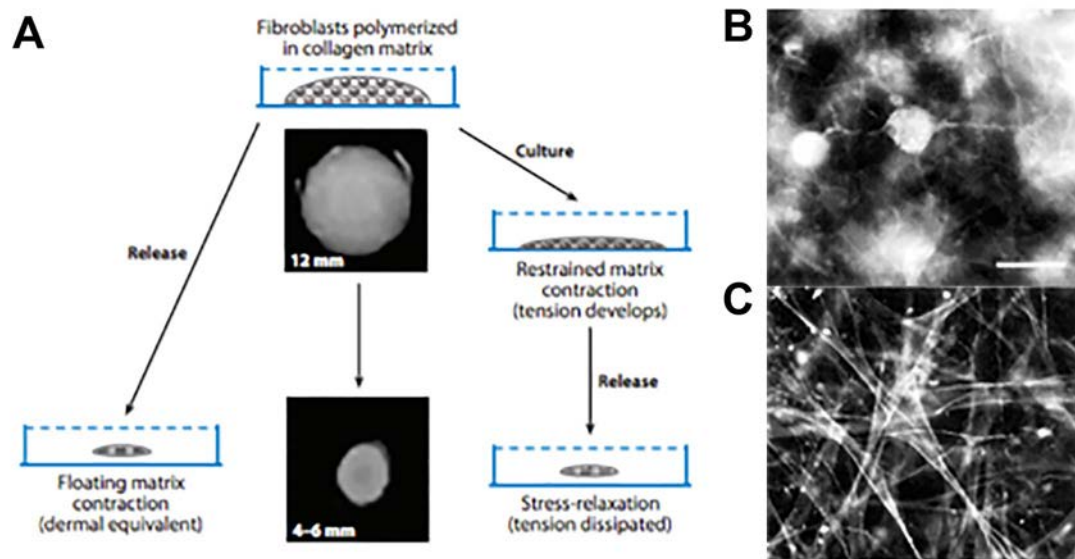
Figure 2. Fibroblast-seeded collagen models A) Fibroblast-seeded collagen gel-based models used extensively to model the effects of endogenous tension on fibroblast behavior, through the application of attached or released boundary conditions. [53] B) Fibroblasts cultured within free-floating collagen gels exhibit a rounded morphology and diminished actin stress fiber formation due to the lack of isometric tension. C) Fibroblasts seeded within attached gel achieve isometric tension and exhibit an elongated morphology that is maintained through the development of a dense, actin-rich cytoskeletal network [48].

The amount of stress that develops within the gel will be affected by the physical boundary conditions imposed on the gel, as well as its geometry. These mechanical relationships were studied in detail by Grinnell *et al.* using fibroblast-seeded three-dimensional collagen gels maintained under fixed boundary conditions (i.e. attached) or under free boundary conditions (i.e. released or free-floating) (Fig. 2). The development of such models lead to identifying the importance of the mechanical environment of the matrix on fibroblast isoform and function [47].

11

1.5.1. Floating matrix contraction

This model consists of a cell-seeded gel released upon polymerization. In this type of model, fibroblasts present few actin stress fibers and focal adhesions. Two types of growth factors stimulate cell-driven matrix compaction and reorganization within this low tensile state: platelet-derived growth factor (PDGF) and lysophosphatidic acid (LPA), involving PAK1 and Rho effector mDia1 [39]. Fibroblasts in this environment assume a dendritic morphology, which allows them to compact the gel through migration, in a process described as cell "ruffling or "hand over hand" [54]. This type of compaction can be compared to attempting to walk on a rug with very low friction. If the rug is not attached to the floor, traction created by walking will cause the rug to ruffle while the person remains in the same position. Given the absence of boundaries, cells migrating through a floating gel cause matrix ruffling which results in area reduction and increased collagen density.

1.5.2. Restrained matrix contraction

The contractile activity of fibroblasts cultured within attached collagen gels is resisted by the fixed boundaries. This resistance to deformation causes an increase in the state of tension within the gel that initiates a mechanical feedback loop that further increases cell contractile activity by stimulating actin stress fiber formation. Under this state of isometric tension, fibroblasts are characterized by an extended, bipolar morphology, reinforced by prominent actin stress fibers (Fig. 2B).

1.5.3. Stress relaxation (released gel)

Fibroblasts seeded in restrained gels develop isometric tension. A sudden change in global tension such as that caused by the release of these cell-inhabited, restrained collagen gels generates significant initial contraction due to recoil, similar to what occurs during a "tug of war". This stress-relaxation causes the disruption of stress fibers, the release of focal adhesions, as well as morphological and behavioral changes in the cells. Upon the disruption of isometric tension, cells are rendered quiescent and sometimes apoptotic due to decreased signaling through the extracellular signal-regulated kinase (ERK) pathway [47, 55]. Fibroblasts under these conditions exhibit a collapsed morphology (Fig. 2C), and reduce their contractile and synthetic activity [48].

These *in vitro* models have provided important insights on the mechanisms that govern fibroblast-guided remodeling of soft connective tissue during wound healing. The fibrin clot that acts as a provisional matrix during wound healing is estimated to be relatively compliant, with a Young's Modulus of approximately 10-1000 Pa [56]. Fibroblasts that are cultured *in vitro*, in three dimensional collagen gels with a similar compliance lack stress fibers and complex focal adhesions. As fibroblasts migrate into the wound bed and initiate wound contracture and granulation tissue formation, the stiffness of the wound bed begins to increase, and cells develop stress fibers and focal adhesions, These changes in stiffness initiate fibroblast differentiation into a proto-myofibroblast phenotype [57]. As proto-myofibroblasts align along the axis of tension, they regulate and maintain the level of stress inside of the substrate. Maintenance of the proto-myofibroblast phenotype depends on a constant feed-back loop between cell-derived tension and extracellular tension. Once the proto-myofibroblast is established it

13

can be stimulated to further differentiate into an α-SMA expressing differentiated-myofibroblast. Studies have shown that stimulus from autocrine production of TGF-β1 induces the expression of α-SMA and enhances the formation of bundles of stress fibers and fibronexus complexes [58]. The characteristics that define the morphology and behavior of each fibroblast phenotype are detailed inF.

Fibroblast differentiation is not limited to biochemical influences alone. Studies using collagen gel models bound to external constraints have highlighted the importance of global tension and increased matrix stiffness on the development of the myofibroblast. In the absence of stress, fibroblasts are unable to differentiate despite the presence of contraction agonists [4].

Table 1. Features of Fibroblast-myofibroblast Differentiation.

Phenotype	Features	In Vivo	In Vitro Models
Fibroblast	• Stellate morphology. • Focal adhesions with ECM.	Normal, healthy connective tissue	• Low-tension and low-stiffness matrices. • Free-floating gels.
Proto-myofibroblast	• Bipolar morphology • Stress fibers that express cytoplasmic actin.	• Normal connective tissue. • Early granulation tissue.	• Medium stiffness and tension substrates.
Differentiated myofibroblast	• Extended, bipolar morphology. • Stress fibers expressing α-SMA. • Fibronexus junctions.	• Late contracting granulation tissue. • Fibrocontractive diseases.	• Medium stiffness substrates in presence of TGF-β. • High stiffness and high-tension substrates. • Attached matrices

14

Mechanical stimulation of myofibroblast differentiation involves the activation of a number of pathways that communicate and translate mechanical cues between the cell and the ECM. The Rho/ROCK pathway is a mechanotransduction pathway that controls actin stress fiber formation and cell contractility through the phosphorylation of myosin light chain (MLC). This pathway is described in greater detail in the following section.

1.5.4. Fibroblast Mechanosensitivity and the Rho/ROCK Pathway

RhoA is a small GTPase that directs the assembly and stabilization of the actin cytoskeleton. Its downstream effectors play two important roles in enabling cell ability to exert forces, controlling actin polymerization, assembly and stabilization, and controlling contractility through activation of myosin light chain (MLC). Rho interacts with integrins and is activated by TGF-beta and mechanical force. Rho-associated kinases (ROCKs) are downstream targets and effectors of RhoA that become activated upon binding of the small GTPase (Fig. 3). In mammalian cells, ROCKs consist of two isoforms: ROCK1, and ROCK2. In their activated form, ROCKs become essential regulators of cell force generation through deactivation of the mysosin binding site of myosin phosphatase (MYPT) and direct phosphorylation of myosin light chain (MLC) at Ser19. Through direct phosphorylation of LIM-kinase, the ROCK1 isoform controls cofilin activity, enhancing actin filament stabilization [59]. ROCKs can maintain stress fibers through their ability to increase contractility through MLC phosphorylation and by stabilizing actin filaments through its activity on LIMK, and cofilin. ROCK also plays an important role in myofibroblast differentiation in response to TFG-β1 stimulation and several

15

studies have demonstrated its importance in controlling collagen synthesis [60]. ROCKs have been found to be at the center of a number of cardiovascular and fibrocontractive diseases due to their role in increasing cell contractility and ECM production [60-62].
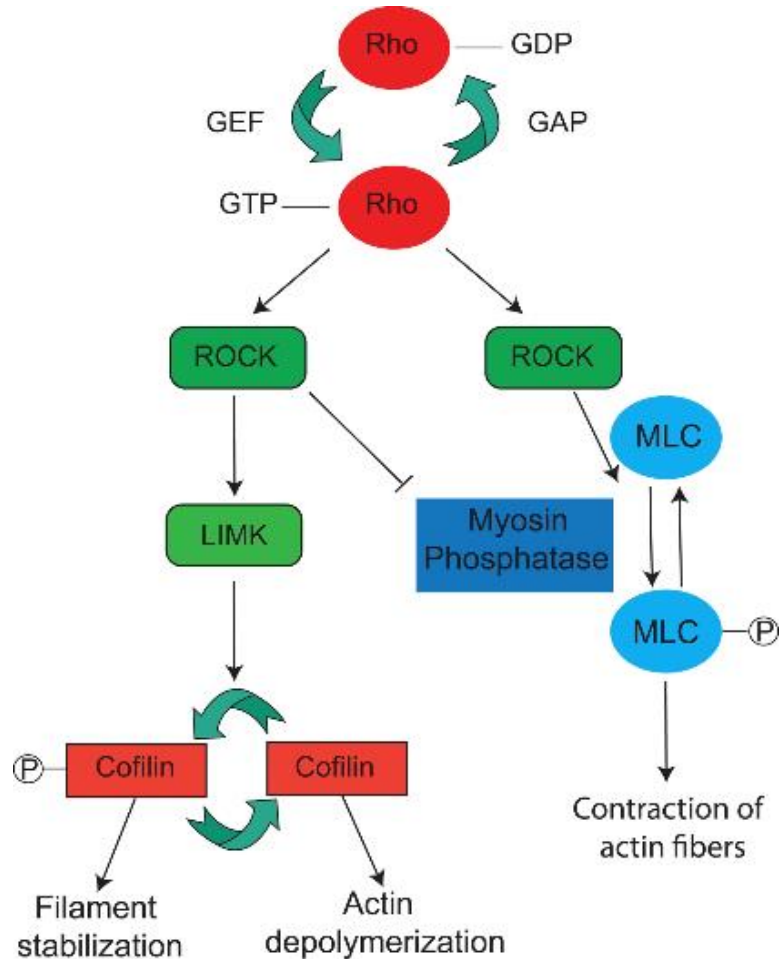
Figure 3. The Rho/ROCK mechanotransduction pathway.

Regulation of cell responses to exogenous stimulus often depends on the dynamic and synergistic activity of more than one pathway. MLC phosphorylation is regulated by a balance between two enzymatic activities: MLC kinases and myosin phosphatase. While ROCKs mainly prevent dephosphorylation of MLC and have the capacity to directly phosphorylate MLC, myosin light chain kinase (MLCK), regulated by

Ca^{2+}/calmodulin, is transiently expressed in response to mechanical stress, and its main known function involves phosphorylation of MLC to regulate the assembly of stress fibers at the cell periphery [63]. As so, the Rho/ROCK pathway plays an important role in fibroblast differentiation into the myofibroblast phenotype, and therefore, is essential to processes that involve tissue maintenance, regeneration, and remodeling. Key components of this pathway are the target of one of the studies presented in this thesis.

1.6. Objectives

The mechanical feedback loop that exists between cell contractility and the properties that define the mechanical environment of connective tissues plays an important role in the maintenance, regeneration and function of tissue. Cells sense mechanical signals and respond by initiating a number of signaling pathways that convert physical signals into chemical signals. This mechanotransduction process allows cells to alter their behavior in response to physical cues. It is a fact that the structural and compositional stability of the ECM is vital in the progression of a number of physiological processes that result in maintaining function of tissue. But, what defines a healthy mechanical environment, how is it regulated, and how can it be altered to manipulate cell behavior are questions that still remain unanswered.

This work involved the development of *in vitro* experimental models used to capture the effects of the dynamic reciprocity between fibroblasts and the mechanical environment on tissue remodeling, and regeneration. These models were to be used to qualitatively and quantitatively assess the microstructural and compositional changes as well as alterations in fibroblast behavior in response to manipulation of the mechanical

17

environment of the cell. The following objectives were defined in order to begin to address such questions:

Objective 1: Set up a system that allows for the assessment of the effects of boundary conditions on short-term structural reorganization of a fibrin gel using human dermal fibroblast explants.

Objective 2: Use the same system to assess the effects of boundary conditions and short-term structural reorganization of a fibrin gel by human dermal fibroblasts on long-term compositional reorganization.

Objective 3: Use local mechanical stimulation to restore function of aged human dermal fibroblast activity through the injection of cross-linked hyaluronic acid into collagen-based dermal equivalent models.

18

CHAPTER 2: DEVELOPING AN EXPERIMENTAL MODEL TO STUDY THE EFFECT OF MULTI-SCALE MECHANICAL INTERACTIONS ON STRUCTURAL REORGANIZATION OF TISSUE

The contents of this chapter can be found in the following publication:

De Jesus, Aribet M., Maziar Aghvami, and Edward A. Sander. "A combined in vitro imaging and multi-scale modeling system for studying the role of cell matrix interactions in cutaneous wound healing." PloS ONE11.2 (2016): e0148254.

2.1. Introduction

Cutaneous wound healing involves the coordination of platelet degranulation, provisional fibrin matrix formation, cellular infiltration, and extracellular matrix (ECM) remodeling, and continues for a period after skin integrity and homeostasis is restored [18]. The repaired tissue formed is fibrotic (i.e., a scar) and lacks the organization and full functionality of normal skin. Additionally, if imbalances between ECM synthesis and degradation arise during the remodeling process, it can lead to abnormal scars, such as hypertrophic scars, that are characterized by excessive fibrosis. These scars can result in disfigurement, distress, discomfort/pain, and permanent loss of function from contracture [64-66]. Abnormal scarring is a major clinical problem, with estimated U.S. annual treatment costs in the billions of dollars [67, 68].

A number of clinical treatments have been explored to manage these scars, including surgical excision, corticosteroid injection, silicone gel sheeting, pressure therapy, and laser therapy [65]. For many of these treatments, the mechanisms underlying a reduction in fibrosis (as well as the range in patient healing response) are not clear.

19

There is, however, increasing evidence supporting the notion that the improvement in scar formation observed with these treatments has a mechanical basis, particularly as fibrosis is believed to be a response to tension [68-70], and these treatments may all act to reduce tension during healing [71-73]. The idea that mechanical environment plays an important role in scar management is also consistent with the surgical practice of making incisions in the skin along Langer's lines to reduce tension and scarring at the wound site. Furthermore, wounds formed in high-tension areas, such as the shoulder and scapula, are more prone to exuberant fibrosis than low-tension areas, such as the scalp and lower legs [69].

In vitro experiments have also demonstrated that mechanical forces modulate the activity of skin-derived cells [34, 74-76], including fibroblast gene expression for inflammatory mediators, growth factors, and ECM proteins [29, 77-79]. Additionally, *in vivo* studies on mice, pigs, and humans have shown that altering skin stress dramatically regulates the extent of scarring [80-82]. Recently, Gurtner *et al*. found that stress shielding abdominal incisions produced significant improvements in scarring compared to within-patient controls [81, 83]. Other important mechanisms are also involved (e.g. oxygen tension, inflammatory agents, biochemical and genetic factors) but clearly there are substantial data supporting a central role for mechanical environment.

Multi-scale mechanical interactions are an important component of this mechanical environment. They are dynamic and reciprocal scale-spanning physical interactions between tissues, cells, and ECM. In the wound site these interactions initially involve fibrin and the structure of the clot, and then gradually change as fibrin is replaced with new ECM, like load-bearing collagen. When loads and constraints are applied at the

20

tissue-level of the skin, they are transmitted down into the provisional matrix and ECM, where they can alter the local environment and affect cell activity. In addition, the constituent fibroblasts themselves also exert traction forces on the ECM in an attempt to close the wound margins and to reach a homeostatic level of ECM tension. Combined, these interactions contribute in an integrated and cooperative manner to produce a global pattern of ECM remodeling [80, 84-86], including during wound healing and scar formation [80, 87].

It is, however, difficult to evaluate what distinguishing parameters from the complex milieu of components involved result in fibrosis, or what measures should be taken to minimize scar formation. Although it is clear that reducing tension at the wound site can reduce scar formation, it is not clear what mechanobiological mechanisms mediate this process or how it can be optimized. With many complicated phenomena operating at multiple scales and governed to varying degrees by the properties of the ECM, mechanical models become a necessary tool for unraveling the relationships between individual ECM and cellular components and the aggregate remodeling response and properties of the healing tissue. As such, these models will be important for evaluating parameters unique to a patient and identifying an optimized strategy for reducing scar.

In addition, while much of the focus on mechanical environment has rightly been placed on the levels of tension at the wound site, a second component involved in multi-scale mechanical interactions that is potentially important is the initial configuration of the clot. This initial structure may control both how macroscopic forces are distributed through the microstructure (and thus the levels of force an individual cell will experience)

21

and how replacement ECM (e.g. collagen, elastin) will be organized; organization will be controlled partly through cell contact guidance with the fibrin matrix and steric constraints on how ECM can be laid down and assembled [88-90]. Recent work suggests that the remodeling response in an *in vitro* setting is strongly influenced by multi-scale mechanical interactions that depend in part on the initial fibrin alignment pattern and the distribution of cell-generated internal forces [86]. Should this proposition hold true, knowing how and when one should intervene (e.g. mechanically or chemically) to alter this pattern and control the remodeling process will be important for optimizing treatments to reduce scar. In strategies that involve changing the mechanical environment of the wound site (e.g. stress shielding sheets, shape memory sutures, sutures with elastic gradients, and adhesives), many important variables are not optimally defined. For example, it is not clear if there is an optimal window in time for stress shielding the wound site, how much or what kind of force should be applied, whether the amount of force should change over time, or how these parameters should change with anatomical site, wound size, and shape.

Here, I report on the experimental work done to develop a system for understanding how multi-scale mechanical interactions regulate wound healing and scar formation so that these sorts of questions can be answered. The experimental data obtained from this *in vitro* dermal fibroblast explant/fibrin gel culture system was later combined with a fiber-based multi-scale computation model, the details of which will not be presented in this dissertation. Experimentally, small, but significant, differences in short-term structural remodeling of fibrin gels by the fibroblasts in response to *Fixed* or *Free* gel boundaries were observed that could impact long-term remodeling.

22

2.2. Experimental Methods

2.2.1. Fibrin Gel Preparation

Fibrin gels were prepared as described previously [86, 91]. Briefly, 0.222 mL of bovine fibrinogen at a concentration of 30.6 mg/mL (Sigma Aldrich, St. Louis, MO) was diluted in 0.444 mL of 20 mM HEPES buffer and combined with 0.167 mL of a solution of bovine thrombin (Sigma Aldrich, St. Louis, MO), and $CaCl_2$ to produce 6.8 mg/mL fibrin gels. Microspheres measuring 4 um in diameter (Life Technologies, Grand Island, NY, Catalog No. F8858) were also added at a concentration of 5 million microspheres/mL and homogeneously distributed in the solution before gelation commenced. The solution was then cast into square polydimethylsiloxane (PDMS) (Dow Corning, Midland, MI) molds measuring 8 mm x 8 mm x 1 mm (length, width, depth). The molds were attached with silicone grease (Dow Corning, Midland, MI) to either the No. 0 coverglass of 35 mm glass bottom Petri-dishes (MatTek Corp., Ashland, MA, Catalog No. P35G-0-20-C) or the viewport glass of a microscope-mounted bioreactor (described below). The solution gelled quickly in the mold and remained at room temperature for approximately 30 minutes until the explants were added. This process produced gels with an estimated average thickness of 798 μm ± 139 μm. This measurement was calculated based on multiplying the optical path length (i.e., the difference between the focal plane of the glass surface and focal plane of the gel surface) and the refractive index of the gel, which we took as the refractive index of water, n = 1.3.

2.2.2. Cell Culture and Explant Preparation

Immortalized TERT-human dermal fibroblasts [92] were cultured in high glucose Dulbecco's Modified Eagle Medium (DMEM) (Life Technologies, Grand Island, NY) supplemented with 10% fetal bovine serum, 1% penicillin-streptomycin, and 0.1% amphotericin B. Fibroblasts were grown to 80% confluency in T-75 tissue-culture flasks maintained in a 37 °C humidified incubator supplied with 5% CO_2 and 95% air. Explants, each consisting of approximately 6,000 cells, were produced by trypsinizing, pelleting, and resuspending the fibroblasts in a low retention 1.5 mL conical tube at a concentration of $2x10^7$ cells/mL, and pipetting 0.3 µL of cell suspension onto the surface of a fibrin gel. Three explants were positioned at the vertices of a triangle with each side measuring approximately 2 mm from explant centroid-to-centroid (c.f., [91]). The cells were then allowed to settle and attach to the fibrin gel for approximately 2 hours before fresh medium with 10 µg/mL aprotinin was added in order to limit the potential for serine protease induced fibrin degradation [93].

2.2.3. Gel Boundary Conditions

In order to study the effects of mechanical constraints and multi-scale mechanical interactions on explant restructuring of the gel, two in-plane boundary conditions, designated as either *Fixed* or *Free*, were examined (Fig. 3). For *Fixed* gels, the sides of the gel remained attached to the PDMS mold. For *Free* gels, the sides of gel were carefully separated from the edges of the mold with a sterile 30G x ½ inch needle (BD Biosciences, San Jose, CA). The gel bottoms remained attached to the glass for both cases.
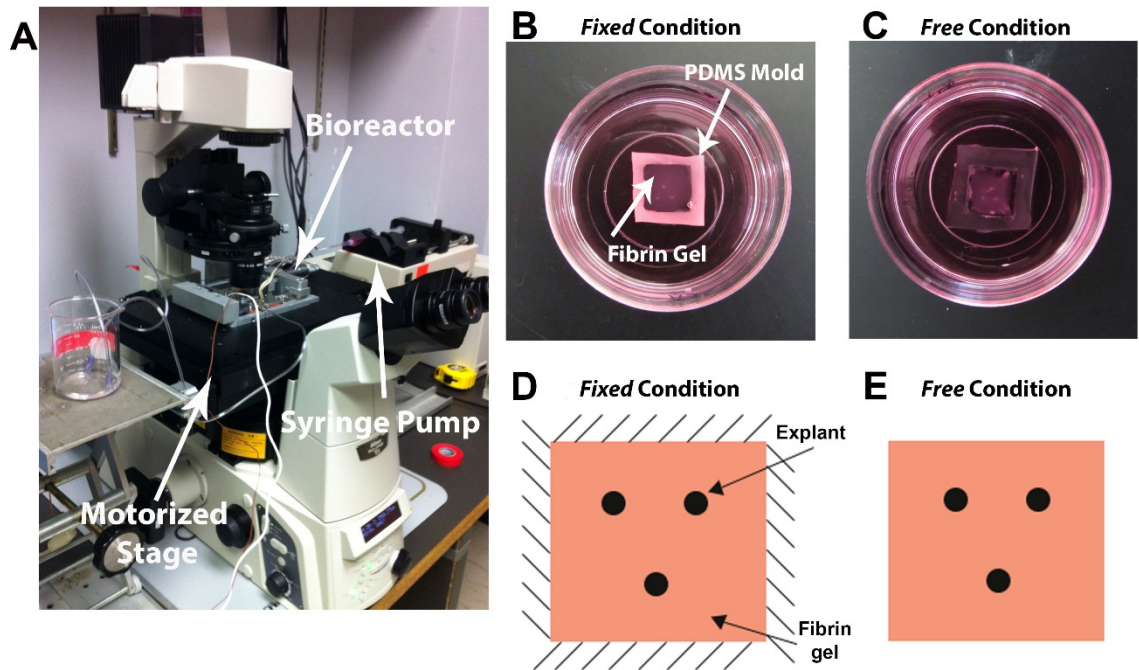
Figure 4. Experimental setup. (A) Samples were prepared in an ADMET BioTense bioreactor and placed onto the automated stage of a Nikon Eclipse TI. Fresh CO_2-treated DMEM was perfused through the chamber of the bioreactor over the duration of the experiment. (B,D) *Fixed* fibrin gels were polymerized in a PDMS mold and remained attached over the duration of the experiment. (C,E) After polymerization, lateral boundaries in *Free* fibrin gels were released, while the bottom boundary of the gel remained attached to the glass-bottom Petri dish.

2.2.4. Experimental Setup and Imaging

Four samples were prepared for both *Fixed* and *Free* boundary conditions, with each gel cast into its own separate 35 mm glass bottom Petri dish. These samples were transferred from the incubator to the microscope and imaged at t = 0 hours, 12 hours, and 24 hours in order to provide an indication of experiment repeatability, which was assessed by monitoring gross structural changes in the gel, such as the changes in explant area and explant centroid-to-centroid distance, and to confirm that suitable environmental conditions were maintained in the bioreactor.

A more detailed view of structural changes in the gels over 24 hours was also obtained by taking time-lapse images of one *Fixed* and one *Free* gel (each gel was imaged separately) in a temperature-controlled, microscope-mounted BioTense Perfusion Bioreactor (ADMET, Norwood, MA), which was maintained at 37°C (Fig. 3A, B). Fresh incubator-conditioned medium saturated with 5% CO_2 was perfused through the bioreactor via a syringe pump at a rate of 0.015 mL/min for the duration of the experiment in order to maintain a pH of 7.4. Outflow medium from the bioreactor was collected and periodically tested with a Combination pH Microelectrode (Cole Parmer, Vernon Hills, IL) to confirm that a neutral pH was maintained. All images were obtained on a Nikon Eclipse TI inverted microscope equipped with a DS-Qi1 Nikon CCD camera and a ProScan II motorized stage. Gels were imaged with a CFI Plan Apo 10x DIC objective. During imaging 36 individual frames were acquired and tiled together. All images were saved as 16-bit jpg2 images and exported as uncompressed 8-bit tiff images for analysis.
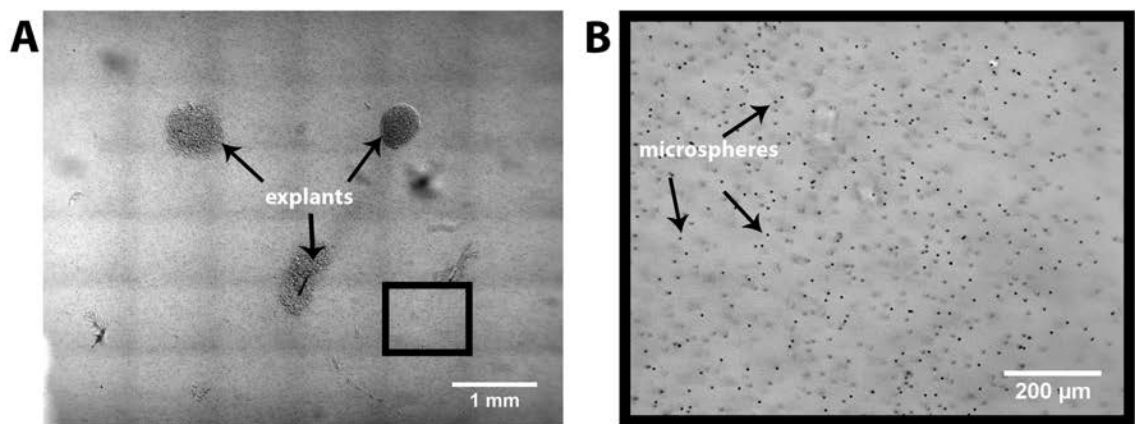
Figure 5. Experimental and multiscale models. (A) TERT-Fibroblast explants were seeded onto the polymerized fibrin gel in a triangular configuration. (B) Microspheres 4 μm in diameter were embedded within the fibrin gel and their movement and displacement was tracked using a custom particle tracking algorithm based on image correlation.

26

Fiber alignment was not clearly visible in these gels with DIC imaging due to light scattering from the microspheres and the thickness of the gel. As a result, fiber alignment was obtained at 24 hours by imaging a set of identical gels (minus the microspheres) fixed with 4% paraformaldehyde. These gels were imaged in reflection mode [94, 95] using a Leica TCS SP5 multi-photon confocal microscope with a HeNe 543 nm laser and a 20x objective (Roy J. Carver Center for Imaging, University of Iowa). Cell nuclei were labeled with Hoescht 33342 (Life Technologies, Grand Island, NY). Images were acquired at adjacent locations as a z-stack consisting of 40 images spaced 4 μm apart through the thickness. All images were saved as 8-bit tiff images.

2.2.5. Image Analysis

2.2.5.1. Changes in Explant Morphological Changes and Cell Migration

Images acquired at t = 0 hours, t = 12 hours, and t = 24 hours were analyzed with ImageJ (NIH, Bethesda, MA) in order to measure morphological changes in explant area and centroid-to-centroid distance. Explants borders were delineated with the free-hand drawing tool in order to calculate the area and centroid of each explant. Cells that migrated past the periphery of each explant were not considered as part of the explant area. The percent change in explant area was calculated by normalizing the explant area at t = 12 hours and t = 24 hours with the area at t = 0 hours. Similarly, the centroid-to-centroid distance between explants was normalized with the corresponding distance between explants at t = 0 hours.

27

Cell migration distance, *CMD*, out of the explant was also assessed from images acquired at 24 hours. Regional distinctions were made between cells traveling axially between explants versus those moving towards the gel boundaries. This distinction between axial and non-axial regions was made in order to determine if fiber alignment generated between explants resulted in enhanced cell migration, since fiber alignment is known to influence cell migration patterns [88, 96, 97]. In each region, radial lines were drawn outward from the explant boundary, through the axis of the migrating cell body, and up to the leading edge of the migrating cells. The average line length and standard deviation was then taken as the *CMD* for the region.

2.2.5.2. Microsphere Displacements

For each of the time-lapse images acquired, the position of a subset of microspheres (17 ± 3 microspheres/image) was tracked during the experiment using a custom semi-automated MATLAB algorithm[34, 98]. The algorithm, which is based on normalized cross-correlation between successive images, was then applied to each individual image sequence. First, a set of clearly visible microspheres was selected in the initial image of the time-lapse sequence and the instantaneous and cumulative displacements of each microsphere were determined and updated via the template-matching algorithm. Similarly, the instantaneous and period average rates of microsphere displacement were calculated, respectively, by either dividing the difference in microsphere displacement between successive frames by the time between image acquisitions (i.e., 15 minutes) or by dividing the difference in the cumulative displacement from 0 to 6 hours, 6 to 12 hours, 12 to 18 hours, and 18 to 24 hours over the

28

time in minutes (i.e., 360 minutes). Note that for the *Free* gel, microspheres in the images making up the far right column were not tracked because the images were not in focus.

During the experiment cell compaction of the gel produced large deformations in the plane and through the thickness of the gel. To compensate, the focal plane was periodically readjusted over the course of the experiment to keep the microspheres in focus. The accuracy of the calculated displacements was visually confirmed frame-by-frame by plotting the displacement vectors on the tracked microspheres in the image. The microsphere displacements associated with each tiled image were further grouped into one of four spatially distinct regions (Fig. 5) to facilitate identifying regional differences in remodeling. These regions include the non-axial region above the explants (Region 1), the lateral non-axial regions (Region 2), the axial regions and the area in the center of the explant (Region 3), and the non-axial region below the explants (Region 4).

2.2.5.3. Fibrin Fiber Alignment

Fiber alignment at 24 hours was measured in the pair of paraformaldehyde-fixed gels using a custom MATLAB algorithm based on the use of Fast Fourier Transforms [99]. The algorithm returns a fiber orientation distribution that is converted to an orientation tensor with major and minor principal directions of alignment. The strength of fiber alignment, α, in the image is then calculated as $\alpha = 1 - \omega_1/\omega_2$, where ω_1 and ω_1 are the eigenvalues of the orientation tensor and $\omega_1 < \omega_2$. α is bounded by values of 0 and 1, which correspond to isotropic and completely aligned fiber distributions in the image.
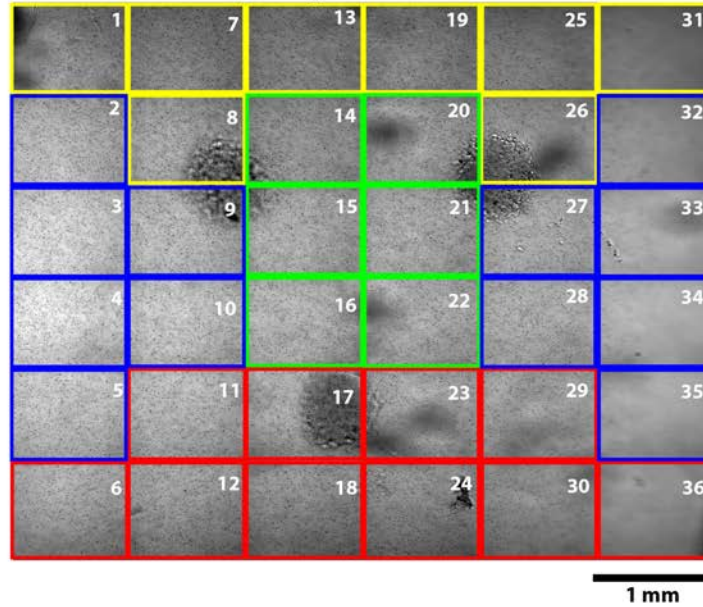
Figure 6. Tiles analyzed for bead displacements. Individual tiles stitched to generate a larger image of the fibrin gel surface were analyzed individually to quantify microsphere displacements in each condition. Tiles are color coded to indicate the region of the gel to which they correspond. Tiles surrounded by a yellow box correspond to Region 1, tiles in blue correspond to Region 2, tiles in green correspond to Region 3, and tiles in red correspond to Region 4.

2.5. Results

2.5.1. Explant Morphological Changes

In all experiments, initially rounded fibroblasts in the explants rapidly reorganized the shape of the explants during the first 6 hours. Over the next 18 hours, the dense mass of cells in the explants continued to shrink in size while individual fibroblasts on the explant periphery began to assume a spindle-shaped morphology and migrate outward from the explant boundary into the fibrin matrix. Small differences in explant morphology were evident between *Free* and *Fixed* gels (Fig. 6, 7). Average initial explant area decreased from 0.47 mm^2 ± 0.01 mm^2 at $t = 0$ hours to 0.31 mm^2 ± 0.07 mm^2 at $t = 24$ hours in *Free* gels, and from 0.46 mm^2 ± 0.08 mm^2 at $t = 0$ hours to 0.33 mm^2 ± 0.12

30

mm^2 at $t = 24$ hours in *Fixed* gels. These values correspond to explant areas that were 66.6% ± 17.9% and 70.9% ± 19.9% of the initial explant areas, respectively. Although explant area decreased more in *Free* gels compared to *Fixed* gels, the difference was not statistically significant.

The explants also moved closer to each other in a manner dependent on the boundary conditions. The average normalized centroid-to-centroid distance between explants after 24 hours was slightly lower (but significantly so, $p < 0.05$) in *Free* gels (0.95 ± 0.02) compared to *Fixed* gels (0.98 ± 0.02). On average, the explants on *Free* gels moved approximately 100 µm closer together, with the average centroid-to-centroid distance decreasing from 2.16 mm ± 0.20 mm at $t = 0$ hours to 2.03 mm ± 0.20 mm at $t = 24$ hours. In contrast, explants on *Fixed* gels remained separated by essentially the same distance (1.96 mm ± 0.24 mm at $t = 0$ hours and 1.95 ± 0.18 mm at $t = 24$ hours).

Small regional differences in fibroblast migration out of the explants were also observed. At $t = 24$ hours, *CMD* values were significantly higher ($p < 0.05$) for cells migrating in axial regions between explants than for cells migrating in non-axial regions in both *Fixed* (291 µm ± 95 µm and 252 µm ± 79 µm) and *Free* gels (268 ± 94 µm and 206 ± 61 µm), respectively. Significant differences ($p < 0.05$) in *CMD* between *Fixed* and *Free* gels were only found for fibroblasts located in the non-axial regions.

2.5.2. Experiments: Fibrin Structural Reorganization

In addition to changes in explant morphology, substantial structural reorganization in the gels was observed and quantified over the duration of the experiment via the displacement of embedded 4 µm diameter microspheres. Long-range

31

communication of cell traction forces between explants, the ECM, and the gel boundaries produced significant spatial and temporal differences in microsphere displacements between *Free* and *Fixed* gels (Fig. 6, 7). Overall in-plane average microsphere displacements (Table 1) were significantly affected by the boundary conditions ($p < 0.001$), with substantially larger average cumulative displacements occurring in the *Free* gel.

Significant regional differences in the microsphere displacements were also observed (Fig. 8A). In both the *Free* and *Fixed* gel, microsphere displacements were statistically no different in the axial regions (Region 3) between explants, except at 24 hours. The average cumulative microsphere displacements in the non-axial regions (Regions 1, 2, and 4) were, however, significantly greater for the *Free* gel than for the *Fixed* gel at all time points. In the *Fixed* gel, displacements in the non-axial regions were essentially the same or slightly lower than in Region 3. A more detailed view of the microsphere displacements from Region 1 and Region 4 is presented in Figure 6. It shows that the cumulative microsphere displacements in both non-axial regions began to plateau noticeably after approximately 12 hours in the *Fixed* gels (Fig. 9A), whereas for the *Free*

Table 2. Overall Average Magnitude and Rate of Microsphere Displacement.

Time	Magnitude (µm)		Time	Rate of Displacement (µm/min)	
	Fixed	*Free*		*Fixed*	*Free*
6 hrs	36.6 ± 12.7	43.6 ± 14.9	0-6 hrs	0.10 ± 0.04	0.12 ± 0.04
12 hrs	53.8 ± 19.6	70.6 ± 23.2	6-12 hrs	0.05 ± 0.02	0.07 ± 0.03
18 hrs	63.7 ± 23.5	92.2 ± 30.9	12-18 hrs	0.03 ± 0.02	0.06 ± 0.02
24 hrs	69.7 ± 25.3	105.6 ± 35.9	18-24 hrs	0.02 ± 0.01	0.04 ± 0.02

32
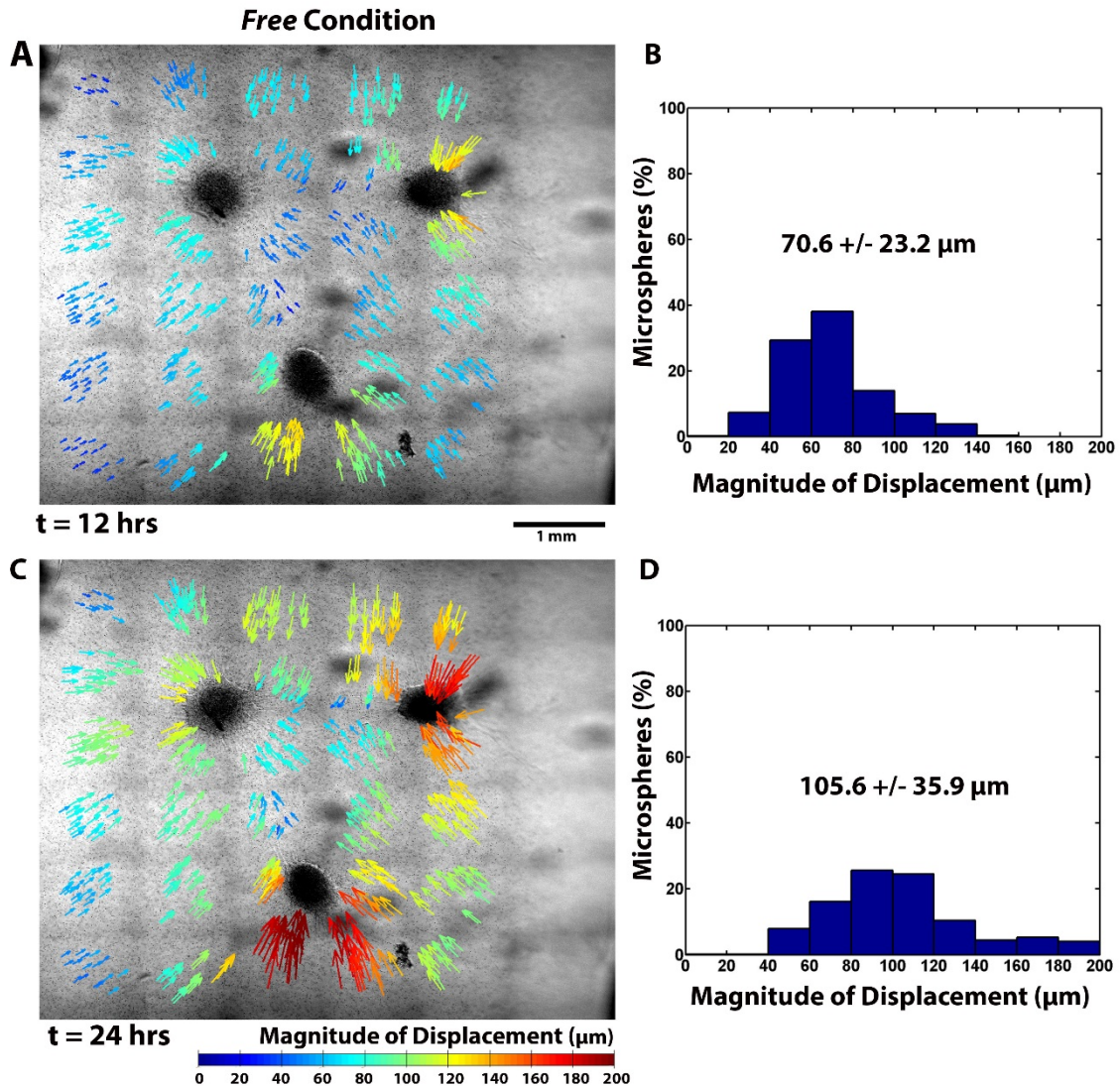
Figure 7. Microsphere displacements in a *Free* gel. Cumulative microsphere displacements at (A,B) t = 12 hours and (C,D) t = 24 are depicted spatially with color coded arrows that indicate the direction and magnitudes. Also shown are the corresponding histograms of microsphere displacement.

gel, the displacements in these same regions increased roughly linearly before beginning

to plateau later in the experiment (Fig. 9B). Microsphere displacement rates also differed

regionally (Fig. 5B). In the *Free* gel, period average rates of displacement were generally

highest in the non-axial regions of the gel.
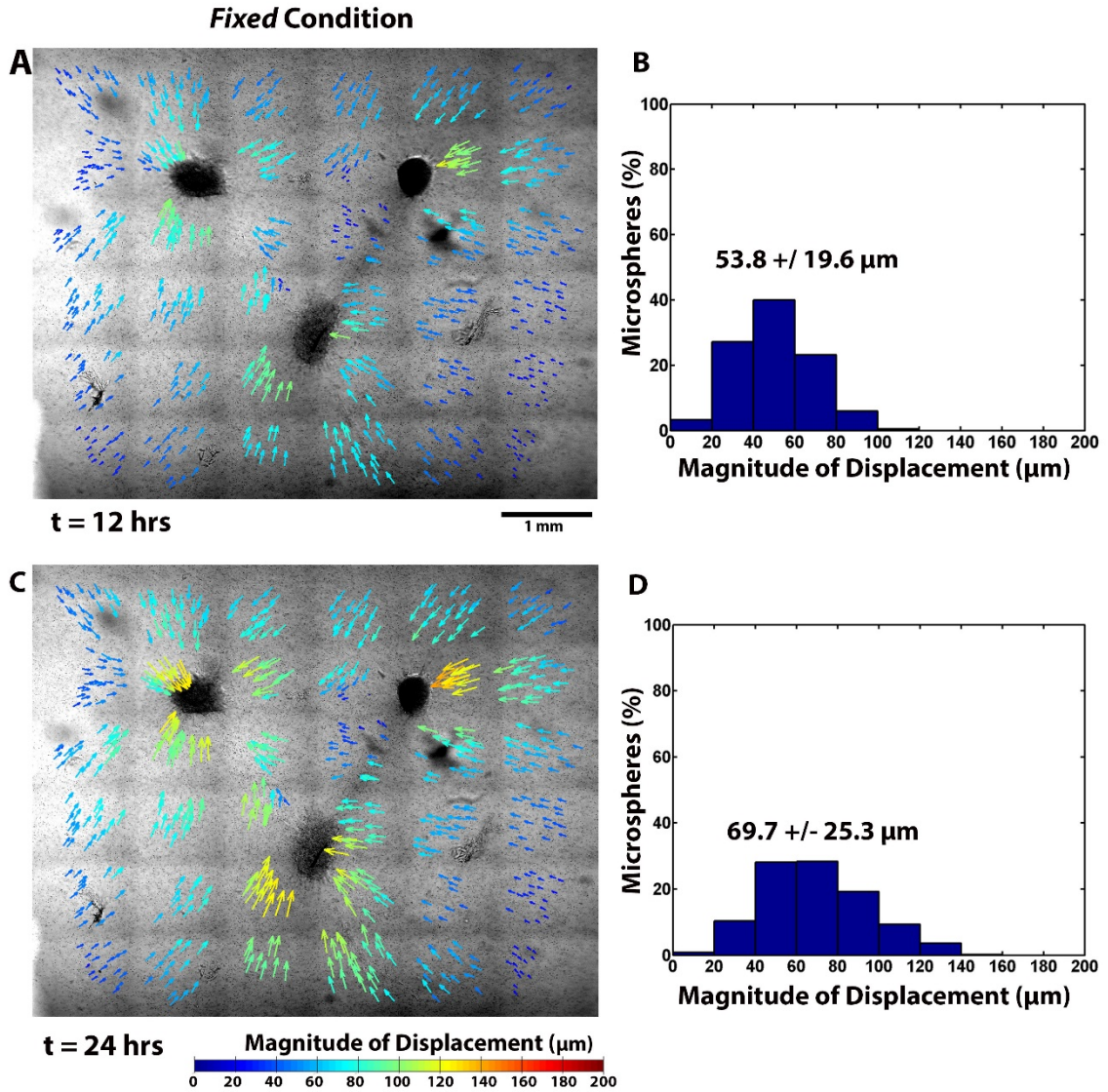
Figure 8. Microsphere displacements in a *Fixed* gel. Cumulative microsphere displacements at (A,B) t = 12 hours and (C,D) t = 24 are depicted spatially with color coded arrows that indicate the direction and magnitudes. Also shown are the corresponding histograms of microsphere displacement.

At six hours, the rates were essentially equivalent, with values of 0.13 ± 0.05 µm/min, 0.13 ± 0.03 µm/min, and 0.13 ± 0.05 µm/min in Regions 1, 2, and 4, respectively. These rates decreased appreciably to 0.08 ± 0.03 µm/min, 0.07 ± 0.02

34

μm/min, and 0.09 ± 0.03 μm/min after 12 hours, and finally to 0.04 ± 0.01 μm/min, 0.03 ± 0.01 μm/min, and 0.05   ± 0.02 μm/min after 24 hours. Period average rates of displacement in the axial region (Region 3), were considerably smaller, with rates of 0.09 ± 0.02 μm/min after six hours, 0.06 ± 0.02 μm/min after 12 hours, and 0.03 ± 0.01 μm/min after 24 hours. In the *Fixed* gel, the period average rates of displacement were generally lower and also decayed faster with time in each region compared to the *Free* gel. The exception to this trend was in Region 3, where even though the rates were lower in the *Fixed* gel, no significant difference in the period average rates between *Fixed* and *Free* gels was found.
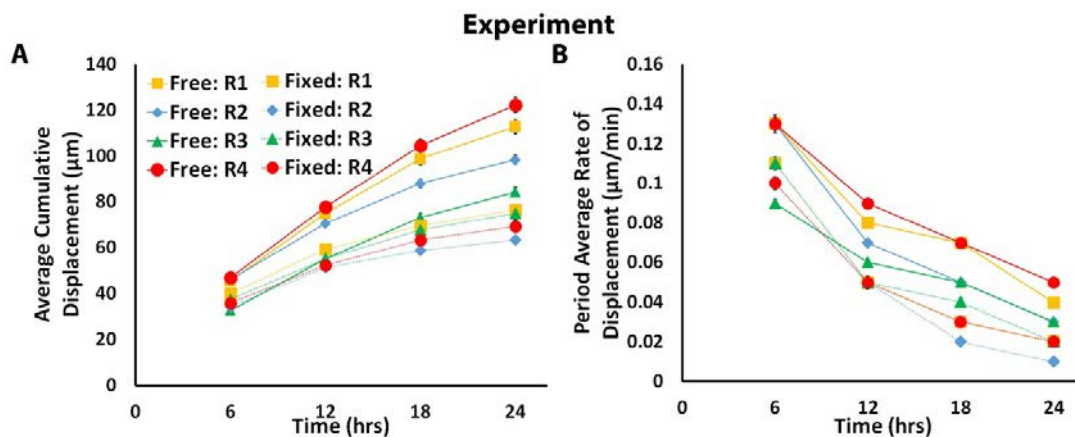
Figure 9. Comparison of regional average magnitude and period average rate of microsphere displacement for each boundary condition and between the experiment and model. (A) Average cumulative microsphere displacement and (B) period average rate of microsphere displacement in the experiment for all four regions and for each boundary condition plotted every six hours. Error bars represent the standard error of the mean.

35
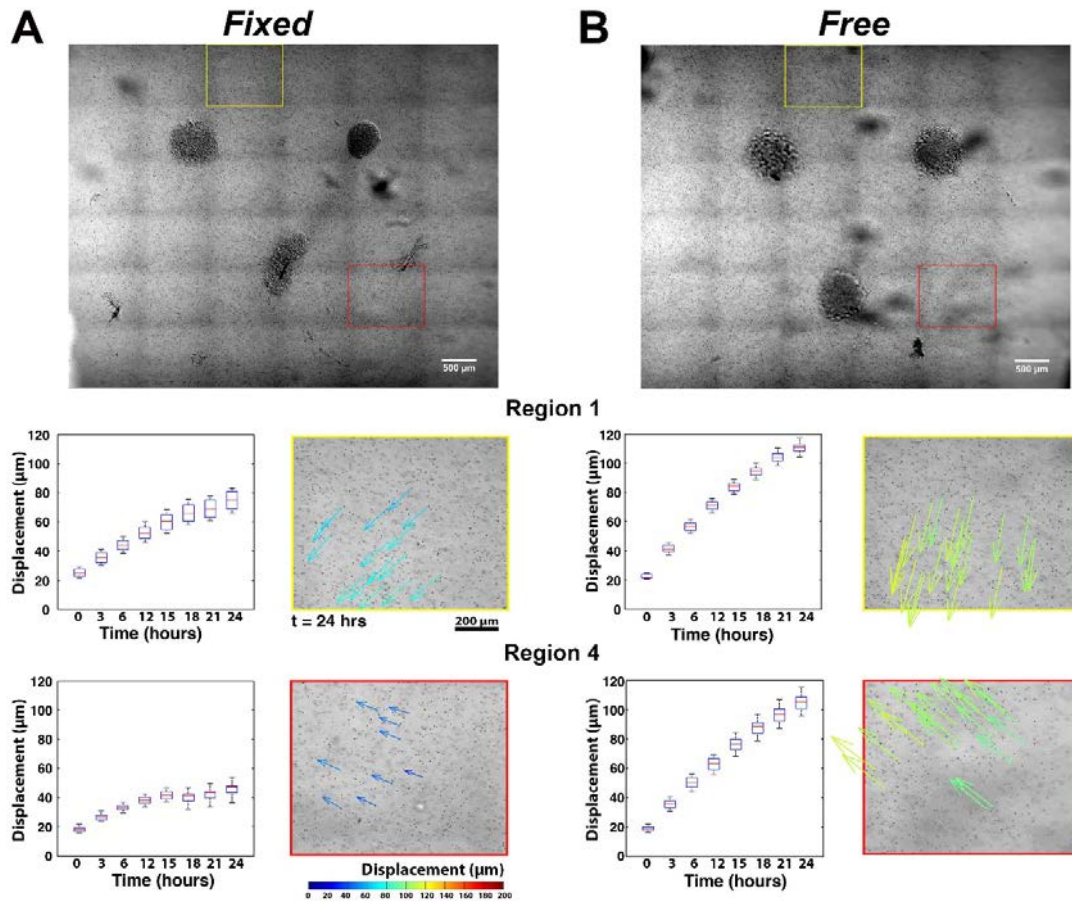
Figure 10. Comparison of regional differences in microsphere displacements. In both (A) *Fixed* and (B) *Free* gels the cumulative displacements of images associated with Region 1 (yellow box) and Region 4 (red box) at each hour are represented with box plots, where the box edges show the 25th and 75th percentiles, the median is depicted with a red line, and the whiskers indicate the full range of the data points. Color-coded arrows show the direction and magnitudes of the cumulative displacements at t = 24 hours. Microsphere displacements are directed towards either the explants or the axial regions between explants. Larger microsphere displacements occurred in the *Free* gel compared to the *Fixed* gel.

Instantaneous rates of displacement generally followed the period average rates of displacement, but were initially higher with maximum measured rates of 0.17 ± 0.06 µm/min and 0.21 ± 0.06 µm/min occurring at $t = 15$ minutes for *Free* and *Fixed* gels, respectively.

36

Fibrin fiber realignment between explants was also apparent after 24 hours in reflection mode confocal images of microsphere-free *Fixed* and *Free* gels (Fig. 10). The average strength of fiber alignment in the *Free* ($\alpha = 0.246 \pm 0.132$) and *Fixed* ($\alpha = 0.209 \pm 0.096$) gels were not significantly different. For both gels, fiber realignment was strongest in the axial regions between explants. Interestingly, strong fiber alignment did not develop equally among all three axes. Instead, one or two dominant axes of fiber alignment developed between the explants. In the *Fixed* gel, strong fiber alignment occurred between the bottom explant and the top-right explant ($\alpha = 0.456$) (Fig. 10C), and between the top two explants ($\alpha = 0.437$). In the axis that developed the strongest alignment the final centroid-to-centroid distance was 1.97 mm, which was smaller than along the other two axes (2.32 mm and 2.38 mm). In the *Free* gel, strong fiber alignment was also observed between the top-right explant and the bottom explant ($\alpha = 0.474$) (Fig. 10D). Similar to the *Fixed* gel, the centroid-to-centroid distance along this axis (2.01 mm) was shorter than the other two axes (2.11 mm and 2.70 mm). Repeat experiments (data not shown) on additional samples confirmed this asymmetrical outcome in fiber alignment, although equal alignment between all three axes was also found in some gels. This result may be due to inherit asymmetries in the positioning of the explants, the number of cells in each explant, or other factors that drive preferential remodeling and fiber alignment along some axes. For both boundary conditions, increased radial fiber alignment was also observed around the explants, with the lowest levels of alignment found in non-axial regions of the gel (Fig. 10 E, F).

37
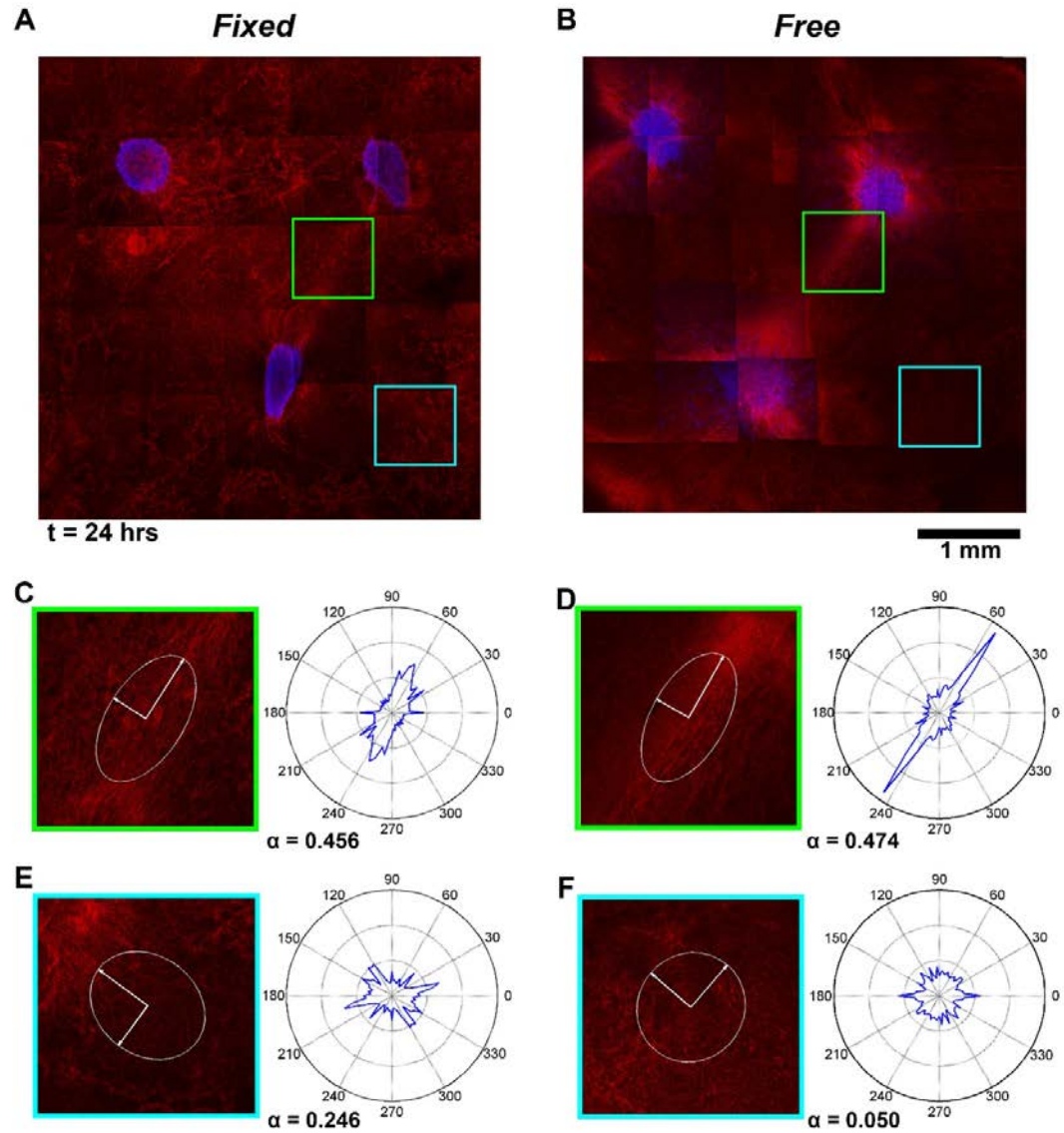
Figure 11. Fibrin fiber alignment in a *Fixed* and *Free* gel at t = 24 hours. Equivalent, microsphere free (A) *Fixed* and (B) *Free* gels were imaged with reflectance mode confocal microscopy and tiled together. Fiber orientation distributions for each image were reduced to major and minor principal directions of alignment and plotted at the center of each image as a pair of axes circumscribed by an ellipse. Highly aligned regions are more elliptical and less aligned regions are more circular. Fiber distributions for highly aligned axial regions (C, D) and less aligned, non-axial regions (E, F) are also shown.

2.6. Discussion

Tissue growth, remodeling, and repair are complex processes that are regulated in part by multi-scale mechanical interactions. To better understand how these interactions contribute to the mechanobiology of the remodeling process in the context of wound healing and scar formation, we conducted *in vitro* experiments on fibroblast-matrix interactions in fibrin gels (as an approximation of the initially formed clot) subjected to either *Free* or *Fixed* in-plane mechanical constraints. Using averaged morphological measurements from the experiments, an idealized, image-based multi-scale model was used to simulate the experiment so that the ability of the model to capture the physics of short-term structural remodeling could be evaluated.

Experimentally, we found that the explant system produced significant differences in explant morphology and fibrin gel reorganization in a manner that depended on whether the lateral edges of the gel were mechanically constrained or not. For the *Fixed* gel the average reduction in explant area and centroid-to-centroid distance was less than in the *Free* gel. Furthermore, much larger microsphere displacements and greater compaction through the thickness were observed in the *Free* gel compared to the *Fixed* gel. In addition, regional cumulative displacement patterns and rates of displacement differed in the non-axial regions (but not the axial regions) of the two gels. Taken together, these data imply that there was less "slack" (i.e., translational and rotational freedom) in the fibrin fiber networks for the *Fixed* gel, a result consistent with other studies involving the role of mechanical constraints on fibrous gels [87, 100-102]. In these studies, cooperative behavior between cell tractions and fiber reorganization resulted in anisotropic gel reorganization that proceeded in a manner that was dependent

39

on the gel geometry, gel boundary conditions, and the spatial patterning of the cells. We interpret the differences in constrained and unconstrained gels in this study as a product of multi-scale mechanical interactions that arise from such cooperative behavior. Initially, the fibroblasts pulled fibrin fibers inward to produce a dense, pericellular matrix around the explants. Distal fibers then rotated and translated inward in response to tensile forces that were propagate through the fiber network. The extent of translation and rotation depended on the existence and distance of mechanical constraints, which consisted of either the in-plane gel attachments to the boundaries of the PDMS mold and glass substrate, or the cell tractions emanating from the explants. Instead of translating inward, constrained fibers, rotated, stretched, and aligned along directions of tension based on their connectivity to other simultaneously deforming fibers in the gel. This collective, multi-scale response produced fiber alignment patterns that then set the pattern for cell migration.

In both *Fixed* and *Free* gels, cell migration distance (*CMD*) in the axial regions between explants was significantly greater than migration into non-axial regions. This finding is consistent with the concept of contact guidance, where cells preferentially migrate along directions of fiber alignment, and has been observed by others in other cell-gel systems [97, 101, 103]. For example, Provenzano *et al.* saw that radial fiber alignment generated by explants enhanced and directed cell migration out of the explants, and then postulated that this mechanism might underlie metastasis into the surrounding stroma for certain cancers [97]. However, it is also possible that the fibroblasts are migrating faster between explants due to a durotactic effect because the aligned fibers are stiffer [104], or to direct sensation of tension from the explant [101], or to a ligand

40

density-dependent haptotactic effect [105], or to some combination thereof. Chemical gradients could also be involved, but the fact that *CMD* in non-axial regions was significantly greater in the *Fixed* condition than in the *Free* condition suggests that a mechanical effect was more likely.

Regardless of the exact mechanism(s) involved, the anisotropy in fiber alignment and cell migration that develops in the fibrin gel should control how ECM remodeling progresses, particularly with respect to the organization and amount of collagen produced [86]. Finally, the experimental data obtained here was used to develop an image-based multiscale model and compare model predictions of short-term remodeling. A comparison of the model with this data can be found in De Jesus *et al.* [10].

41

CHAPTER 3: THE EFFECTS OF INITIAL STRUCTURAL REORGANIZATION ON LONG-TERM COMPOSITIONAL REMODELING OF THE ECM

3.1. Introduction

The ECM is a natural composite that consists of an assortment of proteins that confer mechanical properties and physiological function. Amongst the plethora of proteins that define the ECM, collagen is the most abundant and provides strength and structural integrity to most human tissue. Collagen is a ubiquitous protein that accounts for 30% of the total protein in the human body[106], and provides strength and structural support to most connective tissues and organs. There are approximately 20 different types of collagen [107]. The majority of it is fibrillar collagen type I, which makes up over 90% of total collagen in the human body [108]. Fibers of this load-bearing protein consist of a heterotrimeric structure composed of two α1(I) chains and one α2(I) chain. Cutaneous tissue injury leads to a series of synchronized events that result in the synthesis of collagens type I and type III by resident fibroblasts to replace the damaged tissue.

Wound healing is a complex process that requires the collective activity of multiple cell lineages, growth factors and matrix signals. Pathological phenomena that result in fibrotic wound healing are characterized by the excessive deposition of ECM proteins that cause tissue deformation, reduced mobility due to contracture, pain and discomfort. Excessive ECM synthesis during fibrosis has been associated to the prolonged presence of the myofibroblast after wound contraction. Myofibroblasts are characterized by an increased expression of alpha smooth muscle actin (α-SMA), and large focal adhesions that provide the mechanism necessary for large force generation,

42

essential for wound contraction and remodeling. This specialized phenotype is also responsible for the tissue regenerative activity of ECM protein synthesis.

There is a large body of evidence to support the idea that the state of the mechanical environment of a wound plays an important role in altering the synthetic activity of the dermal fibroblast. Under mechanical load, local stress signals are communicated to neighboring cells that ultimately initiate myofibroblast differentiation [9, 109-112]. Persistent stress developed in wounds during tissue remodeling is hypothesized to be responsible for the prolonged presence of the myofibroblast during fibrosis. Several therapeutic treatments have been developed that involve the reduction of tension at the wound site in order to reduce myofibroblast activity, excessive collagen production and scarring. Although the specific mechanisms by which these procedures are capable of regulating scar formation are yet unclear, there is enough evidence to support the idea that they function through a mechanical basis.

Initiation of collagen transcription can be stimulated by biochemical and mechanical cues. The nature of the biochemical cue (i.e. growth factors, cytokines, etc) and of the mechanical cues (i.e. tensile stress, compression, etc.) as well as the degree of transcription and translation will depend largely on cell type, location, and function. Collagen deposition and organization is dependent on spatial cues from the wound ECM. When cultured in fibrin or collagen gels contractile forces exerted by fibroblasts cause gel compaction and a reorganization of the fibrous structure. *In vitro* studies using these cell-seeded gel matrices have demonstrated the effects of gel geometry and constraints on the patterns of fiber alignment and the structural reorganization that develops [10, 113]. Gels that begin with an isotropic distribution of cells and fibers transform into

43

heterogenous and anisotropic constructs with organized fiber alignment patterns. Patterns of fiber alignment and ECM displacements may provide the cues necessary to guide collagen synthesis and organization. Fiber alignment can, in turn, induce cell alignment through contact guidance.

Compositional remodeling of the ECM during wound healing involves a delicate balance between collagen proteolysis and synthesis. Imbalances that may develop between these two events may lead to hypertrophic scarring or to deficient wound healing [114, 115]. Different types of MMPs are secreted by fibroblasts during wound healing, including MMP-1, and gelatinases MMP-2, and MMP-9. Interstitial collagenase (MMP-1) is an enzyme that initiates mature fibrillar collagen type I degradation and is normally highly expressed during the initial stages of the wound healing process. Physical as well as biochemical stimulation can regulate the synthesis and activity of these MMPs. Studies have demonstrated increased expression and activation of latent MMPs in fibroblast-seeded gels 24 hours after release [116], and a gradual increase in MMP-1 activity with time in both tethered and untethered collagen gels [117]. Cyclic, uniaxial mechanical tension applied to a scratch wound demonstrated an upregulation in collagen expression, accompanied by a downregulation in the expression of MMPs [118]. These studies reported on the short-term effects of changes to the mechanical environment on MMP synthesis and activation to assess the effects of mechanical tension on the expression of important mediators of the wound healing process. But wound healing is a process that normally requires 3 days to 4 weeks to complete.

This chapter encompasses studies performed to investigate the impact that the initial structural remodeling in a clot may have on long-term, fibroblast-mediated ECM

44

compositional remodeling. To test the hypothesis that different boundary conditions can alter the outcomes of short-term structural and long-term compositional remodeling of cutaneous tissue, the studies discussed in this chapter expand upon the *in vitro* wound-healing model presented in Chapter 2. Here, we relate the small differences in short-term structural reorganization of fibrin observed in response to either *Fixed* or *Free* gel boundary conditions to long-term compositional remodeling effects by studying changes in the expression of ECM remodeling genes MMP-1, MMP-2, MMP-9, and COL1A1 and collagen synthesis.

3.2. Experimental Methods

3.2.1. Fibrin Gel Preparation and Boundary Conditions

Fibrin gels were polymerized within square PDMS molds with dimensions of 8 mm x 8 mm x 1 mm (width, length, height), following the procedure described in section 2.4.1. The molds were attached to the bottom of wells in a 6-wells plate with the use of silicone grease (Dow Corning, Midland, MI). Once added to the molds, the fibrin solution gelled quickly and remained at room temperature for approximately 30 minutes until the explants were added. After polymerization, *Free* gels were released from the sides of the mold with the use of a 30 G x 1/2 inch needle while *Fixed* gels remained attached to the mold. The bottom of the gels remained attached to the surface of the wells.

3.2.2. Cell Culture and Explant Preparation

Samples were prepared following the same procedure described in Chapter 2 (c.f. 2.2.2) A triangular explant configuration was also used by positioning three explants at the vertice of a triangle with each side measuring approximately 2 mm from explant centroid-to-centroid (c.f., [91]). The cells were then allowed to settle and attach to the fibrin gel for approximately 2 hours before they were treated with DMEM containing 10% FBS, 1% Penicillin/Streptomycin, 0.1% amphotericin B, and supplemented with 1 ng/mL of TGF-β and 50 µg/mL of ascorbic acid. Samples were maintained in a humidified incubator with a controlled temperature of 37°C and supplied 5% CO_2 for one, two, and four weeks. At each time-point, samples were processed and prepared for histological staining, qPCR analysis, and collagen and cell quantification.

3.2.3. Gene Expression Analysis

Total RNA was extracted using a Qiagen RNEasy Mini kit (Qiagen, Valencia, CA, USA). Cells were homogenized using 0.1% 2-mercaptoethanol in a guanidine-thiocyanate containing buffer and eluted using an RNEasy Mini spin column. A NanoDrop 2000 UV-VIS spectrophotometer was used to measure the quantity and quality of isolated RNA by measuring the absorbance at 260 nm and the ratio of A260/A280. cDNA was synthesized using the Applied Biosystems cDNA Transcription Kit (Applied Biosystems, Foster City, CA) and RT-PCR was performed using a Mastercycler Gradient (Eppendorf, Hauppauge, NY). Primers for COL1A1, MMP-1, MMP-2, MMP-9, and the endogenous control 18S were mixed with cDNA in a 384-well Optical Reaction Plate (Applied Biosystems, Foster City, CA). Reverse transcription

46

reactions were performed using TaqMan Reverse Transcription reagents and were carried out in an Applied Biosystems Model QS-7 FLEX (Applied Biosystems, Foster City, CA). The difference between the quantification threshold (ΔC_t), the cycle at which the DNA primer of interest is detected, for each gene of interest and the housekeeping gene, 18S, was used to compare gene expression levels between *Fixed* and *Free* gels [119].

3.2.4. Histological Staining

Samples cultured for one, two, and four weeks were incubated in 4% paraformaldehyde (PFA) at 4°C for 24 hours. After fixation, samples were washed three times using 1x PBS and incubated in 10% sucrose for 20 minutes, and then in 20% sucrose for another 20 minutes. A final solution of 30% sucrose was then placed on the samples for one hour. Samples were then placed in a cryomold, which was then filled with Tissue-Tek embedment media. A gentle Jane freezer was used to freeze the cryomold and tissue. After freezing, the block was placed in a cryostat and sectioned at 10 μm. The resulting slides were stained using a Mason's trichrome stain.

3.2.5. Hydroxyproline Assay and DNA Assay

Samples representative of each time-point were subjected to a hydroxyproline assay to quantify collagen content [113]. Samples were hydrolyzed in 0.1 M NaOH at 98°C for one hour. After centrifugation, the supernatant containing the soluble protein was dried and hydrolyzed at 110°C using 6 N HCl for 24 hours and dried again.

Cell number was quantified in an identical set of samples that were treated to the same conditions as samples that were used for collagen quantification. DNA content was

47

measured using a Hoescht assay [113]. Briefly, fibrin gels were digested by treatment with 0.5 mg/mL proteinase K in digestion buffer (100 mM Tris, 50 mM EDTA, pH 7.43) at 56°C for 24 hours. Digested samples were diluted by 10x in 10x TNE buffer (100 mM Tris, 2.0 M NaCl, 10 mM EDTA, pH 7.43), and 100 μL of this solution were mixed with 100 μL of 0.2 μg/mL Hoescht 33258 in 10x TNE buffer. Samples were loaded into a clear bottom, black 96-well plate and placed into a microplate reader (brand, company) where fluorescence was measured at 360/460 nm (excitation/emission). Standards were prepared using DNA calf thymus DNA diluted in digestion buffer to determine DNA content over the range from 0 to 50 ng/mL. Cell number was determined assuming 7.6 pg of DNA per cell.

3.2.6. Time-lapse Imaging and Fibroblast Migration

Samples representative of the *Fixed* and *Free* conditions were prepared in a # 0 glass-bottom Petri dish and were placed in a temperature controlled chamber (Okolabs, NA, Italy) on a Nikon Eclipse Ti equipped with a DS-Qi1 Nikon CCD camera and a ProScan II motorized stage. Cell viability was ensured by maintaining the environmental temperature at 37°C and supplying a constant flow of 5% CO_2. Tiled 6x6 images were acquired every six hours using a 10x DIC Plan Apo objective to capture the structural changes that occurred across the surface of the gels as well as patterns of explant and individual cell migration over the course of one week.

48

3.2.7. Statistical Analysis

Data are presented as mean value ± standard deviation. Statistical significance was analyzed using Prism 6 (GraphPad Software Inc., La Jolla, CA). Significance was defined by a p-value < 0.05 and was evaluated by use of a Student's parametric t-test.

3.3. Results

3.3.1. Structural and Morphological Changes

Coarse changes in the morphology and structure of fibrin gels that were seeded with fibroblast explants and cultured under *Fixed* or *Free* conditions were observed by use of a Eclipse Ti equipped with a 10x DIC objective as well as by image acquisition using a Nikon digital camera. While *Fixed* gels retained the same initial surface area over the course of the experiment, fibroblasts cultured on *Free* gels compacted the gels approximately 11.3% after one week, and approximately 31.8% after four weeks (Fig. 12).
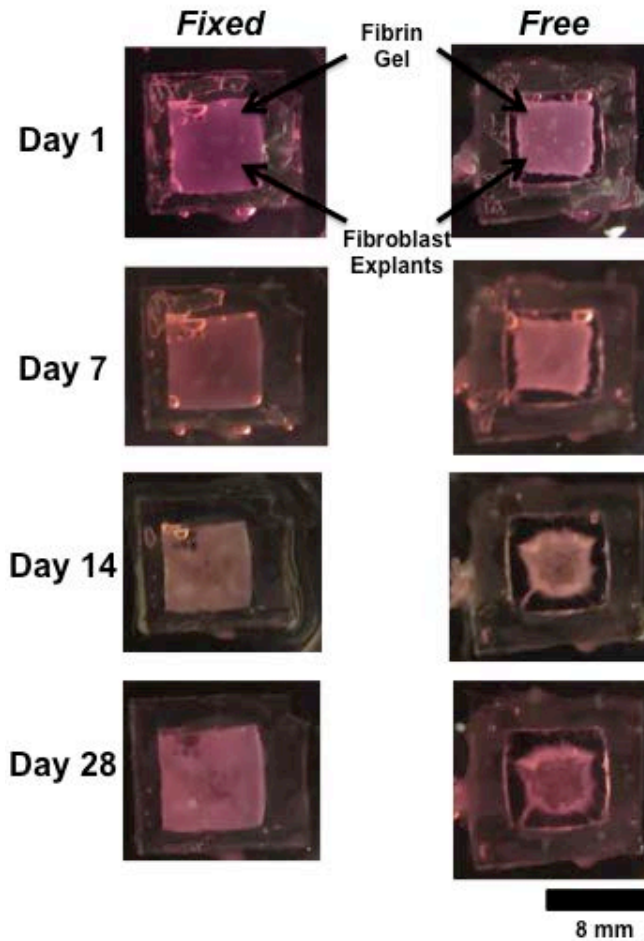
Figure 12. Long-term macroscopic changes in *Fixed* and *Free* gels. Changes in the size and geometry of the gel as well as patterns of fiber densification were monitored in *Fixed* and *Free* gels over the course of four weeks.

Consistent with the behavior observed in the studies reported in Chapter 2, fibroblasts that initially exhibited a rounded morphology at the start of the experiment began to extend and attach to the surface of the fibrin gel, changing the shape of the explant within the first six hours. Over the following 18 to 42 hours, individual cells assumed a spindle-shaped morphology and migrated outward, past the explant boundary (Fig. 13). Over the next three to five days, cell and fibrin fiber densification extended across the surface of the gels, and cell migration distance and proliferation increased.

50

After day three, the perimeter of the explants gradually disappeared as cells invaded regions between the explants (Fig. 13). In *Fixed* gels, dense bundles of fibrin formed along the axis between explants after only 24 hours. As time progressed and fibroblast migration increased, similar bundles began to form between the explants and the boundary of the gel. In *Free* gels the initial fiber densification and alignment observed within the first week was lost. As cells migrated out of the explants, contractile forces generated by the large number of cells at each site, caused explants to move in towards the center of the gel, while also compacting the fibrin gel as was observed in Fig. 12. As observed in previous studies, the average normalized centroid-to-centroid distance between explants was only slightly lower in the *Free* gel (0.94 ± 0.05) than in the *Fixed* gel (0.99 ± 0.03) after 24 hours. This difference increased over the course of a week as the normalized centroid-to-centroid distance decreased to 0.75 ± 0.09 in the *Free* gel and to 0.96 ± 0.04 in the *Fixed* gel (Fig. 14).
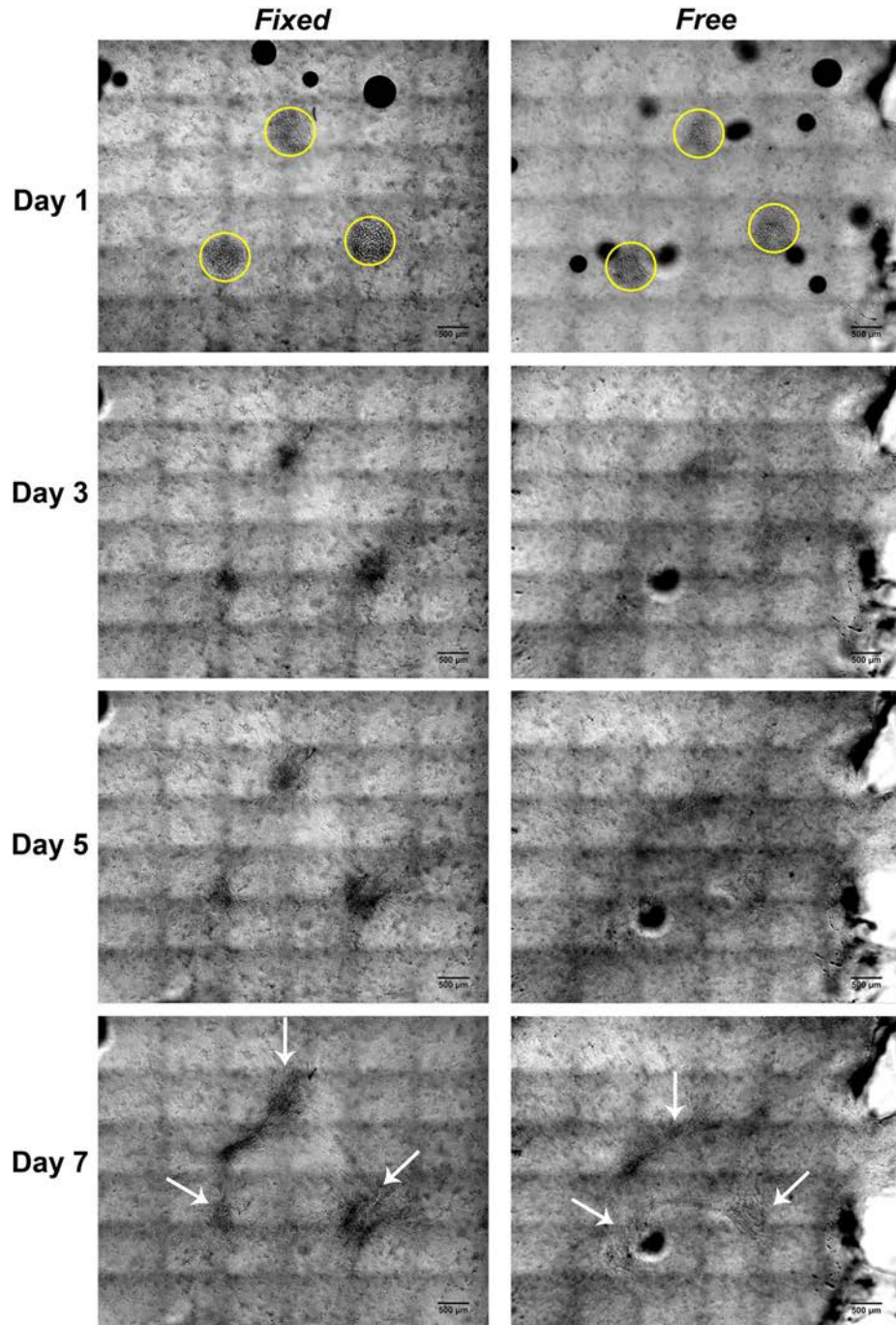
Figure 13. Long-term explant migration in *Free* and *Fixed* fibrin gels. Fibroblast explant migration and morphological changes were captured using DIC microscopy for seven days. Yellow circles and white arrows indicate the location of the explants at the start of the experiment, and after day seven, respectively.
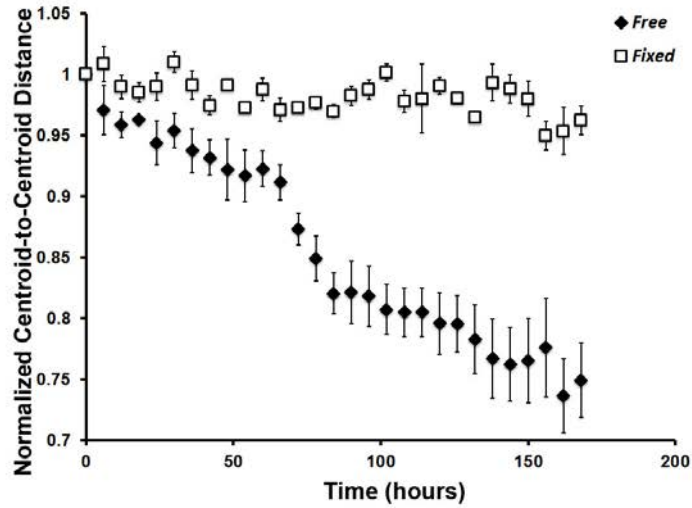
Figure 14. Normalized explant centroid-to-centroid distance in *Fixed* and *Free* gels. Normalized explant centroid-to-centroid distance was quantified every six hours for seven days. Each data point represents the average normalized distance between three explants in one sample per condition ± SEM.

3.3.2. Gene Expression of ECM Remodeling Proteins

The effect of the boundary conditions on pre-translational expression of the collagen type I alpha I chain (COL1A1) was measured using qPCR, and the ΔC_t value was used to compare differences in levels of expression in *Fixed* versus *Free* gels. The average ΔC_t value for COL1A1 gene in *Fixed* gels was found to be 4.45 ± 0.50, 4.62 ± 0.39, and 4.86 ± 0.81 at one week, two weeks, and four weeks of culture, respectively. In *Free* gels, ΔC_t values were found to be 3.92 ± 1.31, 5.23 ± 0.71, and 5.29 ± 0.18 at one week, two weeks, and four weeks, respectively (Fig. 15A). Although no statistical significant difference was found, the level of expression of COL1A1 was 1.5-fold, and 1.5-fold greater in *Fixed* gels as compared to *Free* gels at week two and week four, respectively. Because matrix remodeling also involves ECM degradation, changes in

53
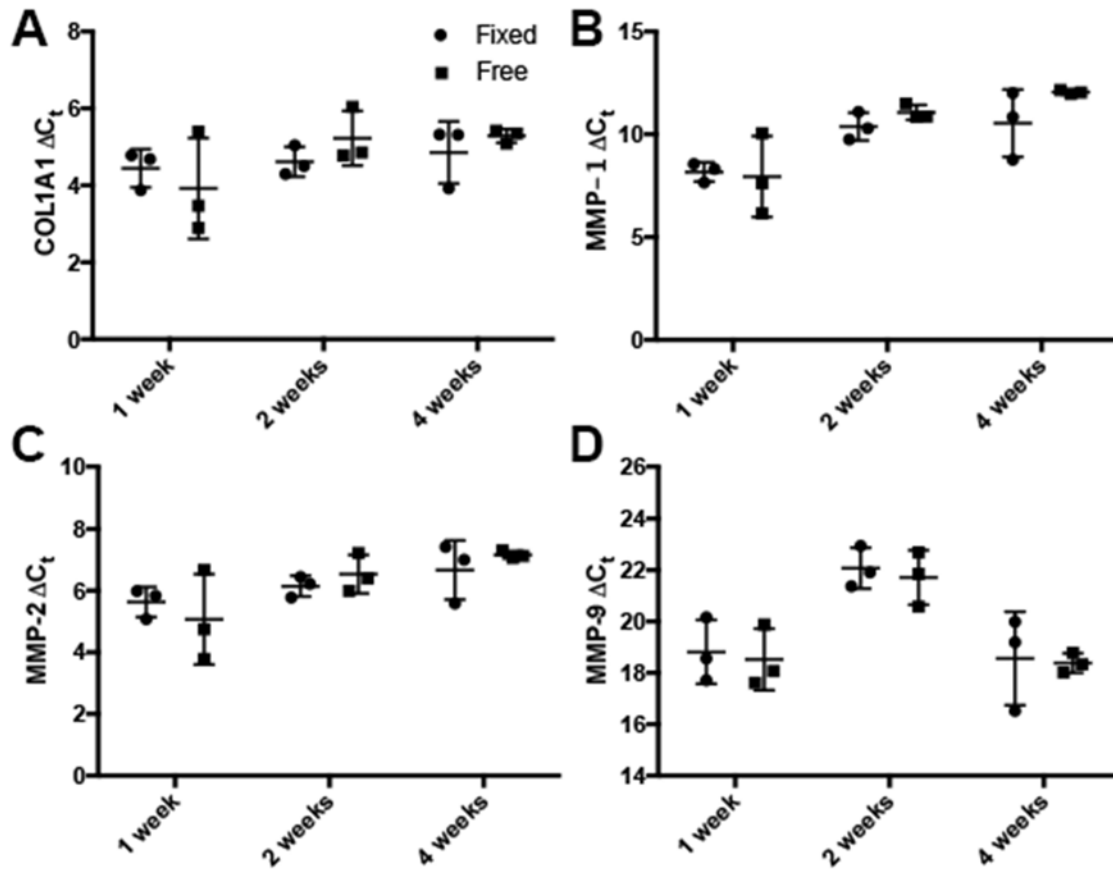
Figure 15. Differences in the expression of ECM remodeling genes. Gene expression of A) COL1A1, B) MMP-1, C) MMP-2, and D) MMP-9 was analyzed in *Fixed* and *Free* fibrin gels after one week, two weeks, and four weeks.

select MMP gene expression was also quantified. Previous studies have reported increases in the expression of MMP-1 in stress-relieved collagen gels [116]. In this study, the average ΔC_t of MMP-1 in *Fixed* gels was found to be 8.17 ± 0.47, 10.38 ± 0.68, and 10.54 ± 1.64 at one week, two weeks, and four weeks (Fig. 15B). In *Free* gels ΔC_t values were found to be 7.95 ± 1.97, 11.07 ± 0.37, and 12.06 ± 0.10 after one week, two weeks, and four weeks, respectively (Fig. 15B). On average, the expression of MMP-1 was found to be 1.6-fold and 4.4-fold in *Fixed* fibrin gels as compared to *Free* fibrin gels at two and four weeks, respectively, though these differences were not statistically

54

significant. A similar behavior was observed in the expression of the gelatinases MMP-2, and MMP-9, as 1.6-fold and 1.5-fold increases were observed in *Fixed* gels, respectively at week four (Fig. 15C, and 15D).

3.3.3. Histological Staining

After two and four weeks, fibrin gel samples cultured under *Fixed* and *Free* boundary conditions were sectioned and stained using a Mason's trichrome stain in order to qualitatively assess the amount and distribution of synthesized collagen. After two weeks, clear histological evidence of collagen production was not found in either *Fixed* (Fig. 16A) or *Free* (Fig. 16B). fibrin gels. After 4 weeks, however, collagen production in both gels was clearly evident. Moreover, more collagen was observed over a greater percentage of the surface area of *Fixed* than in *Free* fibrin gels.

55
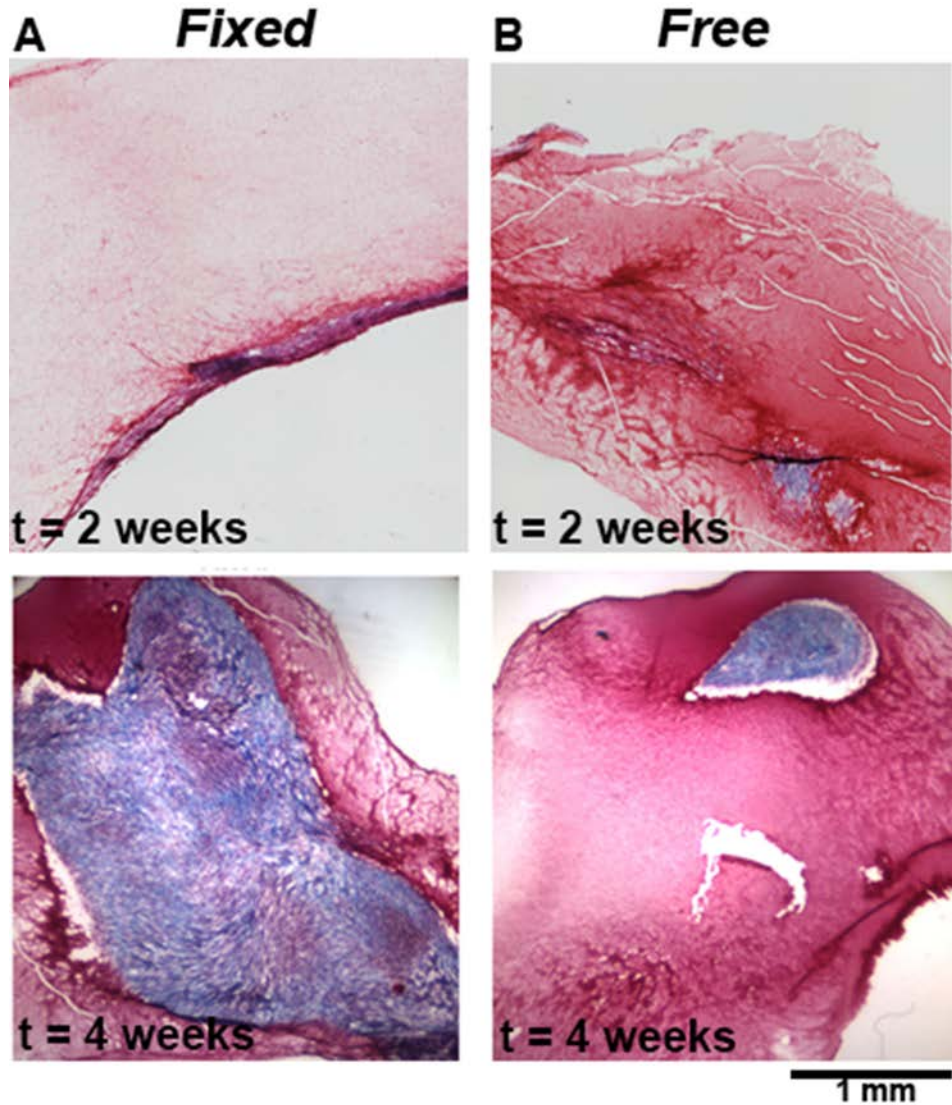
Figure 16. Mason's trichrome staining of sections of A) *Fixed* and B) *Free* fibrin gels after two and four weeks in culture.

3.3.4. Collagen Production

Collagen production in fibrin gels cultured under *Fixed* and *Free* boundary conditions was quantified after one week, two weeks and four weeks in culture using a hydroxyproline assay. The total amount of collagen produced increased from 2.6 ± 0.4 μg in *Fixed* gels and 3.0 ± 0.7 μg in *Free* gels at week one to 47.1 ± 3.5 μg, and 37.8 ± 1.1

µg at week four in *Fixed* and *Free* gels, respectively (Fig. 17A). Total collagen produced significantly increased at each time-point ($p<0.001$) and was found to be significantly greater in *Fixed* gels than in *Free* gels at week four ($p<0.05$). To observe the effects that different boundary conditions may have on stimulating collagen production in individual cells, the total amount of collagen produced was normalized over the average total number of cells in gels cultured under the same conditions. The amount of collagen synthesized per cell significantly increased ($p<0.05$) from 0.012 ± 0.002 ng/cell at week one to 0.045 ± 0.003 ng/cell at week four in *Fixed* gels (Fig 17B). In *Free* gels, collagen production per cell also increased significantly ($p<0.001$) from 0.016 ± 0.004 ng/cell to 0.030 ± 0.001 ng/cell. After four weeks, collagen production per cell became significantly greater ($p<0.05$) in *Fixed* gels than in *Free* gels.
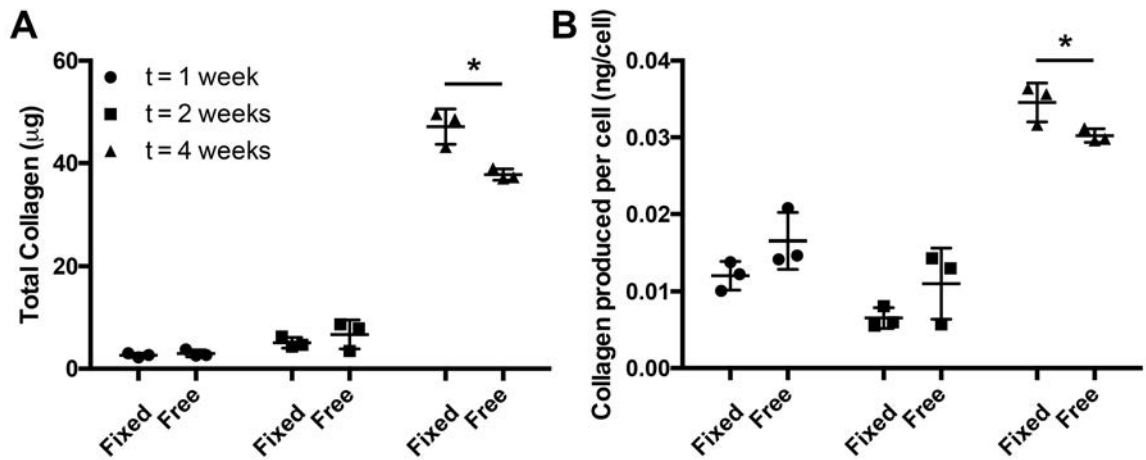
Figure 17. Collagen production in Fixed and Free gels. (A) Differences in collagen production per cell were quantified after one week, two weeks, and four weeks. Measurements with a significant difference ($p<0.05$) are marked with an asterisk. (B) Cell number after one week, two weeks, and four weeks was quantified in *Fixed* and *Free* gels and was used to normalize the amount of collagen produced per cell.

57

3.4. Discussion

Mechanical forces play an essential role in regulating cell and tissue phenotype. Such forces may be applied in the form of external loading or in the development of endogenous stress generated by the contractile activity of fibroblasts, which can also be influenced by the presence or absence of external constraints. Increased collagen production has been associated to an increased state of tension in a number of *in vitro* studies [120-122]. TGF-β activity is enhanced by the presence of tensile forces. The role of tensile forces on myofibroblast differentiation and on excessive collagen deposition has been associated to a number of fibrocontractive diseases, pathological wound healing [123], systemic sclerosis [124] and hypertrophic scarring [28, 125]. How these forces develop, how they are communicated across multiple scales between resident fibroblasts and the wound bed and how they alter compositional remodeling of the wound, are processes that are not yet clear. We have previously demonstrated that by applying different boundary conditions to fibrin gels that were seeded with dermal fibroblasts, differences in structural reorganization of the gel developed, including patterns of deformation as well as fiber alignment [10]. To explore the possibility that the anisotropy of fiber alignment and differences in cell migration and cell-generated tension may control how ECM proteins are synthesized, we performed a study to assess whether substantive differences in long-term remodeling occur between *Fixed* and *Free* fibrin gels even though only small differences in short-term remodeling exist.

The changes in gene expression (mRNA) observed in these studies did not reveal any differential effects caused by culture under different boundary conditions. Collagen type I is abundant in the late stages of wound remodeling and is excessively synthesized

58

in hypertrophic scars. Gene expression studies revealed a small up-regulation in COL1A1 expression in *Fixed* gels at two weeks, but this was not a significant difference. This behavior has been observed with several *in vitro* and *in vivo* studies that have related self-generated tension within wound models caused by restrained boundaries that resist cell contractility, to increased collagen expression and synthesis [126].

Mason's trichrome staining qualitatively demonstrated considerably more collagen production in *Fixed* gels than in *Free* gels (Fig. 16). These observations were supported by quantitative analysis of collagen production using a hydroxyproline assay which revealed a significantly greater amount of collagen produced in *Fixed* gels than in *Free* gels. Although differences in total collagen produced by fibroblasts between *Fixed* and *Free* gels were significant, the difference in the average amount of collagen does not seem to represent the large difference observed in histological samples. This discrepancy may be due to the depth of the fibrin gel sections processed and analyzed histologically. Histological sections were acquired up to approximately 100 μm below the surface of the gel. As part of the hydroxyproline assay, collagen is quantified in the entire fibrin gel. Fibroblasts may have migrated through the thickness of the gel. Restraining the bottom boundary may have caused an increase in collagen production in regions closer to the bottom boundary of the gel that were not histologically stained.

In related work, John *et al*. [127] found that stiff boundaries resulted in more α-SMA expression in fibroblast populated collagen gels compared to compliant boundaries, and that this expression was enhanced with the addition of TGF-β1. α-SMA is a hallmark of the myofibroblast phenotype, which is associated with increased collagen production and abnormal scarring [56]. Although we did not look for α-SMA in this

59

study, it seems likely that the increase in collagen observed in the *Fixed* gels will be also associated with increased α-SMA. More work will be required to quantify these and other differences in ECM synthesis and degradation and how they link to fibroblast mechanotransductive pathways, such as Rho/Rock [97] and ERK [85, 128], particularly as we explore how manipulating the mechanical environment at various time points could be used to control the remodeling process.

CHAPTER 4: USE OF LOCAL MECHANICAL STIMULATION TO MANIPULATE FIBROBLAST BEHAVIOR BY INJECTION OF CROSS-LINKED HYALURONIC ACID

4.1. Introduction

The dermal ECM provides structural support to the skin. It consists mainly of bundles of collagen type I fibrils that afford it strength and resiliency [12]. Resident fibroblasts attach to and extend along these bundles of collagen through integrin-rich focal adhesions. Through this direct interaction with the ECM, cells are able to sense and respond to mechanical forces and stresses that are applied to their surroundings by altering their contractile and synthetic behavior. In this manner, fibroblasts have the ability to modulate the structural and compositional integrity of the dermal ECM.

As we age, an accumulation of alterations to the skin's ECM caused by increases in enzymatic and non-enzymatic collagen crosslinks [129] and photoaging [130, 131] can result in the breakdown of the dermal ECM. The aged dermis is characterized by the appearance of fragmented collagen fibers [42] and a partially degraded network due to the inability of matrix metalloproteinases of digesting crosslinks (Fig. 18). This inefficiently degraded network lacks the structural support required by resident fibroblasts to attach to and achieve homeostatic levels of tension. This loss of mechanical stimulation renders the cells quiescent, causing them to assume a collapsed morphology, and to reduce their contractile and synthetic activity [11]. A gradual decrease in the synthesis of collagen [11] and elastin [132], major structural components of the skin's ECM, and an increase in MMP production [133-136], may be responsible for the formation of wrinkles, increased fragility, and the loss of elasticity in chronologically

61

aged and photoaged skin. Meanwhile, a decrease in the presence of glycosaminoglycans such as hyaluronic acid or hyaluronan [137], could explain the loss of hydration and turgidity.
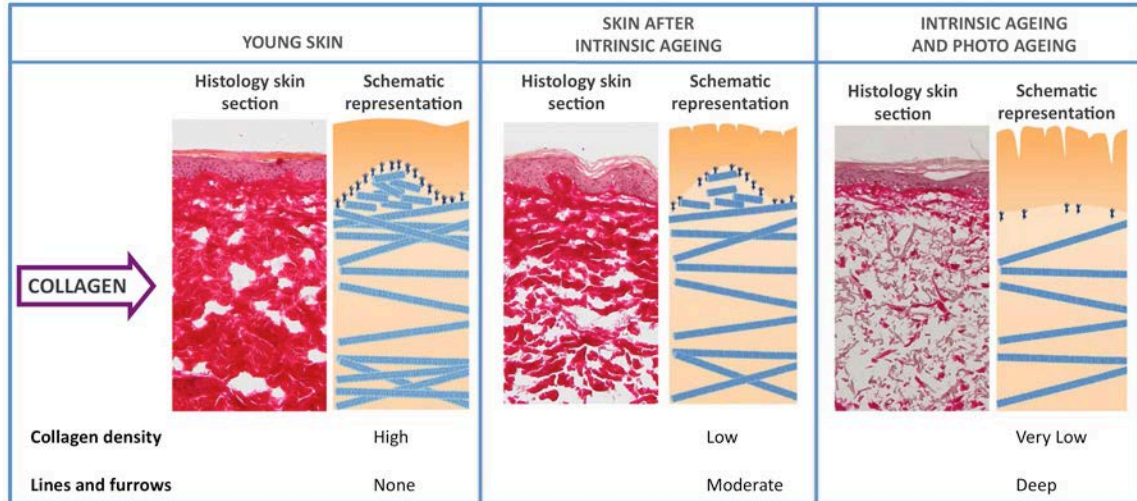
Figure 18. Composition and structure of the aged dermal ECM [1].

The relationship between the state of the mechanical environment of the ECM, fibroblast contractility, and ECM synthesis has been studied through the use of cell-seeded collagen gels. Nakagawa *et al.* used attached and free-floating cell-seeded collagen gel models to prove that fibroblasts that were allowed to achieve high levels of tension in tethered gels were capable of increasing synthesis of collagen. Those cultured under low levels of tension in free-floating gels, synthesized little to no collagen [48]. It has also been reported by Langholz *et al.* that fibroblasts that are grown in these stress-relieved collagen gels down-regulate the expression of genes encoding for collagen while up-regulating MMP1 mRNA through integrin-collagen interactions [49].

The Rho/ROCK pathway is a well-characterized mechanotransduction pathway known for its role in actin polymerization, stress fiber formation, cell contractility, and

62

motility. The pathway begins when RhoA, a small GTPase, is activated by the transmission of external forces to the cell membrane. RhoA then activates Rho associated kinase (ROCK), which in turn regulates actin filament stabilization and myosin-actin engagement and force generation. With structural collapse of the dermal ECM, external forces normally transmitted to the cell, and thus important mechanotransductive cues, might be reduced. Several studies have demonstrated that transforming growth factor β (TGF-β) activation of myofibroblast differentiation and ECM synthesis can be prevented and reduced by inhibition of ROCK [60]. This mechanism could describe the gradual decrease in collagen synthesis observed in the aged dermis as well as the presence of collapsed fibroblasts.

With the aim of reducing the appearance of visible signs of aging on skin, dermal fillers have been developed that consist in the use of natural or synthetic soft tissue fillers that act to lift and smoothen out wrinkles and other skin contour defects. Cross-linked hyaluronic acid (HA) has become a major component in several commercial dermal filler brands. HA is a naturally occurring polyanionic glycosaminoglycan that is found in abundance in skin, and cartilage tissue. It is made up of the repeating disaccharides D-glucoronic acid and N-acetyl-D-glucosamine. HA can bind to cell-surface receptors and is implicated in angiogenesis during wound healing [138-140], cell proliferation [141, 142], differentiation [143], and migration [144, 145]. Its hydrophilic nature, a product of its high fixed-charge density due to the presence of one charged carboxyl group per disaccharide monomer unit, allows it to maintain turgor, and hydration of the skin [146, 147] as well as lubrication in the joints [148-150]. It is this property that has made it an

important component in dermal fillers used in cosmetic surgery for the treatment of skin contour defects, and soft tissue augmentation.

Chemical and physical modifications of the HA polymer, such as cross-linking have made it an attractive building block in the design of polymers for applications in drug delivery and tissue engineering. By altering the amount of HA crosslinking, we can increase the longevity of the polymer when exposed to an aqueous environment, and improve its mechanical integrity. Cross-linked HA is the basis of a number of commercial-brand dermal fillers that make use of its biocompatibility, its space filling effects, as well as its tunable structural properties to achieve different effects in the correction of skin contour defects. Altering the degree of cross-linking, the concentration of HA, and particle size, allows for the control of the degree of swelling, strength, and degradability of the filler. HA dermal fillers with a high degree of cross-linking (20%-23%) exhibit increased stiffness [151] and are commonly used for the treatment of deep wrinkles. The formulation of cross-linked HA used in this study was Juvederm Ultra XC. Juvederm Ultra XC consists of BDDE cross-linked HA (6% crosslinked)

When injected into the dermis HA is eventually degraded by naturally occurring hyaluronidase and removed from the body. Ultrasound studies have revealed a decrease in the volume of injected HA and an increase in its dispersion only three months after injection [152]. Yet, cross-linked HA based dermal fillers have shown long-lasting improvements in the appearance of skin of patients between the ages of 26-80 after only one set of injections.

Several studies have reported on the effects of HA-based dermal fillers on stimulating pro-collagen type I expression, fibroblast elongation, increase in epidermal growth and keratinocyte proliferation [153-155]. A study conducted by Quan *et al.* revealed that within this time-frame, a significant increase in procollagen I synthesis occurred in the area of skin surrounding the sites of injected cross-linked HA, and was also accompanied by changes in dermal fibroblast morphology (Fig. 19) [154]. These results lead them to hypothesize that the effect of cross-linked HA dermal fillers on tissue rejuvenation may be due, in part, to mechanical stimulation.
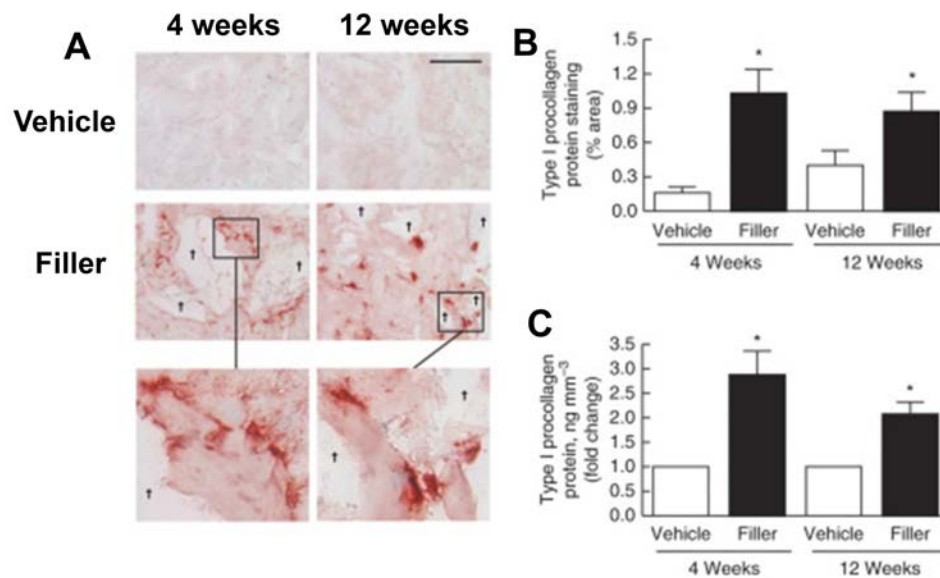
Figure 19. Enhancement of structural support of the aged dermis has been observed to increase procollagen type I secretion [154]. A) Procollagen I staining, B) area % quantification, and C) ELISA quantification in skin sections treated with vehicle (saline), and dermal filler.

Although these reports allude to the role of HA swelling in altering the mechanical environment of the dermis and mechanically stimulating quiescent fibroblasts to initiate contractility and synthesis, this behavior has not been clearly demonstrated. Additionally, none of these studies have characterized the supposed changes in

65

mechanical stress in the environment surrounding the injection. This study aimed to begin to uncover the role of mechanical stimulation and fibroblast mechanosensitivity in the loss of structural integrity and regenerative activity in the aged dermis. We approached this problem by first characterizing the swelling capabilities of a HA-based dermal filler when injected into a collagen gel. We then studied the response of one of several mechanotransduction pathways involved in mediating cell contractility, the Rho/ROCK pathway, to a localized change in the mechanical environment of the ECM via the injection of a space-filling, hydrophilic cross-linked HA dermal filler into two different *in vitro* models of the dermis. A stress-relieved, released collagen gel was used as a model representative of the structurally inefficient aged dermis. An attached collagen gel was used as a model of a young, mechanically stable dermis. The effect of mechanical stimulation on restoring ECM protein expression and synthesis in aged dermal fibroblasts was studied by quantifying by measuring changes in the expression of the COL1A1 gene and synthesis of collagen using hydroxyproline as an index, after treatment with an injection of dermal filler in attached and released fibrin gels. The swelling behavior of the injected HA, and its presence in the gel were associated to the changes in expression levels and synthesis of ECM proteins.

66

4.2. Experimental Methods

4.2.1. Characterization of the Mechanical Effect of HA
Injections In Collagen: Swelling Experiments and Data
Analysis

When placed in a hypertonic solution, HA gels swell due to an increase in osmotic pressure caused by the Donnan effect [156]. This characteristic behavior of HA is hypothesized to cause an increase in stress when injected as filler into the dermis [154, 155]. In order to observe this effect and to estimate the amount of stress that was generated on the collagen network as a result of HA hydration and swelling, HA was injected and allowed to swell in a collagen gel with a concentration of 2 mg/mL. To determine the swelling capability of the pure formulation of HA used for this study, 100 μL of HA (n = 4) was placed within a dialysis membrane and into a solution of water or 1x phosphate buffered saline (PBS) and was allowed to swell for four days (Fig. 20A, and 20B). The height of the water column within the 2 mL pipette inserted into the dialysis tubing at the start of the experiment was measured every hour during the first eight hours, followed by every 12 hours until 72 hours had passed. The change in column height was used to calculate the swelling pressure of the HA filler and the swelling ratio, calculated using the following equation:

$$SR = {V_t}/{V_o} \tag{4-1}$$

A collagen gel with a protein concentration of 2 mg/mL was prepared by mixing 10X PBS, 1 N NaOH, acid solubilized collagen type I from rat tail (Invitrogen™, Grand Island, NY), and DMEM. After one hour of incubation at 37°C each gel was injected

67

with approximately 10 μL of cross-linked HA (Juvederm Ultra XC, Allergan, Irvine, CA) The samples were imaged using DIC microscopy immediately after injection. Samples were then placed in a solution of distilled water or 1x PBS. Swelling kinetics were captured by acquiring microscopic images of the gels every 30 min for 24 hours, using a Nikon Eclipse Ti microscope and 10x Plan Apo objective with DIC capabilities. The area of the sphere formed by the injected HA was measured at each time-point and was plotted every hour.

In order to calculate the Donnan osmotic pressure of HA in different solutions of PBS, we used the following equation:

$$\pi_{Donnan=}\sigma_{hyd} = \rho g \Delta h \qquad (4\text{-}2)$$

where ρ is the density of water, g is gravitational acceleration, and h is the change in the height of the fluid column.

The Donnan osmotic pressure of a swollen HA gel in equilibrium is balanced by the hydrostatic stress of HA, σ_{HA}:

$$\sigma_{HA} - \pi_{Donnan} = 0 \qquad (4\text{-}3)$$

Because the formulation of HA that is being used has a low cross-linking density, when placed into an ionic solution, the gel is not able to resist the osmotic pressure and after approximately two to three hours in solution, it begins to dissolve. As so, we can consider the hydrostatic stress of HA in response to the Donnan osmotic pressure to be negligible.

When injected into a collagen gel, a swollen HA gel at equilibrium would generate a state of stress in the collagen gel that satisfies the following stress balance equation:

68

$$\sigma_{HA} + \sigma_{col} - \pi_{Donnan} = 0 \qquad (4\text{-}4)$$

where σ_{col} is the stress generated in the collagen network and π_{Donnan} is the Donnan osmotic pressure calculated using equation 4-2.

The swelling ratio of the HA dermal filler after injection into an acellular gel was calculated using the following equation:

$$SR = {A_t}/{A_o} \qquad (4\text{-}5)$$

The stress that was generated in the collagen gel by swelling of injected HA was calculated by employing the following method. The Donnan osmotic pressure was measured for the 24 mg/mL HA gel cross-linked at 6%, when placed in water and into a solution of 1x PBS. Hydrostatic stress (σ_{HA}) was plotted against the swelling ratio (SR). Using this plot, and the calculated swelling ratio of the HA dermal filler injected into the collagen gel, the swelling pressure was interpolated. The π_{Donnan} calculated using equation 4-2, was used to estimate the stress introduced into the collagen gel using equation 4-4.

4.2.2. Sample Preparation: *In vitro* Model of the Dermis

Two age groups were defined for the purposes of this study: young and old. The young group was comprised by human dermal fibroblasts extracted from patients between the ages of 14, and 23 years old. The old group was comprised by human dermal fibroblasts from patients between the ages of 56 and 69 years old. Specific details regarding donor information as well as the location of the skin tissue from which the cells were extracted are provided in Table 1. Fibroblast-seeded collagen gels were prepared by mixing together 10X PBS, 1 N NaOH, acid solubilized collagen type I from rat tail

69

(Invitrogen™, Grand Island, NY), and a fibroblast suspension in DMEM to achieve a final protein concentration of 2 mg/mL and a cell concentration of 250,00 cells/mL below passage number 10. The gels were then allowed to polymerize by incubating at 37°C and 5% CO_2 in a humidified incubator. Upon polymerization, samples were fed with DMEM supplemented with 10% FBS/1% Penicillin/Streptomycin/0.1% Amphoterecin B. After 24 hours in culture, fibroblast-seeded collagen gels were either released from the sides of the well to relieve tension generated by fibroblast contractile activity or were allowed to remain attached. A volume of 10 μL of cross-linked HA dermal filler were injected into the center of the collagen gels, 48 hours after polymerization. In order to capture the effects of collagen network disruption caused by puncturing the gel with a needle, a control group was prepared by injecting 10 μL of 1x PBS.

Table 3. Human Dermal Fibroblasts.

Young HDFs			
Age	**Sex**	**Race**	**Location**
14 year-old	Female	Unknown	Breast
16 year-old	Female	Unknown	Breast
18 year-old	Female	Caucasian	Breast
23 year-old	Male	Caucasian	Abdomen
Old HDFs			
Age	**Sex**	**Race**	**Location**
56 year-old	Female	Caucasian	Face
69 year-old	Unknown	Unknown	Unkown
67 year-old	Female	Caucasian	Face

70

The effects of HA injection on fibroblast mechanoresponse were assessed by measuring changes in the expression of genes that encode for various components of the Rho/ROCK pathway using quantitative real-time PCR. Samples were prepared as described in 2.4.2, and 24 hours after collagen polymerization, gels were released from the sides of the wells using a thin spatula. When tethered, tension in a collagen gel develops due to fibroblast contractility. Cells attach to collagen fibrils and generate pulling forces in an attempt to reorganize and consolidate the gel. The increased state of tension that follows, signals the cells to express a multitude of genes and proteins that function to increase contractility and synthesis [48, 157] Releasing tension in the gel reduces the expression of mechanoresponsive genes over the following 24 hours and renders the cells quiescent. At this point, a small volume of approximately 10 μL of HA was injected into the center of the collagen gel.

4.2.3. mRNA Extraction and qPCR Analysis

Total mRNA was extracted from samples that were treated with HA or 1 X PBS for qPCR analysis at two different time-points: 5 minutes after injection, and 24 hours after injection. Samples were washed using 1 X PBS, and were stored overnight at -20°C. Total RNA was extracted using a Qiagen RNEasy Mini kit (Qiagen, Valencia, CA, USA). Cells were homogenized using 0.1% 2-mercaptoethanol in a guanidine-thiocyanate containing buffer and eluted using an RNEasy Mini spin column. A NanoDrop 2000 UV-VIS spectrophotometer was used to measure the quantity and quality of isolated RNA by measuring the absorbance at 260 nm and the ratio of A260/A280. cDNA was synthesized using the Applied Biosystems cDNA Transcription

71

Kit (Applied Biosystems, Foster City, CA) and RT-PCR was performed using a Mastercycler Gradient (Eppendorf, Hauppauge, NY). Primers for COL1A1, RhoA, ROCK1, ROCK2, and the endogenous control 18S were mixed with cDNA in a 384-well Optical Reaction Plate (Applied Biosystems).   Reverse transcription reactions were performed using TaqMan Reverse Transcription reagents and were carried out in an Applied Biosystems Model 7900HT thermocycler. Fold-changes in the expression of genes that were analyzed were calculated using the ΔΔCt method [119].

4.2.4. Hydroxyproline Assay and DNA Assay

Fibroblasts from both age groups below passage number 10 were cultured into fibrin gels at a concentration of 0.5 million cells/mL. Cell-seeded gels were prepared by mixing a suspension of cells in DMEM/10% FBS/1% Penicillin/Streptomycin/0.1% amphotericin B with a solution of fibrinogen at approximately 33.3 mg/mL diluted in 20 mM HEPES at a 1:2 ratio. The fibrinogen-containing solution was then mixed with a solution containing thrombin, 20 mM HEPES, and 2 M $CaCl_2$ at a 1:4:0.75 ratio, to initiate fibrin polymerization. Approximately 0.956 mL aliquots of the total fibroblast-seeded fibrin solution were pipetted into a 24-well plate. After gelation samples were treated with approximately 1 mL of DMEM/10% FBS/1% Penicillin/Streptomycin/0.1% amphotericin B supplemented with 50 μg/mL of TGFβ-1,and 50 μg/mL of ascorbic acid. After 24 hours of incubation at 37°C in a 5% CO_2 humidified environment, gels were released from the sides and bottom of the wells using a thin spatula, to relieve accumulated internal tension and allow them to freely float. Gels were incubated another 24 hours to allow cells to become quiescent under the reduced state of tension, and were

then treated with an injection of approximately 10 µL of dermal filler or PBS. Samples were then incubated for two weeks. Culture medium supplemented with TGFβ-1 and ascorbic acid was replaced every three days. Collagen content was quantified using a hydroxyproline assay. Briefly, samples were hydrolyzed in 0.1 M NaOH at 98°C for 1 hour. After centrifugation, the soluble protein-containing supernatant was hydrolyzed in 6 N HCl at 110°C for 24 hours, and dried in a speed vacuum for 1.5 hours. The amount of hydroxyproline in the supernatant was quantified to estimate the collagen content in each sample assuming 7.46 µg of collagen per µg of hydroxyproline [113, 158].

Cell numbers were quantified in samples that were treated with the dermal filler, and PBS by using a Hoechst assay, in order to normalize the amount of collagen produced over the number of cells in each treated gel. Fibrin gels were digested by treatment with 0.5 mg/mL proteinase K in digestion buffer (100 mM Tris, 50 mM EDTA, pH 7.43) at 56°C for 24 hours. Digested samples were diluted by 10x in 10x TNE buffer (100 mM Tris, 2.0 M NaCl, 10 mM EDTA, pH 7.43), and 100 µL of this solution were mixed with 100 µL of 0.2 µg/mL Hoechst 33258 in 10x TNE buffer. Samples were loaded into a clear bottom, black 96-well plate and placed into a Glomax microplate reader (Promega, Madison, WI) where fluorescence was measured at 360/460 nm (excitation/emission). Standards were prepared using DNA calf thymus DNA diluted in digestion buffer to determine DNA content over the range from 0 to 50 ng/mL. Cell number was determined assuming 7.6 pg of DNA per cell.

4.2.5. HA ELISA

Samples of medium from dermal filler injected cell-seeded collagen gels were stored and HA was quantified 24 hours, 48 hours, 72 hours, one week, two weeks and

three weeks after treatment using an HA ELISA (Corgenix, Broomfield, CO) by following the manufacturer's protocol. Briefly, samples, HA reference solutions, and HA controls were diluted by a factor of 1:10 in reaction buffer and 100 µL of each solution was added into a well coated with hyaluronic acid-binding protein (HABP). In order to account for HA present in the serum used to supplement the DMEM, fresh DMEM supplemented with fetal bovine serum (FBS) was also used as a control. After a one hour incubation at room temperature the wells were washed four times using PBS, followed by a 30 minute incubation at room temperature with a solution of horseradish peroxidase-conjugated HBP. After incubation, 100 µL of a chromogenic substrate solution containing tetramethylbenzidine and hydrogen peroxide was added. The absorbance of each sample, HA reference, and control was measured at 450 nm using a Glomax microplate reader (Promega, Madison, WI). A standard curve was created using the absorbance and known concentration of the HA reference solutions, and a best fit curve was calculated using a third-order polynomial regression as recommended by the manufacturer.

4.2.6. Statistical Analysis

Data in graphs for mRNA expression levels are presented in the form of mean ± standard error. All other data are presented as mean ± standard deviation. Student t-tests were performed using Prism 6 software (Graphpad Software Inc., La Jolla, CA). Significance was obtained at $\alpha = 0.05$.

74

4.3. Results

4.3.1. Cross-linked HA Swelling and Stress Development

Osmotic pressure tests were performed to determine the swelling capabilities of the formulation of cross-linked HA used for this study, as defined by the Donnan effect. When placed into a solution of purified water, the dermal filler absorbed approximately 73.5 ± 20.5 µL in 24 hours and a total of 202.3 ± 34.2 µL after 72 hours (Fig. 20C). Dermal filler exposed to a solution of 1x PBS absorbed approximately an average of 25.7 ± 6.4 µL of water by 24 hours, and of 31.0 ± 8.9 µL by 72 hours. Equilibrium began to occur after only one day, at which point the average swelling ratio of the dermal filler was found to be 1.26 ± 0.06, increasing to 1.31 ± 0.09 by the end of the experiment (Fig. 20C). The change in height of the fluid column was used at each of these time-points to calculate the Donnan osmotic pressure by equating this pressure to hydrostatic pressure. The Donnan osmotic pressure was plotted against the swelling ratio and was used later to estimate the amount of stress generated by the swelling of the dermal filler injected into a collagen gel (Fig. 20D). Focal injection of the dermal filler into acellular collagen gels caused the formation of small pockets that resulted from local expansion of the lattice (Fig. 21A). The average initial area occupied by 10 µL of dermal filler was approximately 4.40 ± 0.87 mm^2. Water absorption after addition of 1x PBS caused the injected filler to swell by approximately 10%, as it expanded in size to approximately 4.83 ± 0.43 mm^2. The swelling ratio of injected dermal filler was defined as the ratio of the area at each time-point over the initial area. After approximately six to seven hours, the change in swelling ratio began to decrease, and equilibrate. The swelling ratio was

75

found to be 1.07 ± 0.01 after only six hours, and 1.10 ± 0.00 after 24 hours (Fig. 21B). This decrease in swelling ratio exhibited by the injected dermal filler as compared to the
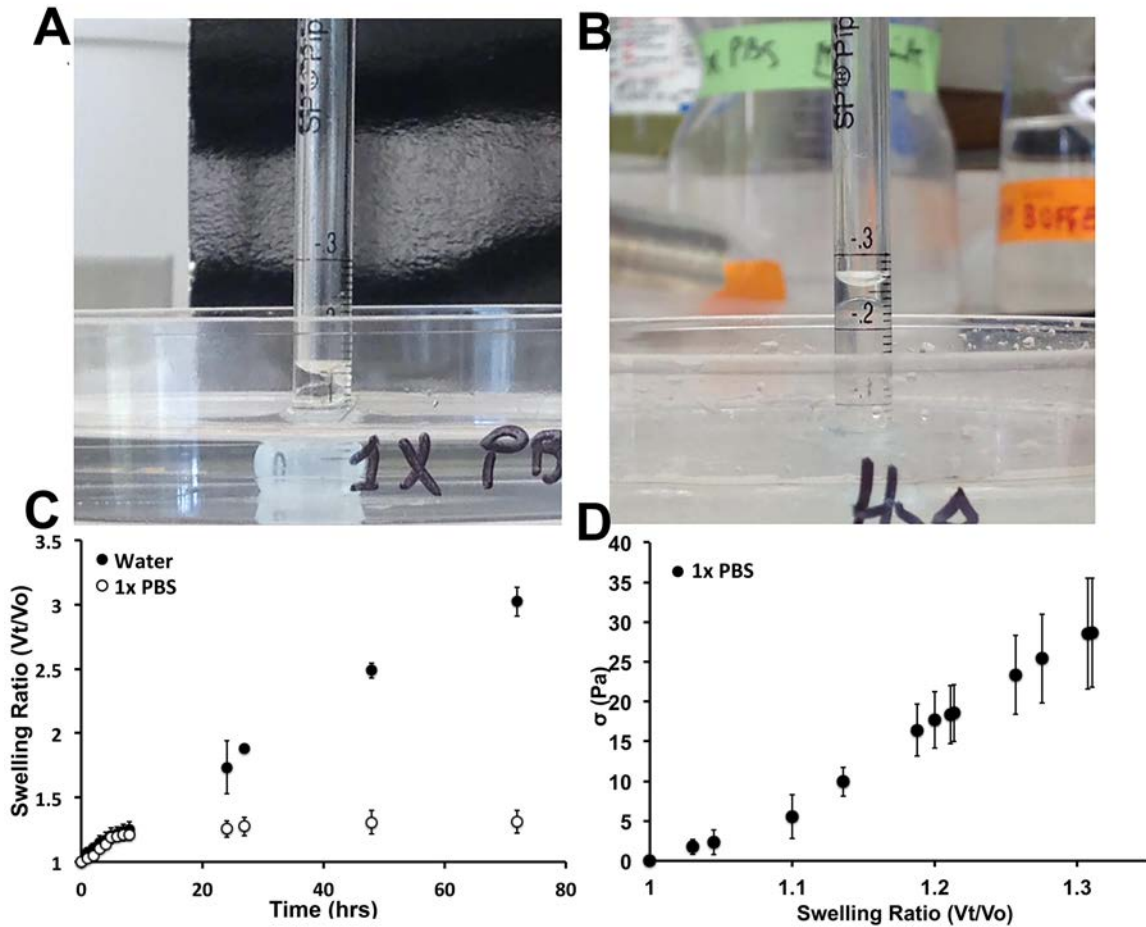
Figure 20. HA dermal filler osmotic pressure tests.

swelling ratio of non-confined dermal filler indicates a resistance to deformation that may be introducing a state of tension on the surrounding fibrous network. Due to the low cross-linking density of the formulation of dermal filler used in this study, we can assume that the hydrostatic pressure of the dermal filler when exposed to an aqueous solution is negligible, which can be confirmed by the dissolution of the dermal filler when placed in water and 1x PBS, after only two hours. The stress generated by swelling of the dermal filler was found by using the swelling ratio of the filler in collagen and interpolating the

corresponding hydrostatic stress using the plot in Fig. 20D. Then, using equation 4-3, I estimated the stress developed by swelling of the dermal filler in collagen to be approximately 20.7 Pa.
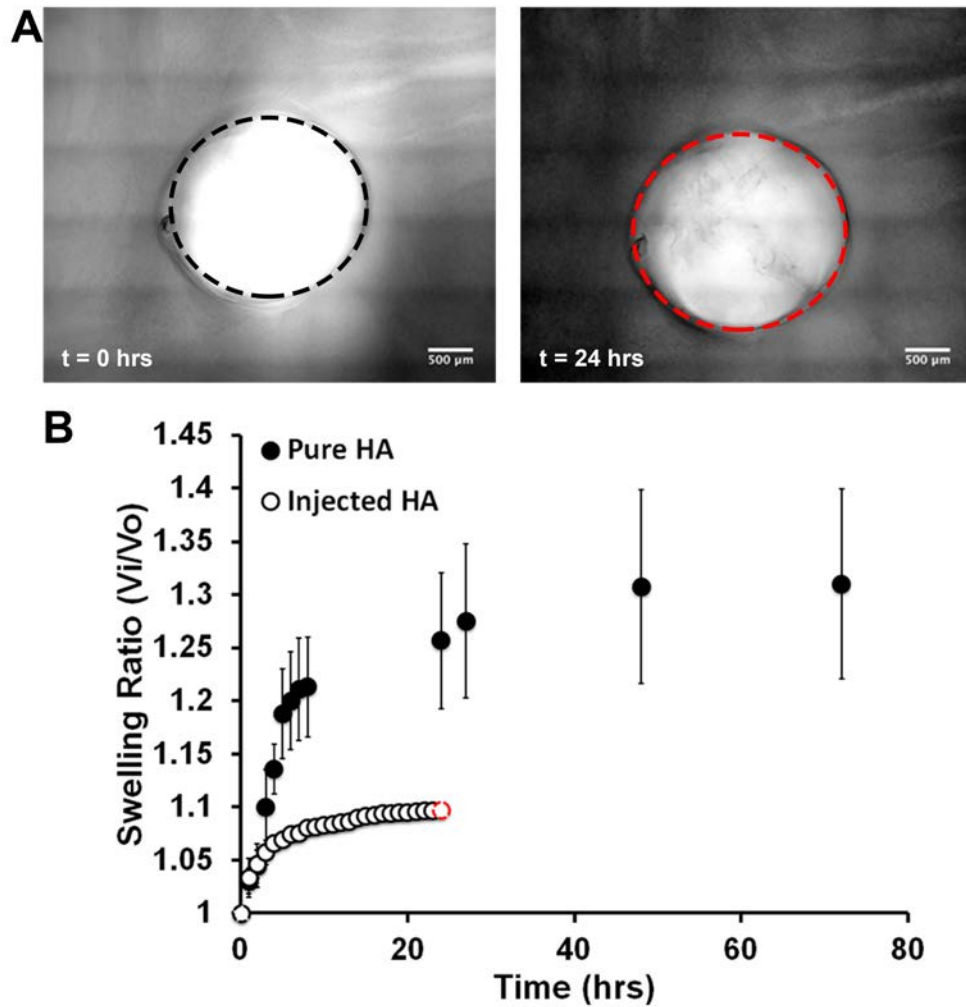
Figure 21. Characterization of swelling behavior of dermal filler in an acellular collagen gel hydrated with 1x PBS. A) DIC images depicting the change in area of an injection of dermal filler due to swelling when exposed to 1x PBS for 24 hours. B) Swelling ratio of pure, unconfined dermal filler, and dermal filler injected into a collagen gel, plotted over time.

4.3.2. Activation of Rho/ROCK Pathway/Fibroblast
Mechanosensitivity

Having demonstrated the swelling capabilities of the HA-based dermal filler and its effect on altering the mechanical environment of a collagen gel, we next considered whether the changes caused to the ECM would be enough to induce mechanotransduction in different aged cells and incite collagen synthesis. Released collagen gels were used to simulate the mechanical environment of the aged dermis by providing a low stress level milieu. Fibroblasts cultured within stress-relieved gels, exhibit a decrease in contractility and in the synthesis of ECM proteins, a behavior characteristic of fibroblasts that inhabit the aged dermis. Primary human dermal fibroblasts (HDFs) extracted from young, and old dermal tissue explants were cultured within collagen gels that were relieved from stress and were then treated with a mechanical stimulus through the injection of a HA-based dermal filler. Age-dependent differences in fibroblast mechanosensitivity were assessed by studying the response of genes that encode for the mechanoresponsive proteins that regulate actin stress fiber formation and contractility, RhoA, ROCK1, and ROCK2. PBS was used as a control, assuming that its injection into a collagen gel would cause a temporary expansion of the lattice. While the dermal filler would absorb water and continue to swell over time, causing small deformations to the surrounding collagen matrix, and introducing a state of stress, we assumed that PBS would eventually diffuse through the porous matrix, causing little to no lasting physical changes and therefore, would provide no mechanical signal to the cells.

Young HDFs cultured in stress-relieved collagen gels that were injected with dermal filler, demonstrated a 2.7-fold increase in the expression of the small GTPase

78

protein, RhoA, and a 2.8-fold, and 3-fold increase in the expression of ROCK1, and

ROCK2, respectively, five minutes after treatment (Fig. 22A). This response was not

sustained after 24 hours in all cell lines within the young age group. Although the average

expression of RhoA, ROCK1, and ROCK2 in dermal filler-injected samples at 24 hours

was found to be 3-fold, 2.7-fold, and 2.6-fold greater than in PBS controls, these levels of

expression were not significantly different.
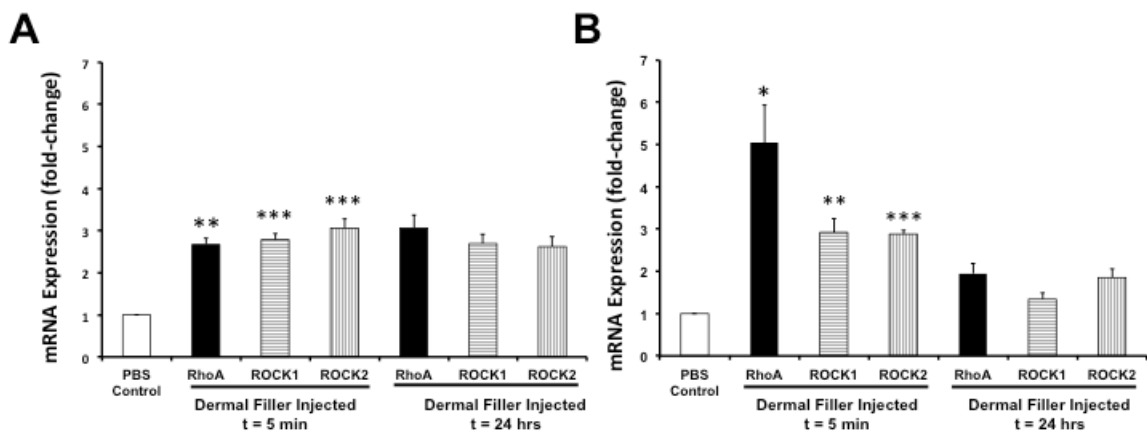
Figure 22. Rho/ROCK expression in young and old HDFs cultured in released collagen gels. Gene expression of RhoA, ROCK1, and ROCK2 was analyzed using qPCR five minutes, and 24 hours after injection of dermal filler into a released collagen gel seeded with A) young HDFs (n=15, *p<0.05, **p<0.01, ***p<0.001 vs. PBS injection) or B) old HDFs (n=9, *p<0.05, **p<0.01, ***p<0.001 vs. PBS injection).

Activation of RhoA, ROCK1, and ROCK2 was also observed in old HDFs in

stress-relieved fibroblasts after dermal filler injection. Levels of expression of RhoA,

ROCK1, and ROCK2 exhibited a 5-fold, 3-fold, and 3-fold increase, respectively, five

minutes after injection of the dermal filler (Fig. 22B). Similar to the behavior observed

in young HDFs, the older cells did not significantly sustain the increased level of

expression of Rho/ROCK genes. No significant differences in levels of expression were

observed between young and old HDFs in response to the injection of the filler.

79

Attached collagen gels were used to represent a simple *in vitro* model of a healthy dermis under homeostatic levels of tension. When cultured within attached collagen gels, as fibroblasts begin to exert forces and remodel the environment, resistance is met by the tethered boundaries of the gel. As tension develops within the gel, fibroblasts assume an active, synthetic activity. Young HDFs cultured within attached collagen gels,
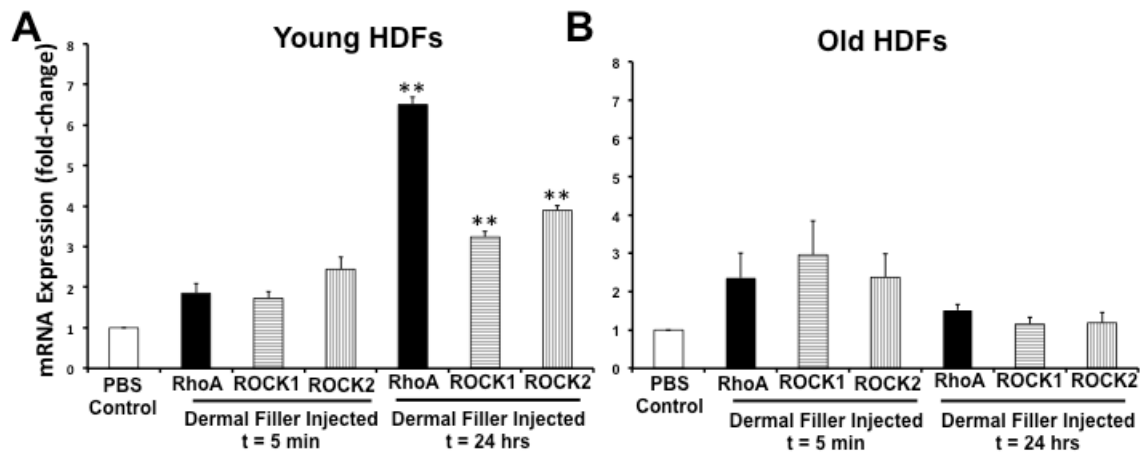
Figure 23. Rho/ROCK expression in young and old HDFs cultured in attached collagen gels. Gene expression of RhoA, ROCK1, and ROCK2 was analyzed using qPCR five minutes, and 24 hours after injection of dermal filler into a released collagen gel seeded with A) young HDFs (n=15, **$p<0.01$, vs. PBS injection) or B) old HDFs (n=9, vs. PBS injection).

demonstrated an approximate 2-fold increase in the level of expression of RhoA, and a 2-fold, and 2.4-fold increase in the expression of ROCK1, and ROCK2 five minutes after treatment, respectively. In contrast to what was observed in fibroblasts cultured under a low-stress level environment, this change in expression continued to significantly increase over the course of 24 hours after treatment (Fig. 23A). In turn, old HDFs showed no immediate response to mechanical stimulation, as no significant change in the expression of RhoA, ROCK1, or ROCK2 was observed five minutes, or 24 hours after injection (Fig. 23B).

80

4.3.3. Cell Number

The number of young HDFs cultured in released fibrin gels increased from an initial estimated 0.25 million cells to a measured average of 1.99 ± 0.38 million cells in dermal-filler treated gels and 2.12 ± 0.57 million cells in PBS controls after three weeks in culture (Fig. 24). Cell proliferation appeared to be lower in old HDFs cultured in released fibrin gels treated with dermal filler (1.72 ± 0.32 million cells) and PBS (1.75 ± 0.38 million cells), as compared to younger HDFs seeded at the same initial density (Fig. 24). With the exception of 69 year-old HDFs treated with dermal filler, all young and old cells cultured within attached fibrin gels demonstrated greater proliferation during the three-week culture after treatment with dermal filler and PBS than in released gels exposed to the same treatment. The number of young HDFs increased from an estimated 0.25 million cells to 2.33 ± 0.50 million cells and 2.59 ± 0.49 million cells in dermal filler-injected and PBS controls, respectively. Old HDFs seeded at the same initial cell density, increased to 1.87 ± 1.06 million cells and 2.48 ± 0.99 million cells in dermal filler-injected and PBS controls, respectively. Treatment with the dermal filler caused no significant change in cell proliferation within age groups when cultured in released or attached gels.

81
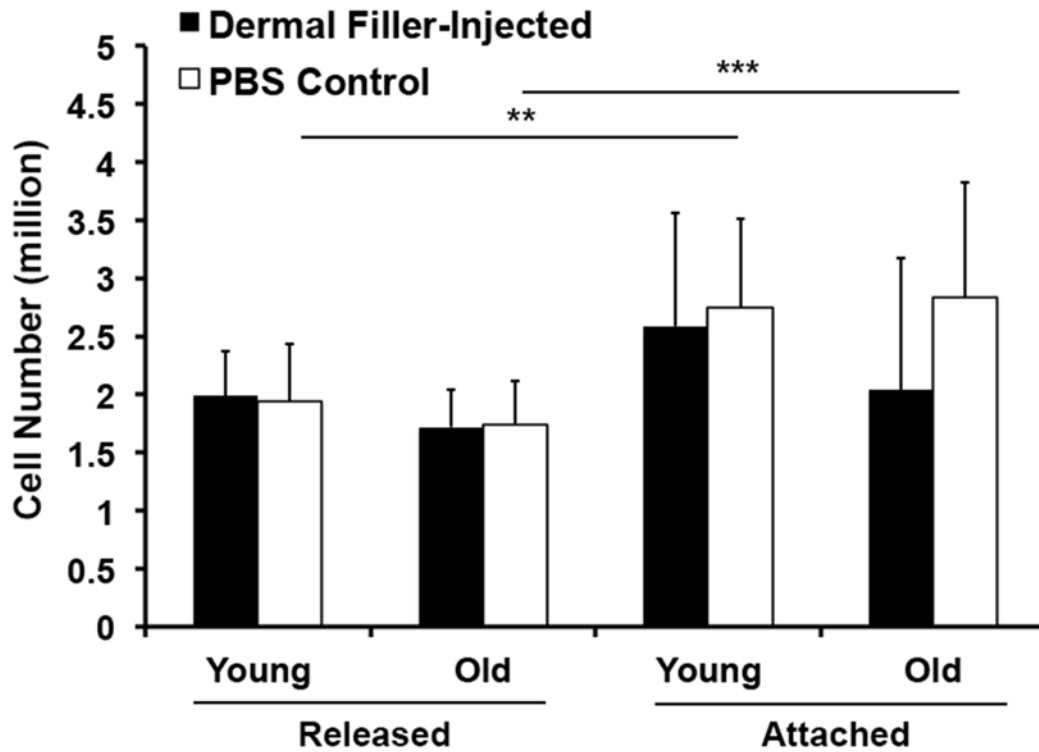
Figure 24. Young and old HDF number in released and attached fibrin gels three weeks after treatment with dermal filler.

4.3.4. Collagen Expression and Synthesis

Having found that the injection of dermal filler and enhancement of mechanical stimulation promotes a change in the expression of mechanosensitive proteins, we next studied the effect of this stimulation on inducing collagen expression and synthesis. Using the same models of healthy and aged dermis we began by studying changes in gene expression levels of collagen type I alpha I (COL1A1). A significant upregulation ($p<0.001$) in collagen expression was observed in both young and old HDFs cultured within released collagen gels five minutes after dermal filler injection (Fig 25A, and B). Stimulation caused by the injection of the filler was not enough to significantly sustain

82

this effect for 24 hours. There may be two reasons for this behavior: the tension caused by the swelling HA within the stress-relieved collagen gel was not sufficient to sustain a large enough increase in collagen expression or the HA began to diffuse out of the gel after injection.
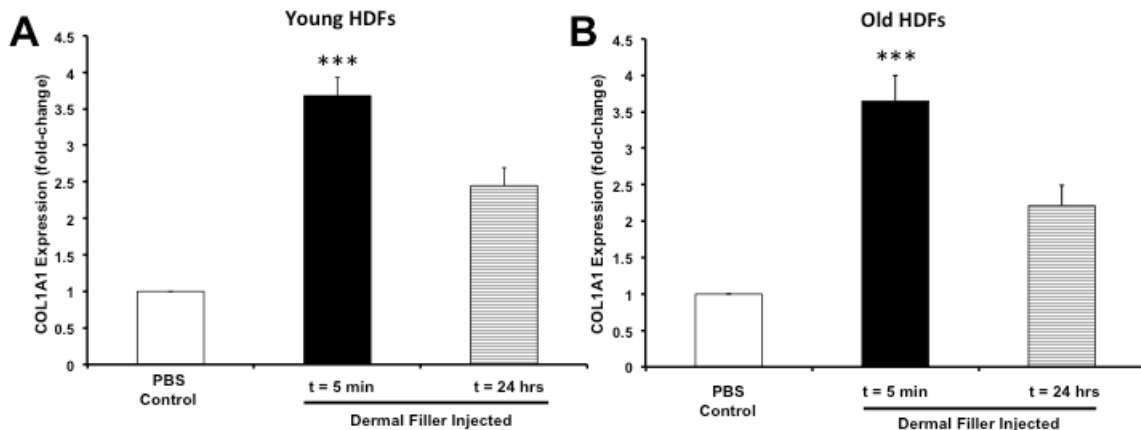
Figure 25. Collagen expression in dermal filler-injected released collagen gels. Gene expression of the collagen type I alpha 1 encoding gene, COL1A1 using qPCR five minutes and 24 hours after injection of dermal filler into a released collagen gel seeded with A) young HDFs (n=14, ***p<0.001, vs. PBS injection) or B) old HDFs (n=9, ***p<0.001, vs. PBS injection).

Following injection of dermal filler into attached collagen gel models, we found a significant increase in COL1A1 in young HDFs 24 hours after treatment (Fig. 26A). When cultured within an environment that provided the mechanical support for cells to achieve homeostatic levels of tension, old HDFs showed no increase in COL1A1 expression five minutes after the dermal filler injection. But, continued swelling of the HA eventually generated a significant increase in COL1A1, observed 24 hours after treatment (Fig. 26B). The fold-change in the expression of COL1A1 in old HDFs, compared to PBS-treated control samples seeded with fibroblasts in the same age group after 24 hours was approximately 4.1, higher than the fold-change observed in young

83

HDFs, which was approximately 3.4. These results indicate that decreased collagen production by aged fibroblasts observed *in vivo* may be a result of a loss of mechanical tension in the dermis. Through the injection of the hydrophilic dermal filler, capable of causing an increase in mechanical stress, normal levels of COL1A1 expression can be restored.
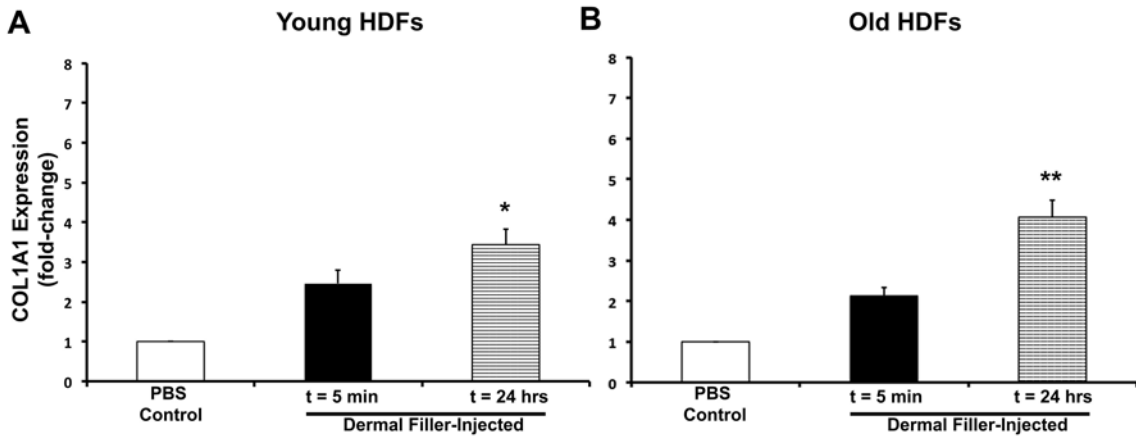
Figure 26. Collagen expression in dermal filler-injected attached collagen gels. Gene expression of the collagen type I alpha 1 encoding gene, COL1A1 analyzed using qPCR five minutes and 24 hours after injection of dermal filler into a released collagen gel seeded with A) young HDFs (n=14, *$p<0.05$, vs. PBS injection) or B) old HDFs (n = 9, **$p<0.01$, vs. PBS injection).

After observing the effect of mechanical stimulation on pre-translational expression of the COL1A1 gene, I evaluated the effect of these changes on the synthesis of collagen. This was studied by quantifying the amount of collagen produced in samples treated with a swelling solution of cross-linked HA dermal filler in released or attached fibrin gels using hydroxyproline as an index for collagen production. In order to account for the effect of cell proliferation on the total amount of collagen produced, cell number was also quantified after a three-week incubation in attached or released fibrin gels, and was used to estimate the amount of collagen produced per cell.

84

Young HDFs produced an average total of 13.6 ± 6.8 µg of collagen when cultured in released fibrin gels and treated with an injection of 1x PBS. The injection of dermal filler did not cause a significant change in the amount of synthesized collagen, as young HDFs produced a total average amount of 12.0 ± 7.0 µg in dermal filler-injected gels (Fig. 27A). No significant difference was found in the amount of collagen produced per cell between control samples (5.9 ± 2.9 pg/cell) and dermal filler-treated samples (6.1 ± 3.0 pg/cell). In released fibrin gels seeded with old HDFs and treated with dermal filler no significant difference in total collagen (13.8 ± 3.1 µg) was observed when compared to PBS-treated controls (13.0 ± 2.4 µg). Collagen produced per cell was approximately 6.4 ± 1.5 pg/cell of collagen in control samples, 21 days after treatment and showed a small up-regulation in collagen synthesis, producing up to 8.0 ± 1.8 pg/cell when treated with an injection of dermal filler (Fig. 27B), though no significant difference was observed.

When cultured in attached fibrin gels, young HDFs produced an average total of 21.9 ± 6.7 µg in PBS controls, and 21.4 ± 5.3 µg when treated with an injection of the dermal filler. Normalized over the average number of cells, young HDFs in control samples produced approximately 8.0 ± 2.3 pg/cell and 8.2 ± 1.6 pg/cell in gels that were treated with the dermal filler. Old HDFs cultured under the same conditions produced an average total of 25.3 ± 4.8 µg of collagen in PBS controls and 24.7 ± 4.6 µg (Fig. 27A). Though no significant differences were observed, old HDFs produced collagen at a rate of 10.4 ± 2.5 ng/cell and slightly increased production to approximately 17.2 ± 8.0 ng/cell in gels treated with an injection of dermal filler (Fig. 27B).

85

Collagen production appeared to be unaffected by age as no differences were observed between age groups. Yet, significant differences ($p<0.05$) were found in the total amount of collagen produced in attached gels as compared to released gels (Fig. 27A), as well as in the amount of collagen produced per cell (Fig. 27B). These results indicate that the expression and synthesis of collagen are dependent on the state of the mechanical environment of the ECM and that this response is not affected by aging in human dermal fibroblasts, but possibly, by the effects of intrinsic and actinic aging on the structural integrity of the dermis. These observations are consistent with the findings of Khorramizadeh *et al*. [159] who demonstrated that collagen production per cell was unaltered by aging in studies conducted on fetal dermal fibroblast and adult human dermal fibroblast monolayers.
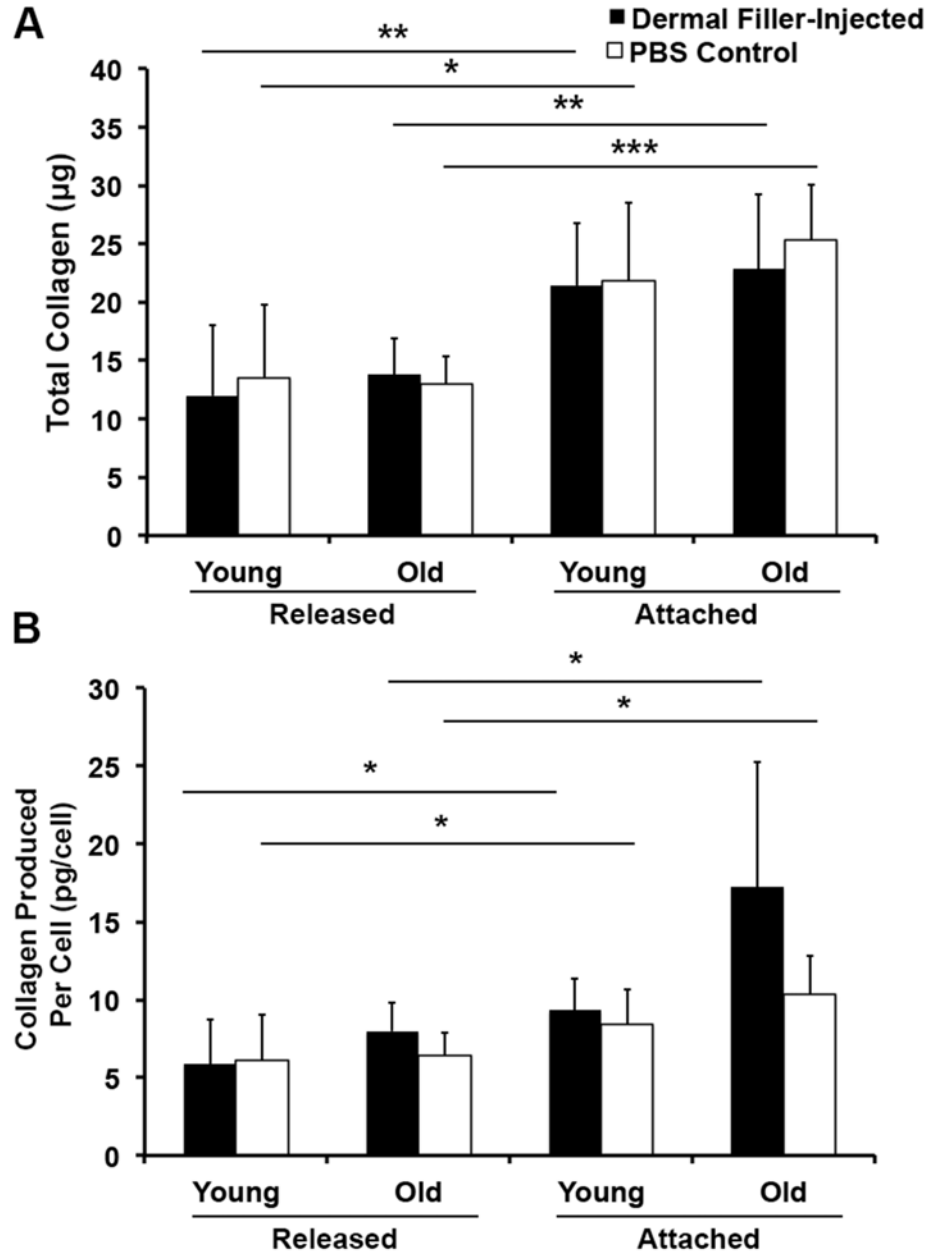
Figure 27. Collagen production in attached and released fibrin gels three weeks after treatment with dermal filler. A) Total collagen produced by young (n = 12, *p < 0.05, and **p < 0.01) and old (n = 9 **p < 0.01, and ***p < 0.001) HDFs cultured in attached and released fibrin gels. B) Collagen produced per cell. (n = 12, *p < 0.05, and **p < 0.01) and old (n = 9 **p < 0.01, and ***p < 0.001)

87

4.3.5. HA Dermal Filler Diffusion

After observing that the injection of the dermal filler did not have significant, lasting effects on collagen synthesis, I hypothesized that the HA was being removed or diffused through the collagen matrix. HA concentration was quantified in samples of DMEM to estimate the amount and rate of diffusion of HA out of the gel and into the medium. With a HA concentration of 24 mg/mL, each 10 µL injection of dermal filler contained 240 µg of HA. During the first 24 hours, approximately 550.8 ± 153.2 ng of HA had diffused out of the gel and into the medium. During the following 48, and 72 hours, the HA found in DMEM was approximately 687.6 ± 214.4 ng, and 504.4 ± 47.4 ng, respectively. HA continued to diffuse out of the gel during the following three weeks, as a cumulative total of approximately 4602.6 ± 278.9 ng of HA was quantified in the DMEM (Fig. 28). This equates to approximately 2% of the total amount of DMEM initially injected into the gel. This amount does not incorporate the HA that may be located in the interstitial space of the collagen gel. Diffusion of HA into the gel and medium may be cause a reduction in the amount of stress generated in the collagen matrix due to HA swelling, and may explain my observations for collagen synthesis in the dermal models used in this study.
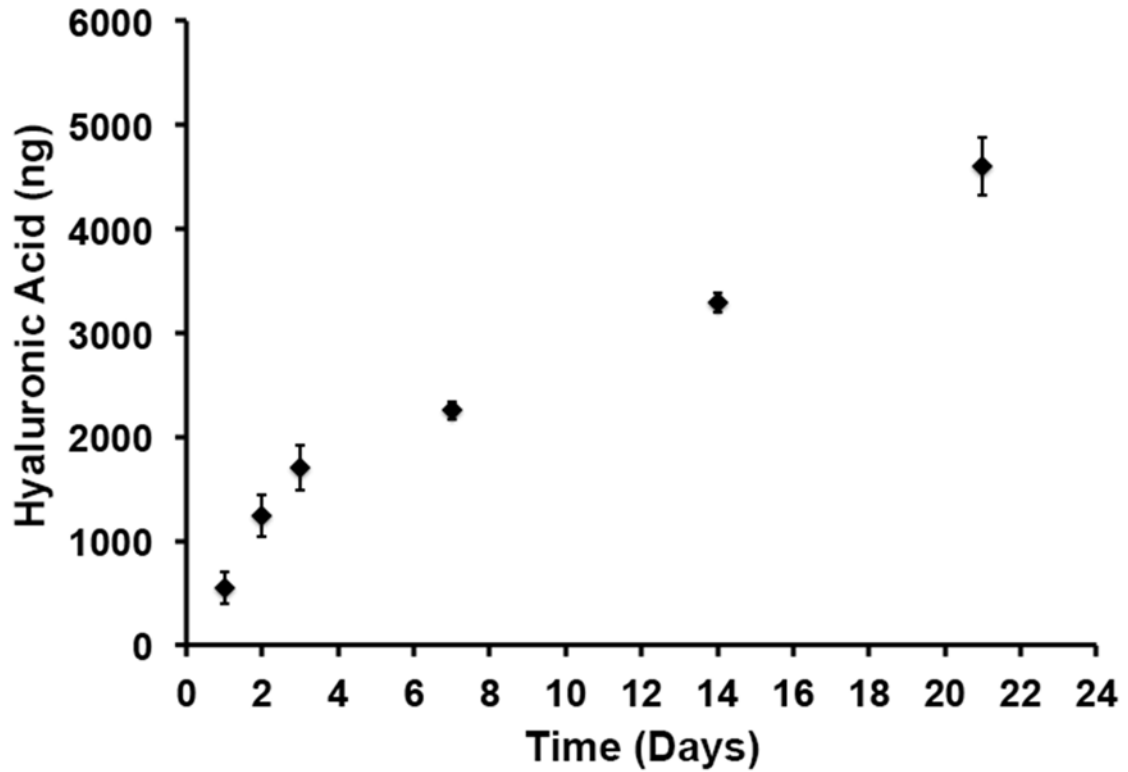
Figure 28. Cumulative amount of HA diffused into medium.

4.4. Discussion

Chronological aging of skin is characterized by drastic changes in the composition and structure of the dermal ECM, such as thinning of collagen fiber bundles [160], and a decrease in collagen and glycosaminoglycan synthesis. The mechanical interaction between fibroblasts and collagen fibrils is essential in regulating cell function and maintaining the structure and function of the dermal ECM [12, 161]. The depletion and destruction of structural proteins, a phenomenon characteristic of intrinsic and actinic aging may be responsible for the loss of mechanical communication between fibroblasts and the ECM. The combination of the inherent changes in cell behavior as we age and alterations in the mechanical feedback loop between cells and the ECM may lead to the

89

development of common signs of aging in skin such as wrinkle formation, increased fragility, delayed wound healing, and decreased elasticity, normally observed in individuals over the age of 60. In the study presented in this chapter, I have explored the role of mechanical integrity and stimulation in inducing the expression of genes responsible for fibroblast regulation and collagen synthesis in young and old HDFs.

Many studies have explored the biochemical effects of HA on fibroblast adhesion, migration, proliferation, and protein synthesis. Its use as a dermal filler is based on its space-filling capability and its biocompatibility. But the long-term *in vivo* effects of cross-linked HA-based dermal filler injections on the activation of collagen synthesis, and changes in fibroblast morphology in the aged dermis suggest that alterations to the mechanical environment caused by its hydrophilicity and swelling capability, or the combination of this and its biochemical activity, may be the factors responsible for this response. In order to test this hypothesis, I began to characterize the swelling behavior of a commercially available 24 mg/mL HA-based dermal filler from Allergan, Inc. by performing osmotic pressure tests. When placed in dialysis tubing and exposed to purified water, the dermal filler increased the volume of fluid in the tubing by approximately 200%. Fluid absorption, governed by the Donnan effect, was decreased when the filler was exposed to an isotonic solution. Exposure to 1x PBS resulted in an increase in volume of fluid in the tubing of 31%. The volume expansion of the filler that occurs due to the ability of cross-linked HA to imbibe large amounts of water, resulted in mechanical stretching and deformation of the fibrous matrix when it was injected into a collagen gel. These deformations introduced a state of stress that was estimated to be approximately 20.7 Pa, and incited behavioral responses in resident HDFs.

90

The Rho/ROCK pathway is a mechanoresponsive pathway that controls actin cytoskeletal organization [162], force traction generation [163], and the formation of actin stress fibers [164]. Few studies have explored the effects of intrinsic aging and the altered structure of the dermis on HDF mechanosensitivity and contractility. In this study, HDFs responded to the injection of the dermal filler by changing the expression of genes that encode for key regulators of the Rho/ROCK pathway in a manner that was dependent on the initial state of tension in the collagen-based *in vitro* model of the dermis. A large increase in the expression of RhoA, ROCK1, and ROCK2 was observed five minutes after injection of the dermal filler in released collagen gels that were cultured under low tension in both young and old age groups. This initial increase may have been caused by mechanical stretching of the collagen matrix as the filler displaced collagen fibers, generating a large, sudden change in the state of stress sensed by surrounding cells. Given the low state of tension that normally characterizes the released collagen gel model, increased stress caused by continued swelling of the dermal filler was not sufficient to cause a significant, lasting effect on the expression of RhoA, ROCK1, and ROCK2 coding genes nor on the expression and synthesis of collagen.

Young HDFs cultured in attached gels demonstrated a sustained response to the behavior of the filler up to 24 hours after injection by maintaining an elevated expression of RhoA, ROCK1, and ROCK2. This response was also accompanied by an increase in the expression of COL1A1, although the stimulation was not sufficient to induce a lasting effect on collagen synthesis. By providing a more stable network that allowed for the generation of endogenous tension and enabled fibroblast connectivity to the collagen ECM, mechanical stimulation through the injection of the hydrophilic dermal filler

91

stimulated fibroblast contractility by increasing the expression of RhoA, ROCK1, and ROCK2. This response was not observed in old HDFs. Injection of the dermal filler into attached models of the dermis resulted in no significant change in the expression of RhoA, ROCK1, or ROCK2 in old HDFs. Aged dermal fibroblasts are characterized by a collapsed morphology, and a rounded shape that differs from the extended shape of fibroblasts in young skin. A disruption in function of the Rho/ROCK pathway may be responsible for the collapsed shape, and reduced ability of the aged dermal fibroblast to maintain structural support of the dermal ECM. These observations are consistent with studies conducted by Kono *et al*., who found that adult fibroblasts exhibited a reduced contractile activity as compared to fibroblasts in childhood [165]. Another study conducted by Fujimura *et al*. correlated the decrease in adult mouse fibroblast contractility to decreased synthesis of ROCK1, and ROCK2 proteins [166]. Results obtained in this study may suggest impairment in the regulation of fibroblast contractility, and actin polymerization resulting from the effects of aging. But, further studies would have to be conducted in order to clearly understand the nature and mechanism of this alteration. Such studies would involve quantification of individual and collective fibroblast contractility, quantification of synthesis and activity of RhoA, ROCK1, and ROCK2 proteins and their effect on the phosphorylation of MLC, and polymerization of actin stress fiber formation in aged fibroblasts.

Interestingly, mechanical stimulation introduced by the filler resulted in an elevation in the expression of COL1A1 that was sustained up to 24 hours after treatment. Furthermore, although the injection of the dermal filler did not promote increased collagen synthesis when compared to PBS-treated control samples, I found that old HDFs

92

were capable of synthesizing collagen at a similar rate as young HDFs. Culturing old HDFs in attached fibrin gels also resulted in an increase in the rate of collagen production per cell, as was observed in young HDFs when compared to collagen synthesis in released gels. Similarly, culturing young HDFs in released fibrin gels that provided a low-tension environment, Although a gradual decrease in collagen production has become a characteristic staple of chronologically aged skin, the fall-off in *de novo* collagen is most evident when skin ECM is damaged and broken down by an increase in MMP production [136]. This seems to indicate that although there may be inherent effects of aging on the cell's ability to compositionally remodel the ECM, the lack of structural support and the absence of mechanical tension play an important role in deactivating ECM synthesis. These results suggest that impaired collagen synthesis in the dermis, normally associated with aging, is caused by a loss of structural stability in the dermis and is not a result of inherent changes in cell behavior caused by intrinsic aging. Although the synergistic activity of fibroblast mechanosensitivity and contractility mediated by the Rho/ROCK pathway and TGF-β1 have been implicated in the activation of collagen synthesis, our results may indicate that fibroblast synthetic activity may not be solely dependent on the Rho/ROCK pathway. Members of the mitogen-activated protein kinase (MAPK) family have been found to be involved in collagen gene regulation [167, 168] and have been shown to interact with TGF-β to control ECM deposition [169]. Further experimentation will involve exploring the role of MAPK and the ERK pathway in modulating collagen synthesis during the aging process.

Although changes in collagen expression and synthesis in aged fibroblasts were associated to the state of the mechanical environment by use of released and attached

93

models of the dermis, no significant, lasting effects were observed due to the injection of a hydrophilic HA-based dermal filler. These results do not concur with in vivo studies that have demonstrated a significant increase in collagen production around areas of the dermis treated with similar formulations of HA-based dermal fillers [152, 154, 155]. By quantifying the presence of HA in samples of medium acquired from dermal filler-injected gels, I found that HA from the filler was diffusing out of the collagen gels within days after treatment. Diffusion of the dermal filler through the porosity of the collagen gel prevents it from continuously mechanically deforming the surrounding matrix by increasing its volume through water absorption. These results lead me to conclude that the models of the dermis developed for this study were not the most suitable for the characterization of long-lasting effects of localized mechanical stimulation via the injection of a hydrophilic, HA-based dermal filler. To improve this *in vitro* model, collagen concentration should be increased to better simulate the protein density in the dermis and ensure stability of the filler at the site of injection.

Furthermore, further improvements can be incorporated in the preparation of released collagen gels to be used as models representative of the environment of the aged dermis. The aged dermis is characterized by a partially degraded and broken down collagen network that causes a decrease in homeostatic tension. Although the released gel provided a low-stress level environment similar to what is observed in the aged dermis, it still consists of an intact collagen network that affords sites for cell attachment. Treatment of the gels with matrix-degrading proteins, such as MMP-1, could allow for the incorporation of the effects of the loss of binding sites and integrity of the collagen fibers on fibroblast quiescence and response to exogenous mechanical stimulation.

94

Despite these limitations, the use of this model allowed me to reveal age-related differences in the synthesis and expression of ECM proteins, and of genes that modulate cell contractility and force generation in human dermal fibroblasts, and their relationship to the mechanical environment of the ECM.

CHAPTER 5: CONCLUSIONS AND FUTURE AIMS

Mechanical forces play an essential role in controlling fibroblast behavior and their ability to regenerate and remodel the ECM of cutaneous tissue. The studies presented in this dissertation provide evidence that demonstrate the effects of multi-scale mechanical interactions between fibroblasts and the ECM on structural and compositional remodeling of wounds and the aged dermis.

The presence of mechanical constraints surrounding *in vitro* models of the wound differentially control the patterns of deformation of fiber alignment generated in the fibrin clot caused by fibroblast contractility. These short-term structural changes have a great impact on the long-term synthesis of ECM-remodeling proteins such as collagen type I, MMP-1, MMP-2, and MMP-9. Dermal fibroblasts cultured on fibrin gels subjected to fixed boundary conditions secreted 21% more collagen type I than those cultured on fibrin gels cultured under free boundary conditions. Demonstrating that the differences in structural reorganization that develop as a result of macroscopic features of the ECM such as geometry, and boundary conditions can determine the extent of compositional remodeling and the outcome of cell-mediated tissue regeneration.

Future work for this project will involve exploring the effects of localized mechanical stimulation on altering the overall structure and cell-mediated organization of the ECM. This would be done by introducing local deformations or inducing changes in fiber realignment in close proximity to cell explants after initial structural reorganization has ensued.

96

Experimentation on the effects of mechanical stimulation on the mechanosensitivity and synthetic activity of human dermal fibroblasts from young and old individuals demonstrated that loss of mechanical stability may be responsible, in part, for loss of fibroblast regenerative capabilities with aging. Injection of a hydrophilic HA-based dermal filler into an *in vitro* model of the dermis altered the mechanical environment of the gel by introducing a state of tension. This stimulation which resulted in an increase in the expression of mechanosensitive proteins of the Rho/ROCK pathway that contribute to mechanotransduction, fibroblast contractility and differentiation in young HDFs was not sufficient to elicit a significant response in old HDFs. These results suggest that intrinsic aging may be accompanied by a reduction in fibroblast contractility and traction force generation. Further evaluation of synthesis and activity of RhoA, ROCK1, ROCK2, and MLC would be required in order to validate initial observations of genetic expression and determine the effects of such changes on fibroblast contractility, and mechanosensitivity. Furthermore, changes in collagen synthesis, normally associated with aging, were found to be unaffected by intrinsic changes in fibroblast behavior. Instead, the effects of natural and actinic aging on the structural support of the dermal ECM may be responsible for the loss of mechanical communication between the ECM and adherent fibroblasts. This communication is essential in controlling fibroblast contractility and synthesis, and therefore, their ability to maintain, remodel, and regenerate cutaneous tissue. Such a finding may prove to be valuable in the investigation of delayed wound healing, loss of strength, and changes in dermal structure and composition in aged individuals.

97

Future work will involve improvement of the *in vitro* model used to represent the aged dermis by increasing protein concentration to decrease the porosity of the gel and prevent diffusion of the injected HA-based dermal filler out of the gel. Once we can characterize the long-term effects of the dermal filler, ensuring its stability, we can then attempt to isolate the mechanical effects of HA swelling on cell behavior from the biochemical effects that may develop from fibroblast-HA interactions. To better simulate the broken-down collagenous network that makes up the environment of the aged dermis, collagen gels would also be treated with matrix-degrading proteins, to minimize fibroblast-matrix interactions by reducing sites for adhesion.

The results for the studies conducted for the completion of this thesis support the idea that mechanical signaling and the dynamic mechanical interplay between cells and the ECM are essential in controlling tissue remodeling and regeneration processes. It also provides a basic framework for better understanding these mechanisms and in identifying the pathways involved in mechanotransduction between cells and cutaneous tissue and how these may affect normal cell behavior during wound healing and aging.

REFERENCES

1. Naylor, E.C., R.E. Watson, and M.J. Sherratt, *Molecular aspects of skin ageing.* Maturitas, 2011. **69**(3): p. 249-56.
2. Gabbiani, G., *The myofibroblast in wound healing and fibrocontractive diseases.* J Pathol, 2003. **200**(4): p. 500-3.
3. Porter, K.E. and N.A. Turner, *Cardiac fibroblasts: at the heart of myocardial remodeling.* Pharmacology & therapeutics, 2009. **123**(2): p. 255-278.
4. Desmouliere, A., I.A. Darby, and G. Gabbiani, *Normal and pathologic soft tissue remodeling: role of the myofibroblast, with special emphasis on liver and kidney fibrosis.* Lab Invest, 2003. **83**(12): p. 1689-707.
5. Lee, C.H., et al., *CTGF directs fibroblast differentiation from human mesenchymal stem/stromal cells and defines connective tissue healing in a rodent injury model.* J Clin Invest, 2010. **120**(9): p. 3340-9.
6. Lee, C.H., E.K. Moioli, and J.J. Mao. *Fibroblastic differentiation of human mesenchymal stem cells using connective tissue growth factor.* in *Engineering in Medicine and Biology Society, 2006. EMBS'06. 28th Annual International Conference of the IEEE.* 2006. IEEE.
7. Alberts, B., et al., *Fibroblasts and their transformations: the connective-tissue cell family.* 2002.
8. Eastwood, M., D. McGrouther, and R. Brown, *Fibroblast responses to mechanical forces.* Proceedings of the Institution of Mechanical Engineers, Part H: Journal of Engineering in Medicine, 1998. **212**(2): p. 85-92.
9. Kessler, D., et al., *Fibroblasts in mechanically stressed collagen lattices assume a "synthetic" phenotype.* Journal of Biological Chemistry, 2001. **276**(39): p. 36575-36585.
10. De Jesus, A.M., M. Aghvami, and E.A. Sander, *A Combined In Vitro Imaging and Multi-Scale Modeling System for Studying the Role of Cell Matrix Interactions in Cutaneous Wound Healing.* PloS one, 2016. **11**(2): p. e0148254.
11. Varani, J., et al., *Decreased collagen production in chronologically aged skin: roles of age-dependent alteration in fibroblast function and defective mechanical stimulation.* The American journal of pathology, 2006. **168**(6): p. 1861-1868.
12. Fisher, G.J., J. Varani, and J.J. Voorhees, *Looking older: fibroblast collapse and therapeutic implications.* Archives of dermatology, 2008. **144**(5): p. 666-672.
13. Cacou, C. and I.F. Muir, *Effects of plane mechanical forces in wound healing in humans.* J R Coll Surg Edinb, 1995. **40**(1): p. 38-41.
14. Wong, V.W., et al., *Focal adhesion kinase links mechanical force to skin fibrosis via inflammatory signaling.* Nat Med, 2012. **18**(1): p. 148-52.
15. MacKenna, D., S.R. Summerour, and F.J. Villarreal, *Role of mechanical factors in modulating cardiac fibroblast function and extracellular matrix synthesis.* Cardiovasc Res, 2000. **46**(2): p. 257-63.
16. Eckes, B., et al., *Fibroblast-matrix interactions in wound healing and fibrosis.* Matrix biology, 2000. **19**(4): p. 325-332.
17. Agha, R., et al., *A review of the role of mechanical forces in cutaneous wound healing.* Journal of Surgical Research, 2011. **171**(2): p. 700-708.
18. Eming, S.A., *Biology of Wound Healing*, in *Dermatology*, J.L. Bolognia, Jorizzo, J.L., Schaffer, J.V., Editor. 2012, Elsevier Saunders: Philadephia.
19. Clark, R., *The molecular and cellular biology of wound repair*. 2013: Springer Science & Business Media.
20. McPherson, J.M. and K.A. Piez, *Collagen in dermal wound repair*, in *The molecular and cellular biology of wound repair*. 1988, Springer. p. 471-496.

21. Schultz, G.S. and A. Wysocki, *Interactions between extracellular matrix and growth factors in wound healing.* Wound repair and regeneration, 2009. **17**(2): p. 153-162.

22. Gabbiani, G., G. Ryan, and G. Majno, *Presence of modified fibroblasts in granulation tissue and their possible role in wound contraction.* Experientia, 1971. **27**(5): p. 549-550.

23. Skalli, O. and G. Gabbiani, *The biology of the myofibroblast relationship to wound contraction and fibrocontractive diseases*, in *The molecular and cellular biology of wound repair.* 1988, Springer. p. 373-402.

24. Ohara, H., et al., *Collagen-derived dipeptide, proline-hydroxyproline, stimulates cell proliferation and hyaluronic acid synthesis in cultured human dermal fibroblasts.* The Journal of dermatology, 2010. **37**(4): p. 330-338.

25. Diegelmann, R.F., I.K. Cohen, and B.J. McCoy, *Growth kinetics and collagen synthesis of normal skin, normal scar and keloid fibroblasts in vitro.* Journal of cellular physiology, 1979. **98**(2): p. 341-346.

26. LeRoy, E.C., *Increased Collagen Synthesis by Scleroderma Skin Fibroblasts in Vitro a Possible Defect in the Regulation or Activation of the Scleroderma Fibroblast.* Journal of Clinical Investigation, 1974. **54**(4): p. 880.

27. Verhaegen, P.D., et al., *Differences in collagen architecture between keloid, hypertrophic scar, normotrophic scar, and normal skin: an objective histopathological analysis.* Wound Repair and Regeneration, 2009. **17**(5): p. 649-656.

28. Aarabi, S., et al., *Mechanical load initiates hypertrophic scar formation through decreased cellular apoptosis.* The FASEB Journal, 2007. **21**(12): p. 3250-3261.

29. Lu, F., et al., *Microdeformation of three-dimensional cultured fibroblasts induces gene expression and morphological changes.* Ann Plast Surg, 2011. **66**(3): p. 296-300.

30. DeBiasio, R., et al., *Five-parameter fluorescence imaging: wound healing of living Swiss 3T3 cells.* J Cell Biol, 1987. **105**(4): p. 1613-22.

31. Fronza, M., et al., *Determination of the wound healing effect of Calendula extracts using the scratch assay with 3T3 fibroblasts.* J Ethnopharmacol, 2009. **126**(3): p. 463-7.

32. Walter, M.N., et al., *Mesenchymal stem cell-conditioned medium accelerates skin wound healing: an in vitro study of fibroblast and keratinocyte scratch assays.* Exp Cell Res, 2010. **316**(7): p. 1271-81.

33. Takei, T., et al., *Effect of strain on human keratinocytes in vitro.* J Cell Physiol, 1997. **173**(1): p. 64-72.

34. Zarkoob, H., et al., *Substrate Stiffness Affects Human Keratinocyte Colony Formation.* Cell Mol Bioeng, 2015. **8**(1): p. 32-50.

35. Bell, E., B. Ivarsson, and C. Merrill, *Production of a tissue-like structure by contraction of collagen lattices by human fibroblasts of different proliferative potential in vitro.* Proceedings of the National Academy of Sciences, 1979. **76**(3): p. 1274-1278.

36. Montesano, R. and L. Orci, *Transforming growth factor beta stimulates collagen-matrix contraction by fibroblasts: implications for wound healing.* Proceedings of the National Academy of Sciences, 1988. **85**(13): p. 4894-4897.

37. Grinnell, F., *Mini-Review on the Cellular Mechanisms of Disease Fibroblasts, Myofibroblasts, and Wound Contraction.* 1994.

38. Carlson, M.A. and M.T. Longaker, *The fibroblast-populated collagen matrix as a model of wound healing: A review of the evidence.* Wound Repair and Regeneration, 2004. **12**(2): p. 134-147.

100

39. Rhee, S., C.H. Ho, and F. Grinnell, *Promigratory and procontractile growth factor environments differentially regulate cell morphogenesis.* Exp Cell Res, 2010. **316**(2): p. 232-44.

40. Rouillard, A.D. and J.W. Holmes, *Mechanical boundary conditions bias fibroblast invasion in a collagen-fibrin wound model.* Biophysical journal, 2014. **106**(4): p. 932-943.

41. Clark, J.A., J.C. Cheng, and K.S. Leung, *Mechanical properties of normal skin and hypertrophic scars.* Burns, 1996. **22**(6): p. 443-6.

42. Lavker, R.M., P. Zheng, and G. Dong, *Aged skin: a study by light, transmission electron, and scanning electron microscopy.* Journal of investigative dermatology, 1987. **88**: p. 44-51.

43. Fligiel, S.E., et al., *Collagen degradation in aged/photodamaged skin in vivo and after exposure to matrix metalloproteinase-1 in vitro.* Journal of Investigative Dermatology, 2003. **120**(5): p. 842-848.

44. Verzijl, N., et al., *Effect of collagen turnover on the accumulation of advanced glycation end products.* J Biol Chem, 2000. **275**(50): p. 39027-31.

45. Smith-Mungo, L.I. and H.M. Kagan, *Lysyl oxidase: properties, regulation and multiple functions in biology.* Matrix biology, 1998. **16**(7): p. 387-398.

46. Xia, W., et al., *Expression of catalytically active matrix metalloproteinase-1 in dermal fibroblasts induces collagen fragmentation and functional alterations that resemble aged human skin.* Aging cell, 2013. **12**(4): p. 661-671.

47. Fringer, J. and F. Grinnell, *Fibroblast quiescence in floating or released collagen matrices: contribution of the ERK signaling pathway and actin cytoskeletal organization.* J Biol Chem, 2001. **276**(33): p. 31047-52.

48. Nakagawa, S., P. Pawelek, and F. Grinnell, *Extracellular matrix organization modulates fibroblast growth and growth factor responsiveness.* Experimental cell research, 1989. **182**(2): p. 572-582.

49. Langholz, O., et al., *Collagen and collagenase gene expression in three-dimensional collagen lattices are differentially regulated by alpha 1 beta 1 and alpha 2 beta 1 integrins.* The Journal of Cell Biology, 1995. **131**(6): p. 1903-1915.

50. Grinnell, F., et al., *Release of mechanical tension triggers apoptosis of human fibroblasts in a model of regressing granulation tissue.* Experimental cell research, 1999. **248**(2): p. 608-619.

51. Maeda, T., et al., *Conversion of mechanical force into TGF-β-mediated biochemical signals.* Current Biology, 2011. **21**(11): p. 933-941.

52. Moustakas, A. and C.H. Heldin, *Dynamic control of TGF-beta signaling and its links to the cytoskeleton.* FEBS Lett, 2008. **582**(14): p. 2051-65.

53. Grinnell, F., *Fibroblast biology in three-dimensional collagen matrices.* Trends in cell biology, 2003. **13**(5): p. 264-269.

54. Glaser, B.M., A. Cardin, and B. Biscoe, *Proliferative vitreoretinopathy. The mechanism of development of vitreoretinal traction.* Ophthalmology, 1987. **94**(4): p. 327-32.

55. Fluck, J., et al., *Normal human primary fibroblasts undergo apoptosis in three-dimensional contractile collagen gels.* J Invest Dermatol, 1998. **110**(2): p. 153-7.

56. Hinz, B., *The myofibroblast: paradigm for a mechanically active cell.* J Biomech, 2010. **43**(1): p. 146-55.

57. Hinz, B., et al., *Mechanical tension controls granulation tissue contractile activity and myofibroblast differentiation.* Am J Pathol, 2001. **159**(3): p. 1009-20.

58. Vaughan, M.B., E.W. Howard, and J.J. Tomasek, *Transforming growth factor-beta1 promotes the morphological and functional differentiation of the myofibroblast.* Exp Cell Res, 2000. **257**(1): p. 180-9.

101

59.   Sumi, T., K. Matsumoto, and T. Nakamura, *Specific activation of LIM kinase 2 via phosphorylation of threonine 505 by ROCK, a Rho-dependent protein kinase.* Journal of Biological Chemistry, 2001. **276**(1): p. 670-676.
60.   Akhmetshina, A., et al., *Rho-associated kinases are crucial for myofibroblast differentiation and production of extracellular matrix in scleroderma fibroblasts.* Arthritis Rheum, 2008. **58**(8): p. 2553-64.
61.   Haudek, S.B., et al., *Rho kinase-1 mediates cardiac fibrosis by regulating fibroblast precursor cell differentiation.* Cardiovascular research, 2009. **83**(3): p. 511-518.
62.   Schram, K., et al., *Regulation of MT1-MMP and MMP-2 by leptin in cardiac fibroblasts involves Rho/ROCK-dependent actin cytoskeletal reorganization and leads to enhanced cell migration.* Endocrinology, 2011. **152**(5): p. 2037-2047.
63.   Totsukawa, G., et al., *Distinct roles of ROCK (Rho-kinase) and MLCK in spatial regulation of MLC phosphorylation for assembly of stress fibers and focal adhesions in 3T3 fibroblasts.* The Journal of cell biology, 2000. **150**(4): p. 797-806.
64.   Chen, M.A. and T.M. Davidson, *Scar management: prevention and treatment strategies.* Curr Opin Otolaryngol Head Neck Surg, 2005. **13**(4): p. 242-7.
65.   Gauglitz, G.G., *Management of keloids and hypertrophic scars: current and emerging options.* Clin Cosmet Investig Dermatol, 2013. **6**: p. 103-14.
66.   Gold, M.H., et al., *Updated international clinical recommendations on scar management: part 1--evaluating the evidence.* Dermatol Surg, 2014. **40**(8): p. 817-24.
67.   Levinson, H., *A Paradigm of Fibroblast Activation and Dermal Wound Contraction to Guide the Development of Therapies for Chronic Wounds and Pathologic Scars.* Adv Wound Care (New Rochelle), 2013. **2**(4): p. 149-159.
68.   Aarabi, S., M.T. Longaker, and G.C. Gurtner, *Hypertrophic scar formation following burns and trauma: new approaches to treatment.* PLoS Med, 2007. **4**(9): p. e234.
69.   Ogawa, R., *Mechanobiology of scarring.* Wound Repair Regen, 2011. **19 Suppl 1**: p. s2-9.
70.   Duscher, D., et al., *Mechanotransduction and fibrosis.* J Biomech, 2014. **47**(9): p. 1997-2005.
71.   Yagmur, C., et al., *Mechanical receptor-related mechanisms in scar management: a review and hypothesis.* Plast Reconstr Surg, 2010. **126**(2): p. 426-34.
72.   Atkinson, J.A., et al., *A randomized, controlled trial to determine the efficacy of paper tape in preventing hypertrophic scar formation in surgical incisions that traverse Langer's skin tension lines.* Plast Reconstr Surg, 2005. **116**(6): p. 1648-56; discussion 1657-8.
73.   Akaishi, S., et al., *The tensile reduction effects of silicone gel sheeting.* Plast Reconstr Surg, 2010. **126**(2): p. 109e-11e.
74.   Evans, N.D., et al., *Epithelial mechanobiology, skin wound healing, and the stem cell niche.* J Mech Behav Biomed Mater, 2013. **28**: p. 397-409.
75.   Hinz, B. and G. Gabbiani, *Mechanisms of force generation and transmission by myofibroblasts.* Curr Opin Biotechnol, 2003. **14**(5): p. 538-46.
76.   Eastwood, M., et al., *Effect of precise mechanical loading on fibroblast populated collagen lattices: morphological changes.* Cell Motil Cytoskeleton, 1998. **40**(1): p. 13-21.
77.   Kessler-Becker, D., T. Krieg, and B. Eckes, *Expression of pro-inflammatory markers by human dermal fibroblasts in a three-dimensional culture model is mediated by an autocrine interleukin-1 loop.* Biochem J, 2004. **379**(Pt 2): p. 351-8.

78.   Derderian, C.A., et al., *Mechanical strain alters gene expression in an in vitro model of hypertrophic scarring.* Ann Plast Surg, 2005. **55**(1): p. 69-75; discussion 75.

79.   Achterberg, V.F., et al., *The nano-scale mechanical properties of the extracellular matrix regulate dermal fibroblast function.* J Invest Dermatol, 2014. **134**(7): p. 1862-72.

80.   Aarabi, S., et al., *Mechanical load initiates hypertrophic scar formation through decreased cellular apoptosis.* FASEB J, 2007. **21**(12): p. 3250-61.

81.   Gurtner, G.C., et al., *Improving cutaneous scar formation by controlling the mechanical environment: large animal and phase I studies.* Ann Surg, 2011. **254**(2): p. 217-25.

82.   Wong, V.W., et al., *Pushing back: wound mechanotransduction in repair and regeneration.* J Invest Dermatol, 2011. **131**(11): p. 2186-96.

83.   Wong, V.W., et al., *A Mechanomodulatory Device to Minimize Incisional Scar Formation.* Adv Wound Care (New Rochelle), 2013. **2**(4): p. 185-194.

84.   Blackstone, B.N. and H.M. Powell, *Morphogenesis and Biomechanics of Engineered Skin Cultured Under Uniaxial Strain.* Adv Wound Care (New Rochelle), 2012. **1**(2): p. 69-74.

85.   Syedain, Z.H., J.S. Weinberg, and R.T. Tranquillo, *Cyclic distension of fibrin-based tissue constructs: evidence of adaptation during growth of engineered connective tissue.* Proc Natl Acad Sci U S A, 2008. **105**(18): p. 6537-42.

86.   Sander, E.A., V.H. Barocas, and R.T. Tranquillo, *Initial fiber alignment pattern alters extracellular matrix synthesis in fibroblast-populated fibrin gel cruciforms and correlates with predicted tension.* Ann Biomed Eng, 2011. **39**(2): p. 714-29.

87.   Rouillard, A.D. and J.W. Holmes, *Mechanical boundary conditions bias fibroblast invasion in a collagen-fibrin wound model.* Biophys J, 2014. **106**(4): p. 932-43.

88.   Tranquillo, R.T., *Self-organization of tissue-equivalents: the nature and role of contact guidance.* Biochem Soc Symp, 1999. **65**: p. 27-42.

89.   Grassl, E.D., T.R. Oegema, and R.T. Tranquillo, *Fibrin as an alternative biopolymer to type-I collagen for the fabrication of a media equivalent.* J Biomed Mater Res, 2002. **60**(4): p. 607-12.

90.   Manwaring, M.E., J.F. Walsh, and P.A. Tresco, *Contact guidance induced organization of extracellular matrix.* Biomaterials, 2004. **25**(17): p. 3631-8.

91.   De Jesus, A.M. and E.A. Sander, *Observing and quantifying fibroblast-mediated fibrin gel compaction.* J Vis Exp, 2014(83): p. e50918.

92.   Kiyono, T., et al., *Both Rb/p16INK4a inactivation and telomerase activity are required to immortalize human epithelial cells.* Nature, 1998. **396**(6706): p. 84-8.

93.   Yuan Ye, K., K.E. Sullivan, and L.D. Black, *Encapsulation of cardiomyocytes in a fibrin hydrogel for cardiac tissue engineering.* J Vis Exp, 2011(55).

94.   Vader, D., et al., *Strain-induced alignment in collagen gels.* PLoS One, 2009. **4**(6): p. e5902.

95.   Hartmann, A., P. Boukamp, and P. Friedl, *Confocal reflection imaging of 3D fibrin polymers.* Blood Cells Mol Dis, 2006. **36**(2): p. 191-3.

96.   Chaubaroux, C., et al., *Cell Alignment Driven by Mechanically Induced Collagen Fiber Alignment in Collagen/Alginate Coatings.* Tissue Eng Part C Methods, 2015.

97.   Provenzano, P.P., et al., *Contact guidance mediated three-dimensional cell migration is regulated by Rho/ROCK-dependent matrix reorganization.* Biophys J, 2008. **95**(11): p. 5374-84.

98.   Raghupathy, R., et al., *Identification of regional mechanical anisotropy in soft tissue analogs.* J Biomech Eng, 2011. **133**(9): p. 091011.

99.   Sander, E.A. and V.H. Barocas, *Comparison of 2D fiber network orientation measurement methods.* J Biomed Mater Res A, 2009. **88**(2): p. 322-31.

100. Fernandez, P. and A.R. Bausch, *The compaction of gels by cells: a case of collective mechanical activity.* Integrative Biology, 2009. **1**(3): p. 252-259.

101. Krishnan, L., et al., *Effect of mechanical boundary conditions on orientation of angiogenic microvessels.* Cardiovasc Res, 2008. **78**(2): p. 324-32.

102. Thomopoulos, S., G.M. Fomovsky, and J.W. Holmes, *The development of structural and mechanical anisotropy in fibroblast populated collagen gels.* J Biomech Eng, 2005. **127**(5): p. 742-50.

103. Dickinson, R.B., S. Guido, and R.T. Tranquillo, *Biased Cell-Migration of Fibroblasts Exhibiting Contact Guidance in Oriented Collagen Gels.* Annals of Biomedical Engineering, 1994. **22**(4): p. 342-356.

104. Miron-Mendoza, M., J. Seemann, and F. Grinnell, *The differential regulation of cell motile activity through matrix stiffness and porosity in three dimensional collagen matrices.* Biomaterials, 2010. **31**(25): p. 6425-35.

105. Engler, A., et al., *Substrate compliance versus ligand density in cell on gel responses.* Biophysical Journal, 2004. **86**(1): p. 617-628.

106. Hall, D.A. and D.S. Jackson, *International review of connective tissue research*. Vol. 10. 2013: Elsevier.

107. Prockop, D.J. and K.I. Kivirikko, *Collagens: molecular biology, diseases, and potentials for therapy.* Annu Rev Biochem, 1995. **64**: p. 403-34.

108. Gelse, K., E. Poschl, and T. Aigner, *Collagens--structure, function, and biosynthesis.* Adv Drug Deliv Rev, 2003. **55**(12): p. 1531-46.

109. Eyden, B., *The myofibroblast: phenotypic characterization as a prerequisite to understanding its functions in translational medicine.* Journal of cellular and molecular medicine, 2008. **12**(1): p. 22-37.

110. Tomasek, J.J., et al., *Myofibroblasts and mechano-regulation of connective tissue remodelling.* Nat Rev Mol Cell Biol, 2002. **3**(5): p. 349-63.

111. Hinz, B., *Formation and function of the myofibroblast during tissue repair.* Journal of Investigative Dermatology, 2007. **127**(3): p. 526-537.

112. Hinz, B., et al., *Alpha-smooth muscle actin expression upregulates fibroblast contractile activity.* Molecular biology of the cell, 2001. **12**(9): p. 2730-2741.

113. Sander, E., V. Barocas, and R. Tranquillo, *Initial fiber alignment pattern alters extracellular matrix synthesis in fibroblast-populated fibrin gel cruciforms and correlates with predicted tension.* Annals of biomedical engineering, 2011. **39**(2): p. 714-729.

114. Eto, H., et al., *Therapeutic potential of fibroblast growth factor-2 for hypertrophic scars: upregulation of MMP-1 and HGF expression.* Lab Invest, 2012. **92**(2): p. 214-23.

115. McCarty, S.M. and S.L. Percival, *Proteases and Delayed Wound Healing.* Adv Wound Care (New Rochelle), 2013. **2**(8): p. 438-447.

116. Mauch, C., et al., *Collagenase gene expression in fibroblasts is regulated by a three-dimensional contact with collagen.* FEBS letters, 1989. **250**(2): p. 301-305.

117. Lambert, C.A., et al., *Pretranslational regulation of extracellular matrix macromolecules and collagenase expression in fibroblasts by mechanical forces.* Laboratory investigation; a journal of technical methods and pathology, 1992. **66**(4): p. 444-451.

118. Rolin, G.L., et al., *In vitro study of the impact of mechanical tension on the dermal fibroblast phenotype in the context of skin wound healing.* J Biomech, 2014. **47**(14): p. 3555-61.

119. Yuan, J.S., et al., *Statistical analysis of real-time PCR data.* BMC Bioinformatics, 2006. **7**: p. 85.

120. Derderian, C.A., et al., *Mechanical strain alters gene expression in an in vitro model of hypertrophic scarring.* Annals of plastic surgery, 2005. **55**(1): p. 69-75.
121. Kook, S.H., et al., *Mechanical force induces type I collagen expression in human periodontal ligament fibroblasts through activation of ERK/JNK and AP-1.* Journal of cellular biochemistry, 2009. **106**(6): p. 1060-1067.
122. Webb, K., et al., *Cyclic strain increases fibroblast proliferation, matrix accumulation, and elastic modulus of fibroblast-seeded polyurethane constructs.* Journal of biomechanics, 2006. **39**(6): p. 1136-1144.
123. Sarrazy, V., et al., *Mechanisms of pathological scarring: role of myofibroblasts and current developments.* Wound Repair and Regeneration, 2011. **19**(s1): p. s10-s15.
124. Jelaska, A. and J.H. Korn, *Role of apoptosis and transforming growth factor beta1 in fibroblast selection and activation in systemic sclerosis.* Arthritis Rheum, 2000. **43**(10): p. 2230-9.
125. Costa, A.M., et al., *Mechanical forces induce scar remodeling. Study in non-pressure-treated versus pressure-treated hypertrophic scars.* Am J Pathol, 1999. **155**(5): p. 1671-9.
126. Tuan, T.-L., et al., *In VitroFibroplasia: Matrix Contraction, Cell Growth, and Collagen Production of Fibroblasts Cultured in Fibrin Gels.* Experimental cell research, 1996. **223**(1): p. 127-134.
127. John, J., et al., *Boundary stiffness regulates fibroblast behavior in collagen gels.* Ann Biomed Eng, 2010. **38**(3): p. 658-73.
128. Weinbaum, J.S., J.B. Schmidt, and R.T. Tranquillo, *Combating Adaptation to Cyclic Stretching By Prolonging Activation of Extracellular Signal-Regulated Kinase.* Cell Mol Bioeng, 2013. **6**(3): p. 279-286.
129. Schleicher, E. and O. Wieland, *Specific quantitation by HPLC of protein (lysine) bound glucose in human serum albumin and other glycosylated proteins.* Clinical Chemistry and Laboratory Medicine, 1981. **19**(2): p. 81-88.
130. Fisher, G.J., et al., *Pathophysiology of premature skin aging induced by ultraviolet light.* New England Journal of Medicine, 1997. **337**(20): p. 1419-1429.
131. Fisher, G.J., et al., *Mechanisms of photoaging and chronological skin aging.* Archives of dermatology, 2002. **138**(11): p. 1462-1470.
132. Sephel, G.C. and J.M. Davidson, *Elastin production in human skin fibroblast cultures and its decline with age.* Journal of investigative dermatology, 1986. **86**(3): p. 279-285.
133. Millis, A.J., et al., *Differential expression of metalloproteinase and tissue inhibitor of metalloproteinase genes in aged human fibroblasts.* Experimental cell research, 1992. **201**(2): p. 373-379.
134. Burke, E.M., et al., *Altered transcriptional regulation of human interstitial collagenase in cultured skin fibroblasts from older donors.* Experimental gerontology, 1994. **29**(1): p. 37-53.
135. Ricciarelli, R., et al., *Age-dependent increase of collagenase expression can be reduced by α-tocopherol via protein kinase C inhibition.* Free Radical Biology and Medicine, 1999. **27**(7): p. 729-737.
136. Varani, J., et al., *Vitamin A Antagonizes Decreased Cell Growth and Elevated Collagen-Degrading Matrix Metalloproteinases and Stimulates Collagen Accumulation in Naturally Aged Human Skin1.* Journal of Investigative Dermatology, 2000. **114**(3): p. 480-486.
137. Ghersetich, I., et al., *Hyaluronic acid in cutaneous intrinsic aging.* International journal of dermatology, 1994. **33**(2): p. 119-122.
138. West, D.C., et al., *Angiogenesis induced by degradation products of hyaluronic acid.* Science, 1985. **228**(4705): p. 1324-6.

105

139.   Sattar, A., et al., *Application of angiogenic oligosaccharides of hyaluronan increases blood vessel numbers in rat skin.* J Invest Dermatol, 1994. **103**(4): p. 576-9.
140.   Gao, F., et al., *Hyaluronan oligosaccharides promote excisional wound healing through enhanced angiogenesis.* Matrix Biol, 2010. **29**(2): p. 107-16.
141.   David-Raoudi, M., et al., *Differential effects of hyaluronan and its fragments on fibroblasts: relation to wound healing.* Wound Repair Regen, 2008. **16**(2): p. 274-87.
142.   Ferguson, E.L., et al., *Evaluation of the physical and biological properties of hyaluronan and hyaluronan fragments.* Int J Pharm, 2011. **420**(1): p. 84-92.
143.   Maharjan, A.S., D. Pilling, and R.H. Gomer, *High and low molecular weight hyaluronic acid differentially regulate human fibrocyte differentiation.* PLoS One, 2011. **6**(10): p. e26078.
144.   Nishida, T., et al., *Hyaluronan stimulates corneal epithelial migration.* Exp Eye Res, 1991. **53**(6): p. 753-8.
145.   Moseley, R., R.J. Waddington, and G. Embery, *Hyaluronan and its potential role in periodontal healing.* Dent Update, 2002. **29**(3): p. 144-8.
146.   Bonte, F., *Skin moisturization mechanisms: new data.* Ann Pharm Fr, 2011. **69**(3): p. 135-41.
147.   Papakonstantinou, E., M. Roth, and G. Karakiulakis, *Hyaluronic acid: A key molecule in skin aging.* Dermatoendocrinol, 2012. **4**(3): p. 253-8.
148.   Klein, J., *Molecular mechanisms of synovial joint lubrication.* Proceedings of the Institution of Mechanical Engineers, Part J: Journal of Engineering Tribology, 2006. **220**(8): p. 691-710.
149.   Benz, M., N. Chen, and J. Israelachvili, *Lubrication and wear properties of grafted polyelectrolytes, hyaluronan and hylan, measured in the surface forces apparatus.* Journal of Biomedical Materials Research Part A, 2004. **71**(1): p. 6-15.
150.   Schmidt, T.A., et al., *Boundary lubrication of articular cartilage: role of synovial fluid constituents.* Arthritis & Rheumatism, 2007. **56**(3): p. 882-891.
151.   Kablik, J., et al., *Comparative physical properties of hyaluronic acid dermal fillers.* Dermatol Surg, 2009. **35 Suppl 1**: p. 302-12.
152.   Turlier, V., et al., *Association between collagen production and mechanical stretching in dermal extracellular matrix: in vivo effect of cross-linked hyaluronic acid filler. A randomised, placebo-controlled study.* Journal of dermatological science, 2013. **69**(3): p. 187-194.
153.   Wang, F., et al., *In vivo stimulation of de novo collagen production caused by cross-linked hyaluronic acid dermal filler injections in photodamaged human skin.* Archives of Dermatology, 2007. **143**(2): p. 155-163.
154.   Quan, T., et al., *Enhancing structural support of the dermal microenvironment activates fibroblasts, endothelial cells, and keratinocytes in aged human skin in vivo.* Journal of Investigative Dermatology, 2012. **133**(3): p. 658-667.
155.   Paliwal, S., et al., *Skin extracellular matrix stimulation following injection of a hyaluronic acid-based dermal filler in a rat model.* Plast Reconstr Surg, 2014. **134**(6): p. 1224-33.
156.   Lai, K.Y.V., *Bioengineered Tissue Mechanics: Experimental Characterization and a Multi-Component Model*. 2013, UNIVERSITY OF MINNESOTA.
157.   Grinnell, F., *Fibroblast–collagen-matrix contraction: growth-factor signalling and mechanical loading.* Trends in cell biology, 2000. **10**(9): p. 362-365.
158.   Dombi, G.W., R.C. Haut, and W.G. Sullivan, *Correlation of high-speed tensile strength with collagen content in control and lathyritic rat skin.* Journal of Surgical Research, 1993. **54**(1): p. 21-28.

106

159.	Khorramizadeh, M., et al., *Aging differentially modulates the expression of collagen and collagenase in dermal fibroblasts.* Molecular and cellular biochemistry, 1999. **194**(1-2): p. 99-108.
160.	Lavker, R.M., *Structural alterations in exposed and unexposed aged skin.* J Invest Dermatol, 1979. **73**(1): p. 59-66.
161.	Dupont, S., et al., *Role of YAP/TAZ in mechanotransduction.* Nature, 2011. **474**(7350): p. 179-183.
162.	Sit, S.-T. and E. Manser, *Rho GTPases and their role in organizing the actin cytoskeleton.* Journal of cell science, 2011. **124**(5): p. 679-683.
163.	Riento, K. and A.J. Ridley, *Rocks: multifunctional kinases in cell behaviour.* Nat Rev Mol Cell Biol, 2003. **4**(6): p. 446-56.
164.	Pritchard, C.A., et al., *B-Raf acts via the ROCKII/LIMK/cofilin pathway to maintain actin stress fibers in fibroblasts.* Mol Cell Biol, 2004. **24**(13): p. 5937-52.
165.	Kono, T., et al., *Correlation between ageing and collagen gel contractility of human fibroblasts.* Acta dermato-venereologica, 1989. **70**(3): p. 241-244.
166.	Fujimura, T., et al., *Loss of contraction force in dermal fibroblasts with aging due to decreases in myosin light chain phosphorylation enzymes.* Archives of pharmacal research, 2011. **34**(6): p. 1015-1022.
167.	Hayashida, T., et al., *TGF-beta1 activates MAP kinase in human mesangial cells: a possible role in collagen expression.* Kidney Int, 1999. **56**(5): p. 1710-20.
168.	Ivaska, J., et al., *Integrin alpha2beta1 mediates isoform-specific activation of p38 and upregulation of collagen gene transcription by a mechanism involving the alpha2 cytoplasmic tail.* J Cell Biol, 1999. **147**(2): p. 401-16.
169.	Douillet, C.D., et al., *Mechanisms by which bradykinin promotes fibrosis in vascular smooth muscle cells: role of TGF-β and MAPK.* American Journal of Physiology-Heart and Circulatory Physiology, 2000. **279**(6): p. H2829-H2837.

107

APPENDIX A: FIBRINOGEN AND THROMBIN PREPARATION

Fibrinogen is a glycoprotein, synthesized by the liver and is known to be one of the main components of the plasma proteins. Converted to fibrin through thrombin cleavage, fibrinogen is a key component of the wound healing process. Upon injury, the body responds by forming a clot to prevent blood loss and to establish a temporary structure or network that allows for the migration of different cells such as macrophages and fibroblasts to the wound site. The formation of this mesh begins with the accumulation of platelets at the wound site and the conversion of prothrombin to thrombin, which proceeds to cleave several polypeptides on molecules of fibrinogen, which then bind together to form fibrin. At the same time, thrombin activates the plasma protein, factor XIIIa, which catalyzes the formation of cross-links that stabilize and strengthen the fibrin mesh.

Time Required: It will take two days to make the fibrinogen stock solution. Start making the fibrinogen stock solution in the morning. The thrombin stock solution is easy to make and will only take a few hours.

Tips:

- Make sure the fibrinogen solution does not exceed 37 °C. Higher temperatures can cause fibrinogen to denature and form a precipitate.

- You can quantify total protein concentration in the fibrinogen stock with a Bradford total protein assay.

1. Materials

1.1. Reagents

- De-ionized water (18kon

108

- Biological grade NaCl (Company, Cat No.)

- HEPES (Sigma, Catalog No. H0887)

- Bovine Fibrinogen (Sigma, Catalog No. F8630)

- Thrombin from bovine plasma (Sigma, Catalog No. T4648)

1.2. Equipment

- Stir plate and stir bar

- (3) 250 mL bottles (at least one autoclaved)

- (3-4) 150 mL 0.45 µ3 Steritop filter (Fischer, Catalog No. 430627)

- (3-4) 150 mL 0.22 µ3 Steritop filter (Fischer, Catalog No. SCGVTO54E)

- (3-4) Glass fiber prefilters (Fischer Catalog No. AP2007500)

- Steriflip 0.22 µm with 50 mL C-tube (Company, Catalog No.)

2. Methods

2.1. Fibrinogen Stock Preparation (~33mg/mL)

Day 1

1.   Make 150 mL of 20 mM HEPES buffered saline by mixing 3 mL of 1M HEPES and 147 mL of 0.9% saline. Use a slightly bigger bottle than the actual amount. Put a magnetic stir bar into the bottle. Depending on the frequency of use and the total volume needed, preparing half of this volume is also recommended because it makes dissolving the fibrinogen in HEPES a much easier process while also consuming less time.

2.   Warm up the solution to 37 °C in the incubator prior to adding fibrinogen.

3.   Measure out 5 g of fibrinogen.

109

4.	Add a small amount of fibrinogen (0.2-0.3 grams) to the bottle containing 20 mM HEPES buffered saline. Swirl the solution around to make sure that the fibrinogen just added is wet.

5.	Put the bottle in the incubator with the stir plate. Set the stir bar at a speed that is just below forming a vortex. You want to minimize forming bubbles but keep the solution from gelling up.

6.	Add more fibrinogen approximately every 15 minutes or so. Make sure that the previously added fibrinogen has gone into solution. It is common to see bits of precipitate floating about.

7.	Prior to dissolving the total amount of fibrinogen, you should allow the solution to mix in the incubator for 6 to 8 hours. Store the solution in the refrigerator overnight.

Day 2

8.	Warm the solution to 37 °C in the water bath for approximately one hour.

9.	Sterile filter the solution using as many 0.45 micron filters as needed. Make sure to use the prefilters to speed up the process.

10.	Repeat the filtering with 0.22 µ0 filters. Make sure to do this step in the hood into a sterile bottle.

11.	Aliquot 0.5 and 1 mL volumes into sterilized microcentrifuge tubes

**2.2.	Thrombin Stock Preparation (25 U/mL)**

1.	Dissolve 500 units of thrombin into 2 mL of ddH_2O and 18 mL of saline (0.9% NaCl).

2.	Filter through 0.22 µm sterile filter into 50 mL tube (use steriflip tubes).

110

3. Aliquot into 125 μ. and 250 μa volumes into sterile microcentrifuge tubes

2.3. Fibrin Gel Polymerization

In order to prepare a fibrin gel, stock solutions of fibrinogen and thrombin must be further prepared. After separately preparing these reagents, you will add fibrinogen, thrombin and a cell suspension or medium with a concentration ratio of 4:1:1.

1. Determine the volume of fibrin gel you want to prepare. Based off of this, calculate the amount of each reagent required knowing that the final ratio should be 4:1:1.

Example:

$$V_T = 4 \, mL$$

$$V_{fibrinogen} = 4 \, mL * \frac{4}{6} = 2.667 \, mL$$

$$V_{thrombin} = 4 \, mL * \frac{1}{6} = 0.667 \, mL$$

$$V_{cell \, suspension} = 4 \, mL * \frac{1}{6} = 0.667 \, mL$$

2.3.1. Fibrinogen Solution

Reagents:

- Fibrinogen stock (~33 mg/mL)

- 20 mM HEPES 0.9% saline solution

Equipment:

- (1) 50 mL C-tube or 1.5 mL micro-centrifuge tube depending on volume

Procedure

1. Prepare a 20mM HEPES 0.9% saline solution as previously described.

111

2. Thaw out an aliquot of fibrinogen from stock in a water bath at 37C for about 5 minutes.

3. Add 1/3 of the total volume of fibrinogen in fibrinogen from stock and 2/3 in HEPES solution to obtain a solution with a ratio of 1:2 and mix together in a 15 ml C-tube.

Example:

$$V_{fibrinogen} = 4 \, mL * \frac{4}{6} = 2.667 \, mL$$

$$V_{fibrinogen \, stock} = 2.667 \, mL * \frac{1}{3} = 0.889 \, mL$$

$$V_{20mM \, HEPES} = 2.667 \, mL * \frac{2}{3} = 1.778 \, mL$$

2.3.2. Thrombin solution

Reagents:

- Thrombin stock (25 U/mL)

- 20 mM HEPES 0.9% saline solution

- 2 M CaCl$_2$

Equipment:

- (1) 15 mL C-tube or 1.5 mL micro-centrifuge tube depending on volume

Procedure

4. Prepare 40 ml of a 2M CaCl2 solution by adding 40 ml of ddH20 to 11.76 g of CaCl2.

5. Filter this solution using a Steriflip C-tube with a 0.22um filter. Store in refrigerator at 4C.

112

6.   Calculate the amount of each reagent needed to obtain a thrombin solution with a final ratio of 1:4:0.075 and mix together into a 15 ml C-tube.

Example:

$$V_{thrombin} = 0.667\ mL$$

$$V_{thrombin\ stock} = 0.667\ mL * \frac{1}{5.075} = 0.131\ mL$$

$$V_{20\ mM\ HEPES} = 0.667\ mL * \frac{4}{5.075} = 0.525\ mL$$

$$V_{2\ M\ CaCl_2} = 0.667\ mL * \frac{4}{5.075} = 0.00985\ mL$$

2.3.3. Fibrin gel solution

7.   Now that each reagent has been prepared in separate containers, add the previously calculated volume of the cell suspension into the 15 ml C-tube containing the fibrinogen solution.

8.   Mix the thrombin solution with the fibrinogen containing the cell suspension and resuspend 5-10 times or until the solution is evenly distributed.

9.   Once adding thrombin, the solution will begin to gel almost instantly, so make sure that you resuspend quickly and add the solution into the petri dish, well or mold where you would like to set your sample.

10.   After solution has set at room temperature, incubate at 37C and 5% CO2 for 15-30min.

11.   Add medium onto the sample and make sure to change it every day or every two days, depending on the concentration of cells used to seed the gel.

APPENDIX B: POLYMERIZATION OF 3D COLLAGEN

HYDROGELS

1. Materials

1.1. Reagents

- Sterile 10x PBS with phenol red

- Sterile 1 N NaOH

- Sterile dH$_2$O or cell suspension in cell culture medium

- Acid solubilized Collagen Type I (Thermo Fischer, Catalog No.

1.2. Equipement

- 50 mL C-tube

2. Methods

2.1. Acellular Collagen Gels

1.   If you are preparing an acellular collagen gel, sterilize dH20 by using a 0.33 um syringe filter or a 0.33 um Steriflip Millipore C-tube.

2.   Dilute the 2 N NaOH to 1 N NaOH and sterilize using a 0.33 um syringe filter or a 0.33 um Steriflip Millipore C-tube.

3.   Keep collagen type I stock solution (3 mg/mL), 1 N NaOH, and 10x PBS with phenol red at approximately 4°C by keeping on ice.

4.   Determine concentration and final volume of collagen needed.

5.   Calculate the amount of reagents needed so that your final solution is at the desired concentration with normal osmolality and neutral pH.

114

$$V_T = Total\ volume\ of\ collagen\ solution$$

$$V_{Collagen} = \frac{(Final\ concentration\ of\ collagen) * (V_T)}{Initial\ concentration\ of\ collagen}$$

$$V_{MEM\ 10X} = \frac{(V_T)}{10}$$

$$V_{NaOH} = (Total\ volume\ of\ collagen\ solution) * 0.025$$

$$V_{dH_2O\ or\ cell\ suspension} = V_T - (V_{collagen} + V_{MEM\ 10x} + V_{NaOH}$$

6.   Mix the calculated volumes of 10X PBS with phenol red, 1N NaOH, and Collagen Type I and resuspend about 5 times, making sure that the solution is well mixed before adding the cell suspension.

7.   Resuspend another 5 times until you obtain a homogenous mixture. (Try to do this quickly before gel begins to polymerize and avoid creating bubbles in the solution).

8.   Pour collagen into desired plates or dishes immediately or store on ice.

9.   Incubate in a 37C, 95% humidity incubator for 30-40 min.

10. After the gel has polymerized, add cell culture medium.

APPENDIX C: HOESCHT DNA ASSAY

The number of cells within three-dimensional hydrogels can be easily quantified with the use of nuclear fluorescent dyes such as Hoechst stains and a plate reader. Hoschst stains are bisbenzamides that bind to the minor groove of double-stranded DNA. Originally developed by Hoechst AG, these stains are commonly used as nuclear fluorescent dyes.

The following protocol was adapted in order to quantify the number of cells cultured for over one week in fibrin gels.

1. Materials:

- Digestion buffer (100 mM Tris, 50 mM EDTA, pH 7.4)

- 10x TNE buffer (100 mM Tris, 2.0 M NaCl, 10 mM EDTA, pH 7.43)

- Proteinase K (Roche, Ref No. 03115 879001)

- Calf Thymus DNA (Sigma, Catalog No. D1501)

- Hoechst 33342 (Thermo Fischer, Catalog No. H1339)

2. Methods:

2.1. Preparation of digestion buffer

Because EDTA can only go into solution at a pH close to 7.4, begin by preparing a 1 M solution of EDTA in ddH$_2$O.

To prepare 250 mL of digestion buffer with a concentration of 100 mM Tris and 50 mM EDTA and a pH of 7.4, add 3.03 g of Tris base to 150 mL of ddH$_2$O in a 500 mL beaker while stirring on a magnetic plate. Add 12.5 mL of 1 M EDTA. Use concentrated HCl to pH the solution as needed in order to achieve a pH of 7.4. Once the solution reaches pH 7.4, add enough ddH$_2$O to obtain 250 mL of solution.

116

2.2. Preparation of 10x TNE buffer

To prepare 250 mL of 10x TNE buffer with a concentration of 100 mM Tris, 2.0 M NaCl, and 10 mM EDTA, and pH pf 7.4, add 3.03 g of Tris base to 100 mL of ddH$_2$O in a 500 mL beaker while stirring on a magnetic plate. Add 29.28 g of NaCl. Finally, add 2.5 mL of 1 M EDTA. Use concentrated HCl to pH the solution as needed in order to achieve a pH of 7.4. Once the solution reaches pH 7.4, add enough ddH$_2$O to obtain 250 mL of solution.

2.3. Preparation of proteinase K

Reconstitute 100 mg of proteinase K in 20 mL of digestion buffer and store solution in a -20°C freezer in 1 mL aliquots.

2.4. Preparation of calf thymus DNA

Calf thymus DNA must be diluted in digestion buffer at 4°C overnight, or until DNA is completely dissolved in solution. The DNA can be aliquoted in 500 µL of 20 µL of 2 stock solution in a -20°C freezer.

2.5. Fibrin digestion

- The night before, dilute Proteinase K aliquoted at a concentration of 5 mg/mL to a concentration of 0.5 mg/mL in digestion buffer. Add 0.5 mL to a 1.5 mL micro-centrifuge tube containing the sample.

- Incubate micro-centrifuge tubes in a heating block at 56°C overnight. One hour after placing tubes in heating block, gently shake tubes so aid in mixing and degradation of the gel. The next day, make sure that samples are completely digested in the digestion buffer. Add additional digestion buffer to sample if needed.

117

2.6. DNA Standard Preparation

- Thaw out one vial of 20 µg/mL of calf thymus DNA to prepare your standards.

- Prepare standards by using the volumes of each reagent specified in Table C.1.

Table C.1. Calf thymus DNA standards

Standard	Concentration (µg/mL)	Volume of Stock (µL)	Volume of 10x TNE Buffer (µL)
1	6	60	140
2	5	50	150
3	4	40	160
4	3	30	170
5	2	20	180
6	1	10	190
7	0.5	5	195
8	0 (Blank)	0	200

- Add 100 µL of each standard to a 96-well black/clear bottom plate.

2.7. Sample and Plate Preparation

- Dilute each sample by 10x into the 96 well plate, 3 wells per sample (10 µL of sample, 90 µL of TNE buffer).

- Determine the volume of Hoechst 33342 at a concentration of 0.2 µg/mL required to add 100 µL to each well, including those containing the standards. Prepare by mixing the volume required of Hoechst stock solution at 10 mg/mL with 10x TNE buffer.

2.8. Fluorescent Quantification

118

- Turn on the Promega plate reader and select the user-defined protocol Hoechst 33342 DNA Assay. Select the wells to be analyzed, and the number of readings. Make sure that the UV filter (360 nM/460 nM) is selected and is placed in the filter slot.

- Select the "Door" icon in the bottom right corner of the screen.

- Place the 96-well plate with well A1 facing the furthermost right corner of the plate holder.

- Close the door by selecting the "Door" icon again.

- Run assay.

2.9. Data Analysis

- After saving results onto a USB, open results using Excel.

- After subtracting the fluorescent value for the blank from the value of fluorescence obtained for all samples, create a standard curve with fluorescence as the independent variable and DNA concentration as the dependent variable.

- Determine the linear trendline and equation for the dataset using:

  $$DNA\ Concentration = Fluorescence * m + b$$

- Using this equation, determine the DNA concentration in each sample by substituting the value for fluorescence measured using the plate reader. Cell number can be determined considering that fibroblasts contain approximately 7.6 pg of DNA.

APPENDIX D: HYDROXYRPOLINE ASSAY

1. **Materials**

•   0.1 M NaOH

•   6 N HCl

•   Hydroxy-L-proline (CAS 51-35-4, MW 131)

•   Stock buffer (25 g of citric acid, 60 g of sodium acetate, 34 g of sodium
    hydroxide, and 6 mL of glacial acetic acid)

•   Chloramine-T solution (0.0352 g of chloramine-T, 1.3325 mL stock buffer,
    0.65 mL of N-propanol, and 0.5175 mL of deionized water).

•   Dimethylaminobenzaldehyde (pDMBA) solution (0.5 g pDMBA, 3 mL N-
    propanol, and 1.3 mL of perchloric acid)

•   Activated charcoal (CAS 7440-44-0)

2. **Methods**

    2.1. Separation Process:

•   Place samples in an eppendorf tube and add 0.5 mL of 0.1 N NaOH to each
    sample and heat on a heating block at 98°C for one hour.

•   Transfer samples into a glass vial and place into a speed vacuum and spin for
    2 hours or until dry.

•   Once samples have dried, add 0.5 mL of 6 N HCl and heat on a heating block
    at 110°C for 24 hours.

•   Transfer vials to the speed vacuum and spin for 1.5 hours or until dry.

    2.2. Sample Preparation

•   Prepare assay buffer by diluting stock buffer 1:10 in water.

•   Add 0.25-0.5 mL of assay buffer to all samples after the last drying step and
    mix.

- Add a touch of charcoal to each solution, recap, and shake to disperse the well.

- Transfer the solution into a new eppendorf tube and spin in a microcentrifuge at 1500 rpm for five minutes.

2.3. Prepare Standard

- Make a 1mg/mL solution by adding 10 mg of hydroxyproline to 10 mL of assay buffer.

- Make 100 μg/mL solution by diluting the 1 mg/mL prepared in the previous step by 1:10.

- Put 200 μL of the 100 μg/mL solution (therefore a total of 10 μg), in the first well of a 96 well plate.

- Put 100 μL of assay buffer in ten additional wells of the row.

- Take 100 μL out of the first well and mix into the second well.

- Take 100 μL of the second well and mix into the third.

- Repeat pattern for all but the last well. Dispose of the extra 100 μL. The wells should have 10,5,2.5, 1.25, 0.625, 0.313, 0.156, 0.0781, 0.029, and 0 μg/mL.

- Repeat steps 8-12 for a second row.

2.4. Assay

- Add 100 μL of one sample per well.

- Add 50 μL of Chloramine-T solution to each well.

- Incubate at room temperature for 15 min.

- Add 50 μL of p-DMBA solution to each well and mix well (including standards).

- Cover with parafilm plate sealer.

- Incubate at 37°C for 30 minutes.

- Determine the optical density using a plate reader set to 570 nm.